



Aalborg Universitet

AALBORG UNIVERSITY
DENMARK

User-Centered Modelling and Design of Assistive Exoskeletons

Christensen, Simon Søndergaard

DOI (link to publication from Publisher):
[10.54337/aau528218520](https://doi.org/10.54337/aau528218520)

Publication date:
2023

Document Version
Publisher's PDF, also known as Version of record

[Link to publication from Aalborg University](#)

Citation for published version (APA):
Christensen, S. S. (2023). *User-Centered Modelling and Design of Assistive Exoskeletons*. Aalborg Universitetsforlag. <https://doi.org/10.54337/aau528218520>

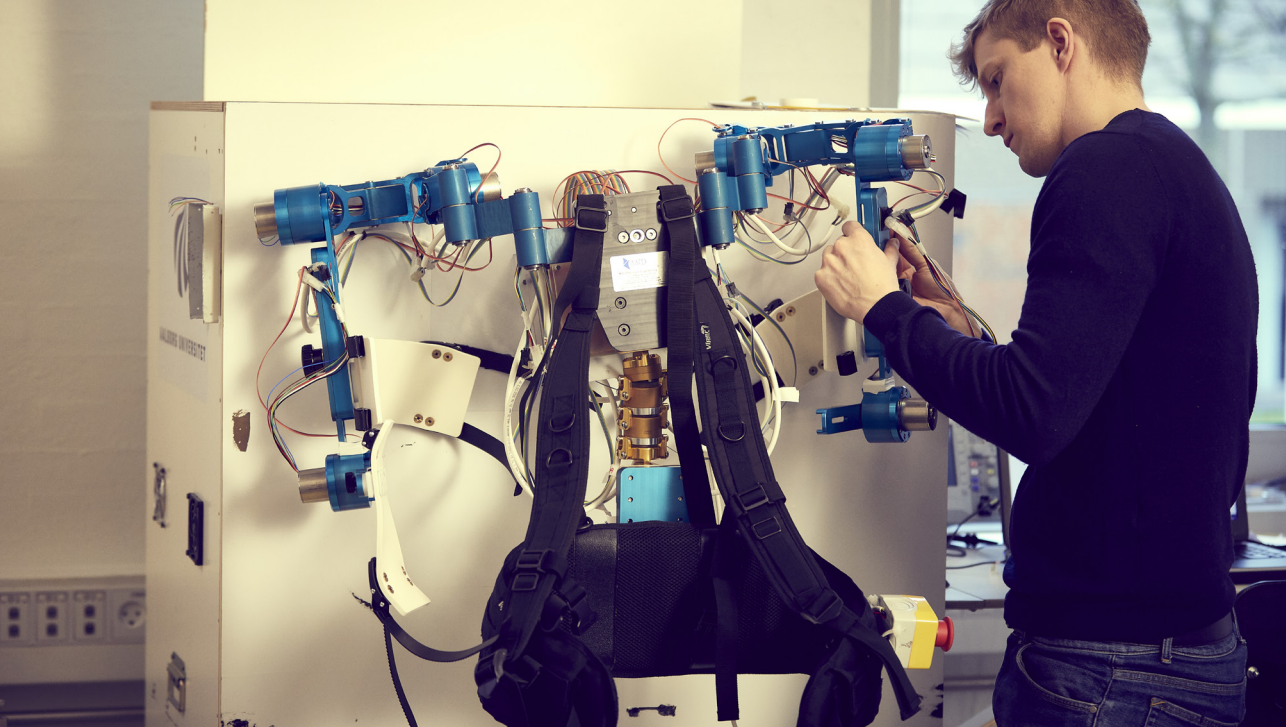
General rights

Copyright and moral rights for the publications made accessible in the public portal are retained by the authors and/or other copyright owners and it is a condition of accessing publications that users recognise and abide by the legal requirements associated with these rights.

- Users may download and print one copy of any publication from the public portal for the purpose of private study or research.
- You may not further distribute the material or use it for any profit-making activity or commercial gain
- You may freely distribute the URL identifying the publication in the public portal -

Take down policy

If you believe that this document breaches copyright please contact us at vbn@aub.aau.dk providing details, and we will remove access to the work immediately and investigate your claim.



USER-CENTERED MODELLING AND DESIGN OF ASSISTIVE EXOSKELETONS

**BY
SIMON SØNDERGAARD CHRISTENSEN**

DISSERTATION SUBMITTED 2023



AALBORG UNIVERSITY
DENMARK

User-Centered Modelling and Design of Assistive Exoskeletons

Ph.D. Dissertation
Simon Søndergaard Christensen

Aalborg University
Department of Materials and Production
Solid and Computational Mechanics Group
Fibigerstræde 16
DK-9220 Aalborg

Dissertation submitted January 21, 2023

Dissertation submitted: January 21, 2022

PhD supervisor: Professor, PhD, MSc Shaoping Bai
Department of Materials and Production
Aalborg University, Denmark

PhD committee: Associate Professor Johnny Jakobsen
Aalborg University, Denmark
Professor Shane Xie
University of Leeds, United Kingdom
Associate Professor Lei Feng
KTH Royal Institute of Technology, Sweden

PhD Series: Faculty of Engineering and Science, Aalborg University

Department: Department of Materials and Production

ISSN (online): 2446-1636
ISBN (online): 978-87-7573-764-2

Published by:
Aalborg University Press
Kroghstræde 3
DK – 9220 Aalborg Ø
Phone: +45 99407140
aauf@forlag.aau.dk
forlag.aau.dk

© Copyright: Simon Søndergaard Christensen

Printed in Denmark by Stibo Complete, 2023

Typeset in L^AT_EX and printed in Denmark by Rosendahls, 2023

Preface

This thesis has been submitted to the Faculty of Engineering and Science at Aalborg University in partial fulfillment of the requirements for the degree of Doctor of Philosophy in Mechanical Engineering. The work has been carried out at the Department of Materials and Production at Aalborg University in the period from December 2014 to December 2021. The work is part of the research project entitled *Assistive exoskeleton suitable for elderly persons - AXO-SUIT* funded by the EU AAL Programme and Innovation Fund Denmark. This support is gratefully acknowledged.

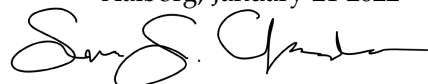
There are several people to whom I am very grateful for their support during my studies. Firstly, I would like to express my sincere gratitude to my supervisor Professor Shaoping Bai for his continuous and unconditional guidance and support. Even after my departure from Aalborg University in 2018, you continued to encourage me to finish my studies. I find it hard to believe that this thesis would ever have come to be without you. For that you have my deepest appreciation.

I would also like to thank the Biomechanics group and particularly, Professors John Rasmussen and Michael Skipper Andersen, for their support in the field of biomechanics and countless aid with the *AnyBody Modeling System*.

A special thanks to my fellow PhD candidates and colleagues at the Solid and Computational Mechanics group for providing a fun and great work environment. It has been a true pleasure.

Finally, thank you to my family for your support throughout the entire journey.

Aalborg, January 21 2022



Simon Søndergaard Christensen

Abstract

This PhD study project was part of the EU collaboration project called AXO-SUIT, funded under the Ambient Assisted Living (AAL) Programme that aims to create a better quality of life for older people by strengthening the development of healthy ageing technologies and innovation. The main objective of AXO-SUIT was to develop modular exoskeletons for assistive applications in the demanding activities of daily living.

An exoskeleton is a mechanism with powered or passive joints and links that correspond to the limbs of the human body. Exoskeletons have shifted the field of robotics in a new era of assistive technology research. The exoskeletons have a potential of assisting and augmenting humans in performing their activities of daily living. The design and development of compact, safe and comfortable exoskeletons is still challenging. Since the human is the centre for these systems, understanding the needs of the end-user is paramount. Involving end-users at an early stage and throughout the development phase can be beneficial for the final design of the exoskeleton.

The objective of this PhD study is to use a user-centered design approach to develop an assistive exoskeleton for general physical assistance for older adults to continue their activities of daily living. End-users are engaged from an early stage to derive the requirements and assess the functionalities and design for the innovative exoskeleton system. This work makes three contributions: 1) the innovative lightweight and compact spherical mechanism, 2) virtual prototyping using musculoskeletal modelling and simulation of a cooperative human-robot system and 3) full-body exoskeleton system design validation including pilot testing.

The first two chapters cover the opening of the dissertation, with the first chapter introducing the background and motivation for the project. Next, the state-of-the-art in portable upper-body exoskeletons is presented, highlighting some of the limitations of the existing solutions. This is followed by the user-centered design approach adopted in the AXO-SUIT project in combination with musculoskeletal simulations. Finally, the overall aim of the project and how this is achieved through the research objectives and questions

is presented.

Chapter 3 presents the first paper, which demonstrates an innovative, lightweight and compact spherical mechanism that is designed for shoulder exoskeleton applications. The three consecutive rotational degrees-of-freedom (DOFs) range of the shoulder is matched by a double parallelogram linkage (DPL) connecting two revolute joints. The kinematics and singularities are analysed for the mechanism as a whole and the double parallelogram linkage on its own. A dimensional analysis is carried out to maximise the range-of-motion (ROM) of the mechanism. The design of the mechanism has several new features compared to the current state-of-the-art, such as a relative large ROM free of singularity, high overall stiffness, lightweight and compactness, which make it suitable for assistive portable exoskeletons.

Chapter 4 presents the second paper, which investigates the physical human-robot interaction through a co-simulation model of the human musculoskeletal system and the exoskeleton robotic system, named UB-AXO. The physical human-robot interaction, i.e., the kinematic and kinetic interaction between the human and exoskeleton, is a major concern for wearable exoskeletons for both functioning properly and interacting safely and comfortably with the human. A co-simulation model comprising the biomechanics of the human upper limb and the dynamics of the exoskeleton, which includes the shoulder joint from chapter 3, is developed in the musculoskeletal modelling and simulation software: *Anybody Modeling System*. The model is used to estimate the effect of physical human-exoskeleton interaction, such as muscle activity, and energy consumption and human joint reaction forces, when performing cooperative motions. Two simulation studies of simple typical activities of daily living are conducted to analyse and evaluate the performance of the exoskeleton system. The simulation results demonstrate that the UB-AXO is able to reduce muscle loading and energy consumption, while maintaining a safe physical human-exoskeleton interaction.

Chapter 5 presents the third and final paper, which demonstrates the design, construction and preliminary testing of a full-body exoskeleton, named FB-AXO. The development of FB-AXO is the result of comprehensive end-user involvement, in which functional requirements and product requirements were obtained. The design challenges including kinematic compatibility and modularity with innovative solutions are addressed, such as the shoulder joint from chapter 3 and a passive supportive spine module. The details of the mechanics, sensors and electronics of the modular system along with specifics of human-exoskeleton interfaces and ranges of motion are also provided. A preliminary test with the exoskeleton modules demonstrates a good compatibility between the user and exoskeleton and some positive effects in

physical assistance.

The final chapter includes a summary of key results from the publications within this dissertation and a discussion regarding the results of the studies. Additionally, limitations of these studies are addressed and recommendations for future research are outlined.

Resumé

Dette ph.d. studium var del af et EU samarbejdsprojekt ved navn AXO-SUIT, som var finansieret af Ambient Assisted Living (AAL) Programme, hvilket er en organisation med formålet om at skabe bedre livskvalitet for ældre borgere ved at styrke udviklingen af innovative hjælpemidler. Det overordnede mål med AXO-SUIT projektet var at udvikle modulopbygget eksoskeletter, der kan støtte bevægelsesfunktioner for de ældre borgere ved krævende daglige aktiviteter, så som at løfte tunge objekter i hjemmet.

Indenfor robotteknologien, er et eksoskelet en mekanisme, der bæres af et menneske for enten at assistere eller forstærke brugers funktionalitet. Som navnet antyder, så består et eksoskelet af en ydre struktur (heraf ekso-), der svarer til kroppens egen struktur. Eksoskelettets led er drevet af enten aktive (f.eks. elektriske motorer) eller passive elementer (f.eks. mekaniske fjedre). Teknologien har med sit store potentiale fået øget fokus indenfor forskning af robotteknologi af personlige hjælpemidler. Design og styring af kompakte, sikre og komfortable eksoskeletter er dog stadig udfordrende. Da mennesket i høj grad er i centrum for disse systemer, er det altafgørende af have en forståelse for slutbrugeren behov . Det kan derfor være yderst gavnligt at inddrage slutbrugeren fra et tidligt stadie af udviklingen og helt frem til de afsluttende tests af det endelige design af eksoskelettet.

Målet med denne ph.d.-afhandling er at anvende en brugercentreret design tilgang til at udvikle et assisterende eksoskelet, der kan hjælpe ældre borgere til at fortsætte deres daglige aktiviteter . Slutbrugere engageres fra et tidligt stadie og er med til at definere krav til systemet, samt at vurdere dens funktionalitet under udviklingen og slutteligt at teste det endelige design. Det vurderes, at resultaterne i denne afhandling har potentiale til at avancere state-of-the-art indenfor assisterende hjælpemidler, hvilket kan være med til at forbedre livskvaliteten blandt ældre borgere.

De første to kapitler omhandler indledningen af afhandlingen, hvor første kapitel er en introduktion, der fremhæver baggrunden og motivationen for projektet. Dernæst præsenteres den seneste forskning indenfor feltet, hvor state-of-the-art eksoskeletter bliver diskuteret og begrænsningerne af de nu-

værende teknologier fremhæves. Herefter præsenteres den bruger-centrerede design tilgang, der er anvendt i AXO-SUIT-projektet i kombination med virtuel prototyping gennem muskuloskeletal simulering. I kapitel 2 præsenteres de overordnede mål med projektet samt de forskningsspørgsmål, der afsøges i afhandlingen.

I kapitel 3 præsenteres den første artikel, som omhandler designet af en kompakt sfærisk mekanisme til skulderledet på et eksoskelet. Mekanismen er bygget op om et dobbelt parallelogram og består samlet set af tre rotationelle frihedsgrader, hvor rotationsakserne er sammenfaldende i et fjernt-liggende punkt. I artiklen analyseres kinematikken og af hele mekanismen samt kinematikken af dobbeltparallelogrammet for sig selv. Efterfølgende gennemføres et parameter studie for at finde det størst mulige bevægelsesområde for mekanismen. Slutteligt er mekanismen fremstillet og integreret i et eksoskelet til overkroppen, hvor bevægelsesområdet afprøves eksperimentelt. Designet af mekanismen har flere attraktive funktioner, som gør den velegnet til portable eksoskeletter, såsom et relativt stort arbejdsområde fri for singularitet, høj strukturel stivhed, letvægt og kompakthed.

I kapitel 4 præsenteres den anden artikel, som omhandler en matematisk modellering og analyse af den fysiske interaktion mellem en musculoskeletal model og et eksoskelet til overkroppen, kaldet UB-AXO. Den fysiske interaktion mellem menneske og robot er et vigtig design faktor for eksoskeletter, da den har indflydelse på performance, men også komfort og sikkerhed. En simuleringmodel, som består af biomekanikken af menneskets overkrop og mekanikken af eksoskelettet, er udviklet i musculoskeletal modellering og simuleringssystemet Anybody Modeling System. Simuleringsmodellen bruges til at estimere effekten af den fysiske interaktion mellem menneske og eksoskelet, såsom muskelaktivitet, energiforbrug og reaktionskræfter i menneskets led, der alle har indflydelse på performance og komfort af systemet. To simuleringstudier, der tager udgangspunkt i simple typiske dagligdagsaktiviteter, benyttes til at demonstrere modellen. Resultaterne fra de to studier viser, at UB-AXO er i stand til at reducere muskelaktiviteten og energiforbrug, samtidig med at den reducerer reaktionskræfterne i menneskets led, hvilket er vigtigt for at opnå en komfortable og sikker fysisk interaktion.

I kapitel 5 præsenteres den tredje og sidste artikel, som omhandler design, fremstilling og præliminær test af det modulopbygget helkrops eksoskelettet FB-AXO. Udviklingen af FB-AXO er resultatet af en omfattende slutbrugerinddragelse, hvori funktionelle og design krav er blevet indhentet. Design udfordringer, såsom kinematik kompatibilitet og modularitet, adresseres med innovative løsninger, som det sfærisk skulder led fra kapitel 3 og et

passivt støttende modul til den nedre ryg region. Detaljer om designets modulære struktur, mekaniske design, anvendte sensorer og elektronik bliver beskrevet sammen med grænsefladerne for interaktionen mellem menneske og eksoskelettet. Den præliminær test med eksoskelet modulerne viser en god kompatibilitet mellem brugeren og eksoskelettet og viser nogle positive effekter i fysisk assistance.

Det sidste kapitel inkluderer et resume af de overordnede resultater fra publikationerne i denne afhandling, samt en diskussion af de anvendte metoder og udbyttet af studierne. Derudover bliver begrænsninger i afhandlingen diskuteret og anbefalinger til fremtidig forskning fremlagt.

Thesis Details

This dissertation serves as an introduction to the research areas of the PhD project. The dissertation is structured as a collection of scientific papers for publication in refereed journals. Three journal papers have been published in refereed scientific journals.

Thesis Title: User-Centered Modelling and Design of Assistive Exoskeletons
Ph.D. Student: Simon Søndergaard Christensen
Supervisor: Prof. Shaoping Bai, Aalborg University

Publications in refereed journals

- [I] **S. Christensen** and S. Bai, “Kinematic Analysis and Design of a Novel Shoulder Exoskeleton using a Double Parallelogram Linkage,” *Journal of Mechanisms and Robotics*, vol. 10, no. 4, pp. 10, 041008, 2018.
<https://doi.org/10.1115/1.4040132>
- [II] **S. Christensen**, X. Li and S. Bai, “Modeling and Analysis of Physical Human-Robot Interaction of an Upper Body Exoskeleton in Assistive Application,” *Modeling, Identification and Control*, vol. 42, no. 4, pp. 159–172, 2021.
<https://doi.org/doi:2021.10.4173/mic.2021.4.2>
- [III] **S. Christensen**, S. Rafique and S. Bai, “Design of a powered full-body exoskeleton for physical assistance of elderly people,” *International Journal of Advanced Robotic Systems*, vol. 18, no. 6, pp. 1–15, 2021.
<https://doi.org/doi:10.1177/172988142111053534>

Publications in proceedings with review

- [1] **Christensen S.** and Bai S., (2017) “A Novel Shoulder Mechanism with a Double Parallelogram Linkage for Upper-Body Exoskeletons,” In: González-Vargas J., Ibáñez J., Contreras-Vidal J., van der Kooij H., Pons J. (eds) *Wearable*

Robotics: Challenges and Trends. Biosystems & Biorobotics, vol 16. Springer, Cham.,

https://doi.org/10.1007/978-3-319-46532-6_9

- [2] **S. Christensen**, S. Bai, S. Rafique, M. Isaksson, L. O'Sullivan, V. Power and G. S. Virk, "AXO-SUIT - A Modular Full-Body Exoskeleton for Physical Assistance," *In: In IFToMM Symposium on Mechanism Design for Robotics (pp. 443-450). Springer, Cham.,*

https://doi.org/10.1007/978-3-030-00365-4_52

- [3] S. Bai, **S. Christensen**, "Chapter Nine - Biomechanical HRI Modeling and Mechatronic Design of Exoskeletons for Assistive Applications," *Editor(s): Jun Ueda, Yuichi Kurita, Human Modelling for Bio-Inspired Robotics, Academic Press, 2017, Pages 251-272,*

<https://doi.org/10.1016/B978-0-12-803137-7.00010-0>

Patent

- [A] Simon Christensen and Shaoping Bai, "A Spherical Mechanism with Double Parallelogram Linkages". IPC no. PCT/DK2017/050100, Patent No. WO 2017/167349. October 5 2017.

This thesis has been submitted for assessment in partial fulfillment of the PhD degree. The thesis is based on the submitted or published scientific papers that are listed above. Parts of the papers are used directly or indirectly in the extended summary of the thesis. As part of the assessment, co-author statements have been made available to the assessment committee and are also available at the Faculty. The thesis is not in its present form acceptable for open publication but only in limited and closed circulation as copyright may not be ensured.

Contents

Preface	iii
Abstract	v
Resumé	ix
Thesis Details	xiii
List of Figures	xvii
List of Tables	xix
Nomenclature	xxi
1 Introduction	1
1.1 Background and Motivation	1
1.2 Brief Introduction to Exoskeletons	3
1.3 State-of-the-art in Upper Body Exoskeletons	6
1.3.1 Passive Upper Body Exoskeletons	7
1.3.2 Active Upper Body Exoskeletons	10
1.4 User-Centered Design of AXO-SUIT	18
1.5 Musculoskeletal Modelling in Exoskeleton Design	22
2 Research Challenges and Objectives	25
2.1 Objectives of the PhD Project	25
2.2 Scope of Work and Project Methodology	27
2.3 Thesis Outline	28
3 Paper I	31
Kinematic Analysis and Design of a Novel Shoulder Exoskeleton using a Double Parallelogram Linkage	33

4 Paper II	45
Modeling and Analysis of Physical Human-Robot Interaction of an Upper Body Exoskeleton in Assistive Application	47
5 Paper III	63
Design of a Powered Full-Body Exoskeleton for Physical Assistance of Elderly People	65
6 Summary of Results and Conclusion	81
6.1 Summary of Results	81
6.2 Contributions	86
6.3 Limitation and Future Work	88
References	91

List of Figures

1.1	Full body exoskeleton developed in the AXO-SUIT Project . . .	2
1.2	General Electric's Hardiman Exoskeleton	3
1.3	Examples of state-of-the-art exoskeletons	4
1.4	The degrees-of-freedom in the human upper extremity	5
1.5	Examples of passive upper body exoskeletons	7
1.6	Examples of active upper body exoskeletons	11
1.7	Examples of acquisition of the user intention	13
1.8	Range-of-motion and joint torques during the overhead reach .	21
1.9	Member of the Focus Group wearing the UB-AXO.	22
1.10	Human-Exoskeleton Model in AnyBody Modelling Systems . .	23
2.1	Scope of work for the PhD study.	27
6.1	Conceptual design of the UB-AXO	84
6.2	Admittance based control strategy for UB-AXO	85
6.3	General application of the admittance based control strategy .	90

List of Tables

1.1	Overview of passive upper body exoskeletons	9
1.2	Overview of active upper body exoskeletons	16
1.3	Characteristics of end-user questionnaire study participants . .	19
1.4	Highest priority body motions	20
1.5	Motion study activities conducted in laboratory settings.	20

Nomenclature

The important and non-trivial abbreviations and nomenclature used in this thesis are presented in the following. Conventional calculus and linear algebra notations, as well as the metric system are used throughout the thesis.

Abbreviations

3R	Three-Revolute Joints
4R	Four-Revolute Joints
AAL	Ambient Assisted Living
ADL	Activities of Daily Living
cHRI	Cognitive Human-Robot Interaction
DC	Direct Current
DOF	Degrees-of-freedom
DPL	Double Parallelogram Linkage
DPM	Double Parallelogram Mechanism
E-EF	Elbow Extension & Flexion
E-PS	Elbow Pronation & Supination
EEG	Electro-Encephalography

EMG	Electro-Myography
FB	Full-Body
FB-AXO	Full-Body AXO-SUIT exoskeleton
FEA	Finite Element Analysis
FMG	Force-Myography
FEM	Finite Element Method
GH	Glenohumeral
HRI	Human-Robot Interaction
LB	Lower-Body
LB-AXO	Lower-Body AXO-SUIT exoskeleton
MMA	Maximum Muscle Activity
MVC	Maximum Voluntary Contraction
pHRI	Physical Human-Robot Interaction
PID	Proportional, Integral, Derivative
PMA	Pneumatic Muscle Actuators
RC	Remote Centre
ROM	Range-of-motion
RPW	Rating of Perceived Exertion
S-AA	Shoulder Abduction & Adduction
S-ED	Shoulder Elevation & Depression
S-EF	Shoulder Extension & Flexion
S-IE	Shoulder Internal & External Rotation

S-PR	Shoulder Protraction & Retraction
SEA	Series Elastic Actuators
SMA	Shape Memory Alloy
UB	Upper-Body
UB-AXO	Upper-Body AXO-SUIT exoskeleton
VSA	Variable Stiffness Actuators
W-EF	Wrist Extension & Flexion
W-RU	Wrist Ulnar & Radial Deviation

Greek Symbols

θ	Joint Angle	[rad]
μ	Manipulability index	[-]
τ	Torque	[Nm]
ϕ	Offset Angle	[rad]
ω	Rotational speed or velocity	[rad/s]

Latin Symbols

A	Area	[m ²]
f	Force	[N]
L	Length	[m]
m	Mass	[kg]
p	Pressure	[Pa]
v	Linear speed or velocity	[m/s]
V	Voltage	[V]

Chapter 1

Introduction

1.1 Background and Motivation

This research project, part of the AXO-SUIT project [1], funded under the Ambient Assisted Living (AAL) Joint Programme Call 6, focuses on supporting occupational work and daily activities of elderly persons by developing assistive devices (exoskeletons) designed to comfortably fit the human body and actively help the wearer. The project brings together three universities and five companies that are active and experienced in R&D of assistive devices. The objective of the project is to develop a portable and modular full body exoskeleton to assist the elderly in their daily living—see Figure 1.1. Aalborg University was the project coordinator and led the development of the upper body exoskeleton (assisting the shoulder and elbow complex) named UB-AXO, to which the research area of this PhD project is assigned.

Today's problems of an ageing population affect both individuals and society as a whole. At the individual level, natural ageing causes degradation in personal mobility and handling capabilities and a loss of independence. Studies have shown that a key issue for the elderly to maintain their quality of life is to keep their personal functional ability [2]. After retirement, most elderly persons are still healthy but occasionally lack the physical endurance to continue their activities at home, in the garden or during social events. By wearing robotic assistive devices, such as exoskeletons, that supports motor functions, like walking or lifting objects, elderly persons are able to move around more easily, reach for objects and manipulate them to perform various physical tasks [3–5]. This type of exoskeleton can be categorised as a medium-duty exoskeleton¹, as it is supposed to assist the human limb(s) and

¹A light-duty exoskeleton would be able to assist the human limb alone or to carry a light object, while a heavy-duty exoskeleton would be able to amplify human strength.

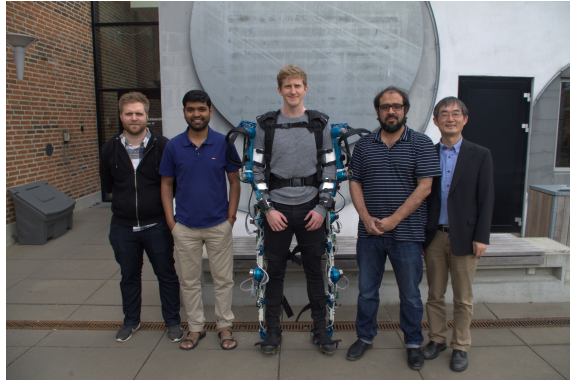


Fig. 1.1: Full body exoskeleton (FB-AXO) developed in AXO-SUIT project.

provide support for a substantial load (approx. 5 kg) to be manipulated. The need for assistance with these tasks might not necessarily be for the entire body. For that reason, modularity is included in the design of the AXO-SUIT exoskeleton.

Determining the needs and requirements is of key importance for any system development, including exoskeleton designs. However, designing a system that achieves the required technical performance is not sufficient; technology acceptance is equally important [6–8]. Providing comprehensive modular support implies that a high number of DOFs should be complemented, which may lead to a bulky and heavy design that is not ideal for wearable devices. As a result, such conspicuous solutions may not be acceptable to the end-user [7, 8]. Thus, adopting a user-centered design approach, where the end-user is involved in the design phase at an early stage, could contribute to user acceptability of the technology.

Musculoskeletal modelling could be used to perform simulation-based designs using bio-mechanical models of the upper extremity and a mechanical model of the exoskeleton. Starting from an early conceptual design and progressing to detailed designs, the models can be used to assess the performance of the exoskeleton and iterate the design before manufacturing physical prototypes. Obviously, this method requires knowledge of the task(s) the exoskeleton has to solve.

Thus, this PhD research aims to develop a modular assistive upper body exoskeleton that helps elderly persons to do everyday tasks and stay active by using an user-centered design approach and biomechanical modelling.

1.2 Brief Introduction to Exoskeletons

The exoskeleton is a technology within the field of wearable robotics. In general, a wearable robot can be defined as a technology that is capable of either extending, complimenting, substituting or even enhancing its human user [9, 10]. In this context, the wearable robot can be a substitution to the human limb(s) or act as an extension to the human body. Exoskeletons or powered orthosis are mechanical devices that are worn by a human user. Typically, the term "orthosis" describes a device that is used to assist a wearer with a limb impairment or disability, while "exoskeleton" describes a device that augments able-bodied wearers [9, 11].

Research on exoskeletons dates back to the 1960s, when General Electric Co. developed the hydraulically-powered Hardiman exoskeleton for the US Army/Navy, shown in figure 1.2. The suit was able to augment the strength of its operator with a maximum lifting capability of 1,500 pounds (~680 kg). The Hardiman exoskeleton was actually two exoskeletons in one. The inner exoskeleton was attached to the operator, while the external exoskeleton carried the objects. Hence, the suit had a robotic master-slave configuration. Due to its large weight, control complexity and power issue, the Hardiman remained at the prototype level [12].

In 1990, Kazerooni [13] presented the concept of "extenders" or "body extenders", where the master-slave configuration is replaced with a direct physical interaction between the exoskeleton and its human operator. With this concept, the operator becomes an integrated part of the exoskeleton, feeling a small portion of the load carried by the exoskeleton.

From the early of 2000s, research in exoskeleton-type systems has truly exploded with systems such as Body Extender [14], BLEEX [15], ONYX [16], XOS2 [17], MIT [18], EKSO [19] and HAL-5 [20]. These newly developed exo-



Fig. 1.2: General Electric's Hardiman Exoskeleton



Fig. 1.3: Examples of state of the art exoskeletons; (a) Body Extender [14] (b) BLEEX [15] (c) ONXY [16] (d) XOS2 [17] (e) EKSO [19] and (f) HAL-5 [20]

skeleton technologies possess a wide range of applications such as military, industry, medical for rehabilitation, commercial and even sport.

To design a portable, comfortable and well-performing motion assistive exoskeleton, it is necessary to consider the kinematics and kinetics the human body. The upper extremity, i.e., the human arm, is constructed for high dexterity. The majority of the muscles groups are placed proximally with respect to the joints, such that the articulated mass and inertia are minimised, e.g. the elbow joint is articulated by muscles in the upper arm. Excluding the hand, the upper body (from shoulder and out) comprises nine main DOFs. There are five DOFs at the shoulder (three DOFs at the glenohumeral joint, and two DOFs at the sternoclavicular), two DOFs at the elbow joint and two DOFs at the wrist joint—illustrated in Figure 1.4. Hence, the exoskeleton for the upper body, should complement these properties, through its kinematic and kinetic design.

Kinematic compliance or compatibility is achieved this by matching the kinematics of the human limbs [9]. Since the exoskeleton is worn by the operator, the device is attached to the arm segments, i.e., upper arm and forearm, and a base, typically the trunk or waist. As a result, there is a direct map-

1.2. Brief Introduction to Exoskeletons

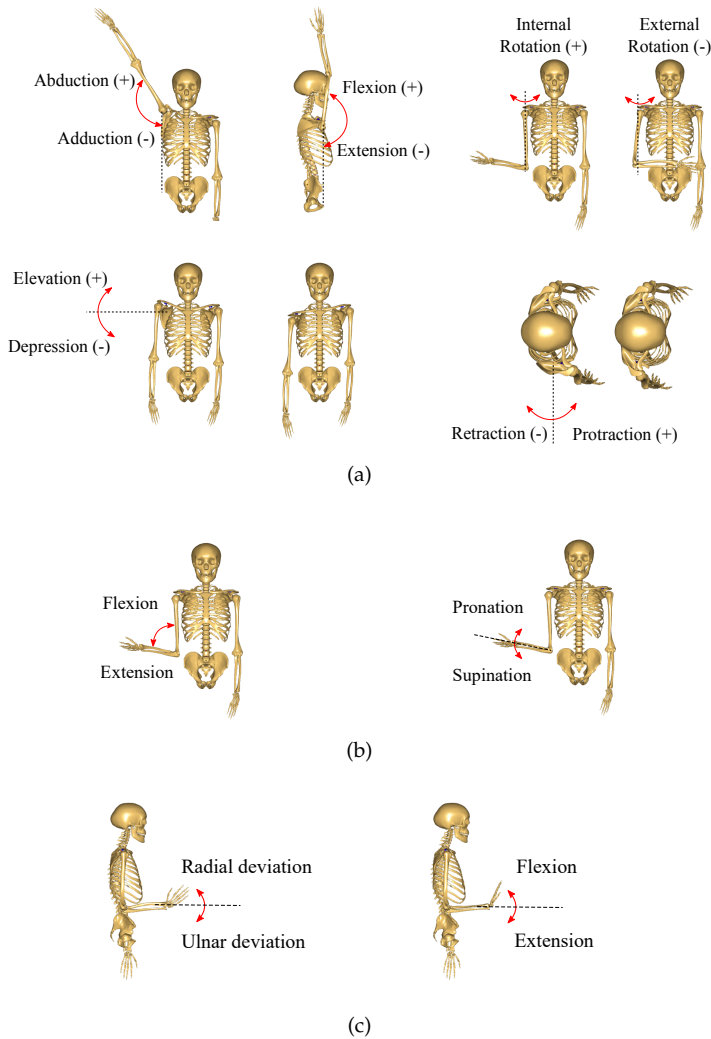


Fig. 1.4: The degrees-of-freedom (DOFs) in the human upper extremity, i.e., (a) shoulder, (b) elbow and (c) wrist.

ping between the exoskeleton joints and the anatomical joints of the human. Typically, this means that the exoskeleton acts in parallel with the human limbs. Note, that it is not strictly required for an assistive device to span all DOFs of the human to be functional. The only requirement is that the exoskeleton joint complies with the respective anatomical joints of the user to avoid potential discomfort and harm. Discomfort arises from undesired internal forces due to axis misalignment between the human to exoskeleton

joint axis [21, 22]. It is, however, desirable for exoskeletons to span the entire anatomical workspace, as this leads to unhindered movements of the user. In addition to the anatomical joint, the exoskeleton also has to adapt to the different size of the operators, i.e., length and width of body segments.

Aside from the kinematics, interaction between the human and exoskeleton can be characterised by how the forces or power is transferred between the two systems. The concept of power transfer depends on the purpose of the exoskeleton. Pons et al. defined the force/power interface as either an *external force system* or *internal force system* [9].

For external force systems, the environmental loads are transferred through the mechanical structure of the exoskeleton to the ground. Hence, the loads and weight of the exoskeleton bypass the human. For such systems, the exoskeleton does not have to act strictly parallel with the human limbs but can have a nonanthropomorphic structure, where the joints of the robot do not align with the anatomical joints. Hence, the designer is less limited in the mechanical functionalities for the exoskeleton but with the drawback of more bulky designs [14, 17, 23]. Note that the external force system exoskeleton is commonly used for stationary exoskeletons in rehabilitation, which require a large number of DOFs but do not have strict limitations on weight and volume. Examples of such exoskeleton robots include ARMin III (6-DOF) [24], CADEN-7 (7-DOF) [25–27], MEDARM (6-DOF) [28] and Armeo©Spring (6-DOF) [29].

For internal force systems, the exoskeleton is not grounded. Instead, the force and power is transmitted between the body segments through the exoskeleton. Upper-body exoskeletons are internal force systems, as they transfer loads from the upper arm and/or forearm to the trunk. A consequence of this is that the human has to carry the full weight of the exoskeleton. The total weight of the exoskeleton is therefore a limiting factor in the design of these systems. This often leads to designs with a few assisted DOFs, as most of the weight of the exoskeleton is related to the force-/power-providing elements of the device [30].

1.3 State-of-the-art in Upper Body Exoskeletons

In the recent decades, several upper body exoskeletons have been developed, some of which have become commercially available, while others remain research prototypes. This section outlines the state-of-the-art of upper body exoskeleton designs and the design approach utilised in their development. Besides field of application, exoskeletons are frequently classified based on the force/torque transferring joint in the devices. In the literature, two main groups are used: passive and active exoskeleton [3, 30–36]. Passive exoskele-

tons utilises mechanical elements, such as springs, to compensate for external loads acting on the arm segments. Active exoskeletons are externally powered elements, i.e., actuators. It is also worth mentioning a third group, which is the truly passive joint. This joint is not driven by the exoskeleton but by the human operator. Hence, the joint is not an assistive joint but one that is introduced for increased ROM or as a self-aligning mechanism for improved kinematic compliance [37, 38]. The obvious drawback of this is, of course, that the human operator must use effort to drive the joint. Some exoskeletons utilise a combination of one or more of the three types of joints. In this state-of-the-art review, these types of exoskeletons are considered as active exoskeletons. Finally, all the exoskeletons reviewed are portable devices, meaning they can be carried by the user and do not require a mobile/stationary platform.

1.3.1 Passive Upper Body Exoskeletons

The passive upper body exoskeletons utilise mechanical elements to store potential energy that is then used to augment the strength of the user. Typically, elastic elements, such as tensional springs or rubber bands, are used to store the potential energy in the exoskeleton [3, 39], however, counterweights can in principle also be used. For an upper body exoskeleton, this option has been disregarded as it adds weight, volume and inertia to the system, which compromises the wearability of the device². In general, the passive upper body exoskeleton systems utilise a gravity-balancing principle like the one presented in [40], to reduce or remove the gravitational load of users' limb and/or an object manipulated by the user.



Fig. 1.5: Examples of passive upper body exoskeletons; (a) CDYS [41] (b) WREX [39] (c) ROBO-MATE [42]

²In passive lower body and full body exoskeletons used for lifting heavy tools, counterweights are used to keep the operator steady. In this case, the additional inertia causes less of a concern for wearability, as the weight of the exoskeleton and tool is directly transferred to the ground.

An overview of some the state-of-the-art passive exoskeletons is listed in Table 1.1 including their concepts of operation. The majority of the passive exoskeletons are targeted industrial applications and designed to support the upper arm (i.e., shoulder joint) during overhead activities, such as the Ekso EVO [43], PAEXO Shoulder [44, 45], ShoulderX [46, 47] and Skelex360-XFR [48, 49]. Nevertheless, some of the passive industrial exoskeletons are designed to support activities below shoulder height. These systems are typically attached to the forearm to elevate the entire arm (i.e., shoulder and elbow joints) like the ROBO-MATE [42, 50, 51], Shiva EXO [52] and ARMOR-MAN [53]. Commonly, these devices are not designed to enhance the strength of the user but to reduce fatigue by decreasing the stress on the arms and prevent work-related musculoskeletal disorders caused by manual handling tasks [54, 55].

In general, the passive upper body exoskeletons provides support to the user by transferring the load from the upper arm or forearm to the trunk through an anthropometric structure. Hence, they only utilise two anchor points on the user. For designs that supports the shoulder, a serial linkage structure is typically used, which can be kept fairly compact as the kinematic chain is kept relatively short (trunk to upper arm), as illustrated with the CDYS exoskeleton in Figure 1.5(a). For devices that support both the shoulder and elbow joint (trunk to forearm), the serial linkage chain is replaced with an auxiliary parallelogram structure, as illustrated with the WREX and ROBO-MATE exoskeletons in Figures 1.5(b) and 1.5(c), respectively. The use of parallelogram structures contributes to a bulky design, as the distance between the two anchor points is made longer. Hence, to maintain a large ROM and avoid collisions between the exoskeleton and user, the design becomes bulky [3].

Some passive exoskeletons utilise more than two anchor points between the exoskeleton and user to give more comprehensive support. These are typically used for medical application, where joint level assistance is required. An example is the AAU cable-driven exoskeleton developed at Aalborg University [56–59]. This exoskeleton does not have a serial architecture; instead, it is composed of three elements: a body armour, an upper- and lower elbow bracket and a spring box. A total of five springs are mounted in the spring box to store the elastic potential energy and compensate the weight of the upper arm and forearm, separately. A cable is attached to each spring to distribute the load from the elbow mechanism to the spring box, which is placed at the lower back of the wearer. Three of the cables are connected to the upper elbow bracket (assisting the shoulder joint) and two to connect the lower elbow bracket (assisting the elbow joint).

1.3. State-of-the-art in Upper Body Exoskeletons

Table 1.1: Overview of passive upper body exoskeletons with technical specifications

Exoskeleton Name	Application	Weight [kg]	Points of Attachment	Concept of Operation
EksoEVO [43, 60]	Industrial	6.5	Trunk and upper arm	Assisting elevation of upper arm using a passively actuated torque mechanism that gradually increases assistance over head
PAEXO Shoulder [44, 45]	Industrial	1.9	Trunk and upper arm	Passively actuated cable pulley mechanism to support overhead activities
Skelex360-XFR [48, 49]	Industrial	2	Trunk and upper arm	Passively actuated cable driven mechanism
ShoulderX [46, 47]	Industrial	3.17	Trunk and upper arm	Supports the shoulder in chest to ceiling level tasks using a cam based cable driven passive mechanism
ROBO-MATE [42, 50, 51, 61]	Industrial	2.3	Trunk and forearm	Assists the entire arm using a two-segment parallelogram structure with tensional steel springs bands
AIRFRAME [62, 63]	Industrial	2.7	Waist and upper arm	Supports the shoulders at chest level and above using a patented technology comprised of a spring-cable-pulley system
BESK [64]	Industrial	3.5	Trunk and Upper arm	Supports the user's upper arms to maintain proper postures and lighten loads for repetitive tasks in either horizontal positions or overhead positions using passively actuated serial linkage system
CDYS [41]	Industrial	2.4	Waist and upper arm	The shoulder is supported during overhead activities using at adjustable spring loaded cable system at the located at the waist
Exy ONE [65]	Industrial	3.55 to 4.3	Trunk and upper arm	The shoulder is assisted in four levels using a passive mechanism
LIGHT [66]	Industrial	2.9	Trunk and upper arm	Support of shoulder movements for overhead activities with a passive mechanism
MATE-XT [67]	Industrial	3	Trunk and upper arm	Supports shoulder flexion movements using a passive spring-based mechanism for in- and outdoor occupational activities
PLUM [68]	Industrial	1.5	Trunk and upper arm	Support of shoulder movements during overhead activities
Shiva EXO [52]	Industrial	-	Thigh, trunk, upper arm and forearm	Supports the back/hip and shoulder for pick-and-place operations and overhead work using fiberglass springs designed to provide an iso-elastic thrust at the arm
Armor-Man [53]	Commercial	14.7	Trunk and Forearm or Hand	Supports the elevation of the arms using a spring loaded parallelogram linkage system that either connects directly to a tool (camera gimbal) or the forearms

Table 1.1: Overview of passive upper body exoskeletons with technical specifications (cont.)

Exoskeleton Name	Application	Weight [kg]	Points of Attachment	Concept of Operation
WREX [39, 69–71]	Medical	-	Base or trunk and forearm	Assists the upper arm and forearm using a two-segment parallelogram structure with elastic bands
AAU Cable-Driven Exoskeleton [56–59]	Medical	-	Trunk, upper arm and forearm	Assist the upper arm and forearm separately using five tensional springs connected to an elbow bracket
EksoUE [72]	Medical	-	Trunk, upper arm and forearm/wrist	Supports both shoulder and elbow using spring loaded joints in a serial linkage system

1.3.2 Active Upper Body Exoskeletons

Compared to the passive exoskeletons, the active exoskeletons can provide higher force augmentation and can assist as needed by use of control. The key advantage of the active exoskeleton over the passive is their ability to supply the wearer with additional power using actuators. An overview of some the state-of-the-art active exoskeletons is listed in Table 1.2 including their supported movements and concepts of operation. For the supported movement, the number of active and passive joints are typically highlighted together with the respected movement denoted with joint and anatomical motion, e.g., **S-FE**. The following notations are used:

Joint notation:

S = Shoulder
E = Elbow
W = Wrist

Anatomical motion notation:

ED = Elevation & Depression
PR = Protraction & Retraction
AA = Abduction & Adduction
EF = Extension & Flexion
IE = Internal & External Rotation
PS = Pronation & Supination
RU = Ulnar & Radial Deviation

The actuators are either placed locally at the specific joints or stored at the back, where the force/torque is transmitted via cables from the trunk. The majority of the exoskeletons in Table 1.2 use locally placed actuation, due to its simplicity and ease of control. When the actuators are placed locally at the joints, the mass of the distal actuators has to be supported by the proximal actuators. As a result, this accumulative effect leads to a need for high force/torque capacity for the proximal actuators. To address this issue, some designs include passive gravity compensating support mechanisms, such as the Stuttgart Exo-Jacket [74, 76], EduExo Pro [77, 78] or Mobile Wearable

Upper-Limb Exoskeleton [79, 80].

Distal placed actuators, using cable driven transmission or serial-linkage systems, require less force/torque capacity, compared to the direct drive actuators, as they only carry the weight of the mechanical structure of the exoskeleton. Moreover, this concept benefits from a more compact design with actuators being "hidden" at the torso, like the Muscle Upper [81–83], Parallel Actuated Exoskeleton [84], CRUX [75, 85, 86], Soft wearable exosuit [87, 88] and Soft Exosuit [89]. The last three examples are so-call "soft" exoskeletons or exo-suits [34], where the mechanical structure of the exoskeleton is replaced with soft-couplings to the human, such as braces or straps. Hence, these devices pose fewer kinematic constrains for the user compared to the "hard" exoskeletons. However, the cable-drive transmissions via bowden cables are generally more complex than the direct-drive in terms of routing, additional moving parts and increased friction in the tubes.

The majority of active exoskeletons are electrically actuated, due to the high speed, high accuracy and advanced motion control provided by electric motors [4]. However, some devices uses pneumatic actuation, typically in the form of a Pneumatic Muscle Actuators (PMA), such as Muscle Upper [81–83]. The PMA have similar actuation as a human muscle, meaning they can only preform one-way actuation. Their lightness, good power/weight ratio and flexible structure make them desirable for portable exoskeletons. Namely, the flexible/compliance structure is an advantage over the electric motors, as they lead to a safe human–robot interaction and comfortable exoskeleton [90]. On the other hand, the PMAs exhibit a highly non-linear behaviour, which makes them more complicated and in general less accurate

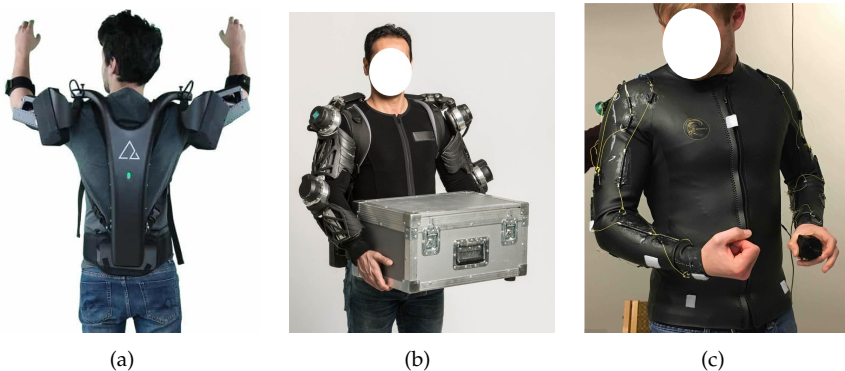


Fig. 1.6: Examples of active upper body exoskeletons; (a) AGADEXO [73] (b) Stuttgart Exo-Jacket [74] (c) CRUX [75]

than the electric motors, and they require an air-compressed tank to be truly portable [35, 90]. Electric actuators can exhibit compliance through advanced control, such as impedance control. This approach has shown success, but it adds another layer of complexity to the control [91]. Mechanical/passive compliant actuation can also be achieved for electric motor by including a spring in the design, as seen with the Series Elastic Actuators (SEAs) used in AGADEXO [73, 92]. Since SEAs have a constant stiffness, the dynamic performance is limited and the stiffness property has to be set as a trade-off between the required bandwidth and torque resolution. To overcome this problem, Variable Stiffness Actuators (VSA) have been introduced [93, 94]. The basic concept of VSAs is to add a second actuation that makes it possible to change the compliance and hence the bandwidth of the actuation.

Electric motors are combined with a geared transmission to achieve a lighter design and good power/weight ratio. On the other hand, gears tend to introduce resistance in the transmission, which then affects the backdrivability of the system. Backdrivability is a measure of how easily a torque or force on the output axis drives the input axis and thus the motor. Certain gears, like worm gears, are not backdriveable, meaning the output shaft cannot drive the input shaft. Such gears are not ideal for exoskeletons, as the joint becomes locked if power is cut to the motors. Hence, backdrivability is a critical design criterion for exoskeletons. A harmonic drive gear [95] is a gear reducer commonly used in robotic mechanisms and known for their high gear ratio, compact design and backdrivability [9]. The harmonic drive gears are used in the Stuttgart Exo-Jacket, HAL Single Joint, UMI and more.

Since active exoskeleton utilise actuators, they also require a form of power supply, sensors and controllers. The control problem for exoskeletons is two-fold. The first problem is sensing the user's intention to move, and the second problem is to convert that intention into assistive interactive motion [91, 96]. The acquisition of the user intention can generally be identified by measuring the interaction between the exoskeleton and human [9, 91]. The decision-making of a human is performed through cognitive processes that are based on information about their surroundings, which are acquired through various senses (visual, tactile and auditory). When a human cooperates with an exoskeleton robot, this cognitive processes is influenced by the robot and vice versa, the motion of the robot is influenced by the cognitive process of the human. This is referred to as human-robot interaction (HRI) [9, 11, 91]. From a control aspect, the human and the exoskeleton, as a human-robot cooperation system, form a closed loop system. Depending on the measurement method of the HRI, the exoskeleton is either based on a cognitive human-robot interaction (cHRI) or a physical human-robot interaction (pHRI). The cHRI-based control system measures common electric signals from the central nervous system to the mus-

culoskeletal system of humans and uses them as inputs for the exoskeleton control, such as electro-encephalography (EEG) [97, 98], electro-myography (EMG) [20, 78, 92, 99, 100] or force-myography signals (FMG) [101–104]. Both EEG and EMG are techniques that extract electrical signals using electrodes on the human body, where EEG tracks the electrical activity of the brain by placing the electrodes on the skull, and EMG records the electrical impulses generated by muscle activity by placing the electrode on the muscles. FMG is a technique that measures force or pressure change resulting from muscular bulging during muscular contraction. With cHRI, the human intent is identified before the occurrence of the actual motion of the user and the required torque/velocity/position for the motion of human joints can subsequently be predicted [23, 91, 105]. On the other hand, the pHRI-based control system measures the force [38, 76, 88, 106] or motion [80, 84, 107–109] changes that are the results of the motions by the human musculoskeletal system, which is then used as inputs to the exoskeleton control. Other techniques include manual inputs, such as joystick [75], breach operated switch [83] and voice commands [89].

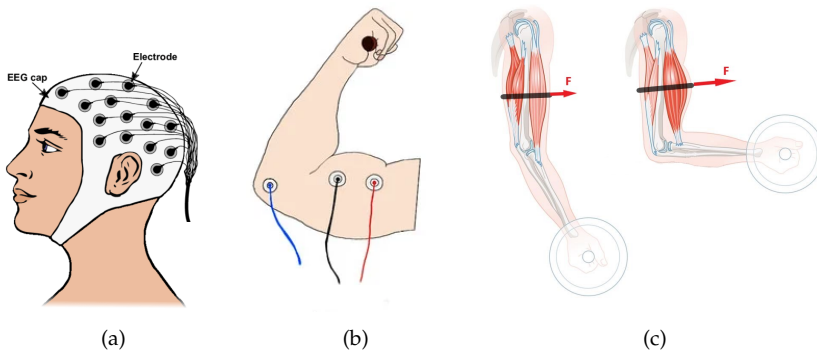


Fig. 1.7: Examples of acquisition of the user intention through; (a) electro-encephalography (EEG) [97] (b) electro-myography (EMG) [92] (c) force-myography (FMG) [101]

Concerting user intention into motion is achieved through interaction controllers. From a control aspect, the exoskeleton and human user together form a closed loop. Hence, both the user and the exoskeleton must be considered, when developing controllers for the exoskeleton system. Most commonly, the interaction controller are in form of either impedance or admittance controllers [96, 110], however, there are also examples of hybrid force/position controllers [9, 105].

The concept of impedance/admittance control was introduced by Hogan et. al. [111, 112] in the 1980s for robotic manipulators and their interaction with the surrounding environment, e.g., welding or assembly robots.

Mechanical impedance is defined as a body's resistance to motion when subjected to a harmonic force, and it is given as the ratio of velocity to force [111]. The inverse of the impedance is admittance. The general idea of "impedance/admittance control" is to regulate the robot's dynamic behaviour at its ports of interaction with the environment. The interaction port is defined as a location, where energy may be exchanged between the robot and its environment. Hence, the strategy with impedance/admittance control is to specify a dynamic relationship between motion and force at the port of interaction and implement a control law that minimises the deviation from this relationship [113, 114].

Only a few active exoskeletons are commercially available, like the Muscle Upper from Innophys [81], AGADEXO from AGADE [73] and HAL Single Joint from Cyberdyne [115]. Similar to the passive devices, they are developed and used for industrial applications. Notably, these commercial devices do not support the entire arm but only a single DOF in the upper body, i.e., shoulder or elbow. The AGADEXO, short for Anti-Gravity Active Device for Exoskeletons shown in Fig. 1.6(a), uses a SEA to support shoulder flexion/extension. The shoulder abduction/adduction and internal/external rotation is achieved through a single passive joint and the cuff on the upper arm. The cuff only imposes a cylindrical type of kinematic constraint, meaning the upper arm can rotate freely in the cuff. This simplifies the structural design of the exoskeleton but with the cost of not knowing the configuration of the human arm directly from the exoskeleton. Like its passive counterparts, such as CDYS or PAEXO Shoulder, the AGADEXO supports gravitational loads. However, unlike the passive devices, AGADEXO can turn the assistance on and off autonomously using a bracelet on the forearm that senses if the user is carrying an object. Using this input, the interaction controller of the exoskeleton transitions between a transparent and assistive mode, thus providing assistance as needed [73]. This is one of the main advantages of the active exoskeletons over the passive as they have an enhanced possibility for various applications through software control. However, with a weight of 4 kg, the AGADEXO is nearly twice as heavy as CDYS and PAEXO.

In general, the active upper exoskeletons are used to compensate for gravitational loads carried by the user (Table 1.2) either for a single joint, e.g., elbow flexion/extension, or joint complex, e.g., the shoulder. A few devices provide more comprehensive support for the shoulder, elbow and/or wrist, such as the Mobile Wearable Upper-Limb Exoskeleton [79], UMI [108] and CRUX [75], illustrated in Fig. 1.6(c). All of these devices are used for rehabilitation and are only designed to support the weight of the arm; hence, the actuation can be designed lighter compared to the devices for industrial application. Since these devices provide support at joint level kinematic compliance becomes more complex to achieve—particularly for the shoulder

complex. Whereas single joint exoskeletons can utilise the cuffs to achieve kinematic compliance, these devices have to realise it with the exoskeleton itself. The shoulder glenohumeral joint behaves as a hollow ball-and-socket joint; hence, the shoulder mechanism must be designed with a remote centre-of-rotation, that replicates the three rotational DOFs. The most common solution to solve this problem is using a series of curved linkages that are connected by revolute joints. The simplest form of this design is using three revolute joints, also referred to as 3R joints. Typically, the axis of rotation are perpendicular to each other, such that they form a gimbal mechanism [26, 28, 116]. However, these devices have limited workspace due to singular configurations and/or links colliding with the wearer. Alternative solutions to these issues have been proposed, such as designing the mechanism with its singular configurations at postures that are less likely for the wearer to reach [117] or using redundant linkages (i.e., a 4R mechanism) [118]. Alternative designs have been proposed, such as the CXD (short for Compact X-scissors Device), which is a curved spherical scissors linkage mechanism [119]. This design stands out from the 3R mechanisms, as it is free of singularities within its workspace and compactness. However, due to the scissor-type structure, all three rotational DOFs are coupled, which adds complexity to the actuation.

The Stuttgart Exo-Jacket [74, 76, 120] is a notable medium-duty upper body exoskeleton. The device is designed for industrial logistics and montage applications that either require a stabilization of the arm during assembly tasks or a force boost in logistics tasks [74]. The exoskeleton can actively support the abduction/adduction and flexion/extension of the shoulder and flexion/extension of the elbow joint. Additional nine passive DOFs are introduced to complement the remaining DOFs of the shoulder and elbow and micro-misalignment between human arm joints and exoskeleton joints. One of the passive DOFs includes a gas-spring mechanism to support shoulder girdle movements (shoulder elevation/depression—see Fig. 1.4). The shoulder and elbow joints generate 40 Nm and 25 Nm, respectively. However, the total weight of the Stuttgart Exo-Jacket is unknown from literature.

Table 1.2: Overview of active upper body exoskeletons with technical specifications

Exoskeleton Name	Application	Weight [kg]	Points of Attachment	Supported Movements	Concept of Operation
AGADEXO [73, 92]	Industrial	4	Trunk and upper arm	1-Active (S-FE) 2-Passive (S-AA & S-IE)	The device uses a bracelets on the forearm to detect payloads in the hand and transition between a transparent mode and assistive mode. A Hybrid SEA is used to vary the level of assistance to the user
Muscle Upper [81–83]	Industrial	8.1	Hip, trunk and hand	2-Active (Hip and arm)	A breath-operated switch is used to control the device to disable and enable a gravity offloading control. A total of 4 PMA also referred to as McKibben artificial muscle are used to support hip flexion and arm elevation at the hand. The suit is powered using an external compression not worn by the user
Stuttgart Exo-Jacket [74, 76, 120]	Industrial	-	Trunk, upper arm and forearm	3-Active (S-AA, S-FE & E-FE) 9-Passive (S-ED, S-IE, E-PS & five alignment joints)	Force sensors in the users gloves are used to detect a load and a force controller is used supply assistance. The three active joint are composed by direct-drive using DC motors and harmonic gears. Moreover, some of the passive joints are equipped with spring mechanism for weight compensation of the device
Soft Exo-suit [89]	Industrial	~10	Trunk, upper arm and forearm	2-Active (shoulder and elbow flexion) 2-Passive (S-AA & S-IE)	A voice-based controller is used to initiate a gravity compensation control. DC-motors with a cable-pulley transmission supports shoulder and elbow flexion movements. Bowden-cables are use to route the cables to two anchor points on the elbow module. The elbow module is mechanically decouple from the trunk module, thus allowing unconstrained S-AA and S-IE movements
HAL Single Joint [20, 104, 115]	Commercial	1.5*	Upper arm and forearm	1-Active (E-FE)	The HAL single joint is a module of the full body HAL exoskeleton. EMG signals are used to detect the user intention on the upper arm. The elbow joint is powered with a DC motor
EduExo Pro [77, 78]	Commercial	5.2*	Trunk, upper arm and forearm	1-Active (E-FE) 2-Passive (S-FE & S-IRE)	EMG sensors on the upper arm is used to detect motion of the elbow joint. The joint is powered by a direct drive DC motor with position and force feedback. A torsional spring in the S-FE joint compensates for the weight of the E-FE joint

* Single arm only

1.3. State-of-the-art in Upper Body Exoskeletons

Table 1.2: Overview of active upper body exoskeletons with technical specifications (cont.)

Exoskeleton Name	Application	Weight [kg]	Points of Attachment	Supported Movements	Concept of Operation
Elbow Exoskeleton [99]	Commercial	>1*	Upper arm and forearm	1-Active (E-FE)	EMG sensors on the upper arm are used to detect the intention of the user which is feed to an impedance controller. DC motor with cable-pulley transmission are used to power the elbow joint
SMA Exoskeleton [107, 121]	Medical	>1*	Upper arm and forearm	2-Active (E-FE & E-PS)	The active joints are actuated with four SMAs (Shape Memory Alloy) in antagonist movement, each with a PID controller for position control
MyoPro [100, 122]	Medical	-	Upper arm, forearm and hand	2-Active (E-FE & Hand) 1-Passive (W-FE)	EMG signals from the upper arm are used to drive the elbow joint using a DC servo motor, while EMG signals in the forearm is used to assist hand grasping
Mobile Wearable Upper-Limb Exoskeleton [79, 80]	Medical	4.2*	Trunk, upper arm and forearm	4-Active (S-FE, S-IE, E-FE & E-PS) 1-Passive (S-ED)	IMU sensors are used to adopt a gravity compensation control strategy. The active joints are powered by DC motors and either cable-drive or belt-drive transmissions. The passive joint is a gravity balancing mechanism using a spring loaded parallelogram
UMI [108, 123]	Medical	-	Trunk, upper arm and hand	4-Active (S-AA, S-IE & S-FE) 3-Passive (S-RD, S-ED & E-FE)	The UMI follows a predefined trajectory for user to follow using a position based adaptive sliding mode control law. The active joints are powered using direct drive DC motors and gearing
RUPERT [109, 124]	Medical	0.63*	Trunk, upper arm and forearm	4-Active (Shoulder flexion, elbow flexion and supination and wrist extension)	Impedance based control using position feedback is used to determined the level of assistance required for the user to follow a trajectory. A total for four PMAs are used to supply one-way actuation to the users
CRUX [75, 85, 86]	Medical	1.3*	Jacket with six anchor points for cable-drive	3-Active (S-AA**, E-FE & W-PS)	The CRUX (Compliant Robotic Upper-Extremity Exosuit) is a soft exoskeleton***, that utilises 6 cable-driven mechanism with DC motors and bowden holsters to drive the respective joints using paired antagonistic anchor points. The suit is control manually using a two-axis analog joystick

* Single arm only

** Only shoulder abduction is supported

*** Soft exoskeletons distinguish from "hard" exoskeleton by not relying on a mechanical structure. Instead, they only rely on the anatomical joints and limbs

Table 1.2: Overview of active upper body exoskeletons with technical specifications (cont.)

Exoskeleton Name	Application	Weight [kg]	Points of Attachment	Supported Movements	Concept of Operation
Parallel Actuated Exoskeleton [84]	Medical	4*	Trunk and upper arm	2-Active (S-AA & S-IE) 4-Passive (S-FE & alignment joints)	Trajectory based impedance control is used to actuate two DC motor based SEA in a parallel mechanism. The actuators are placed remotely on the back to obtain a compact design. The shoulder flexion/extension is supported with a gravity balancing mechanism based on a steel tension spring and a parallelogram structure
Upper limb exoskeleton [102, 103]	-	-	Trunk, upper arm and forearm	2-Active (S-FE & E-FE) 5-Passive (S-PR & S-AA)	The intention of the user is determined using a FMG type sensor that measures the bulking of the upper arm. The two active joints are driven by direct-drive DC motors using Harmonic Gears
Soft wearable exosuit [87, 88]	-	-	Trunk, upper arm and forearm	1-Active (E-FE)	An admittance based controller is used to provide a position dependent force profile to assist gravitational loads. The elbow joint is driven by an electric motor through a Bowden cable transmission anchored at two points

* Single arm only

1.4 User-Centered Design of AXO-SUIT

Determining the needs and requirements is of key importance for any system development, including exoskeleton designs. However, designing a system that achieves the required technical performance is not sufficient; technology acceptance is equally important [6, 7, 125, 126]. One of the notable passive exoskeletons, Wilmington Robotic Exoskeleton (WREX) [39, 69–71], was developed for children with limited muscle strength and can be mounted on both wheelchairs and the body using a back brace and attachments to the forearm. The development of the WREX included focus group meetings with approximately 20 participants [71], where needs and ideas were discussed and prototypes were tested. A similar approach was used for the Ekso EVO, which was developed in collaboration with end-users and physical therapists addressing the specific challenges of industrial applications [43]. However, there is limited, if any, literature available to describe this process. Nevertheless, the use of such user-centered design approaches has proven to lead to a higher acceptance of the technology [8].

A user-centered design approach was adopted throughout the development of the AXO-SUIT exoskeletons, which involves a review of end-users'

needs through questionnaire, focus groups and interviews, kinematic and kinetic motion study, expert reviews and useability and performance testing [125–127]. End-users were defined in three categories [125]:

Primary End-User are the person who will wear the AXO-SUIT exoskeletons.

Secondary End-User are persons or organisations who are in direct contact with a primary end-user. E.g., family members, friends, neighbours, care organisations etc.

Tertiary End-Users are institutions or organisations that are not directly in contact with the AXO-SUIT exoskeleton, but who somehow contribute in organizing, paying or enabling them. E.g., public sector service organisers, social security systems or insurance companies.

A range of methodologies were used to ensure that appropriate end-user input is obtained, e.g., questionnaires, focus groups and interviews. In the first stage, a questionnaire study was undertaken among end-users in each partner country [125]. For the second and third stages, end-user demonstration events/focus groups were undertaken to obtain feedback on AXO-SUIT designs and physical prototypes, as well as end-user opinions on matters relating to commercialisation.

Table 1.3: Characteristics of end-user questionnaire study participants (n=34).

Variable	Primary (n=31)	Secondary (n=3)
Age (years)	71 (59-86)	29 (27-29)
Gender (%females)	77.4%	66.6%
Height (cm)	165 (152-189)	170 (169-179)
Body Mass (kg)	72 (45-110)	60 (58-75)

The primary end-users prioritised for inclusion in end-user engagement activities were adults aged 50 years and over that only had mild or moderate limitations in their ability to perform activities of daily living (ADLs) [125]. A limited number of secondary end-users were also included. End-user requirements were established at the outset of the project, prior to commencing AXO-SUIT designs. Throughout the project, the requirements and designs were revisited to ensure that a user-centred focus was maintained. A total of 34 participants completed the questionnaire; 12 in Ireland, 6 in Sweden and 8 in Denmark. Table 1.3 summarises the characteristics of the sample from the questionnaire. The questionnaire content and methods are reported by O’Sullivan et. al. [125]. The questionnaire participants ranked the highest priorities for assistance for the lower body, upper body and full body motions, as listed in Table 1.4.

Table 1.4: Highest priority body motions ranked by questionnaire participants.

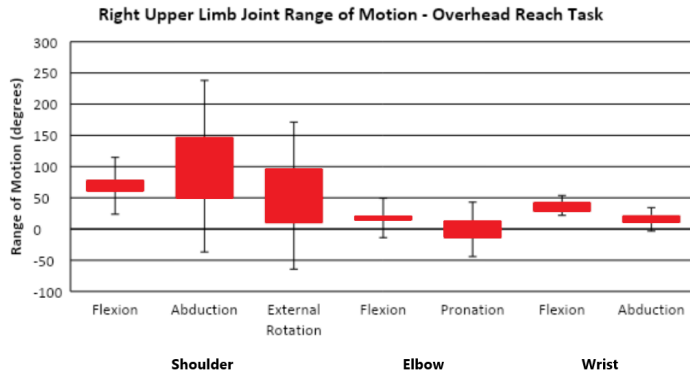
	Lower Body	Upper Body	Full Body
1	Sit-to-stand	Lifting/dropping without grasping	Getting up from kneeling
2	Walking and turning	Reaching to the side over-head/opposite shoulder	Getting up from squatted position
3	Standing	Carrying an object in front with both arms	Carrying small objects with one hand
4	Bending down to the floor	Pushing/pulling horizontally	Bending over/stooping to the floor/ground

The design implications and technical feasibility of assisting the end-users with the prioritised tasks were discussed among the AXO-SUIT consortium before finalising the target motions to assist. To aid the development even further, a set of human kinematic and kinetic data was gathered for 10 of the 12 tasks (see Table 1.5). The motion capture data was acquired in a laboratory setting using eight participants [126]. The motion capture data and anthropometric data for the test subject was subsequently imported into the bio-mechanical simulation software AnyBody Modeling System [128] to create simulations of the participants performing the tasks. From each of

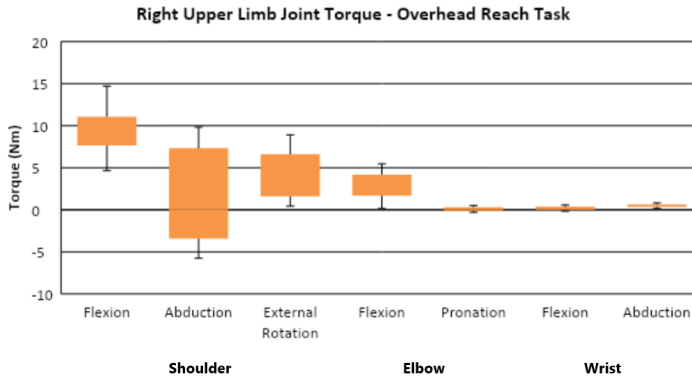
Table 1.5: Motion study activities conducted in laboratory settings.

No	ADL	Description
1	Sit to stand/Stand to sit	Getting up/sitting down from chair without using hands for assistance
2	Walking	Walking without a load to carry
3	Standing	Standing quietly, e.g., at a table/kitchen sink
4	Lifting/dropping	Lifting/lowering an item from floor to table
5	Reaching to side over-head/opposite shoulder	Opening/closing a curtain
6	Push/pull in standing	Pushing/pulling an item (2 kg approx.) across a table surface
7	Holding object in front (2 hands)	Standing while holding a 4 kg item
8	Getting up from kneeling	Both knees on floor, step forward with one foot, rise to standing (without leaning on external object for support)
9	Getting up from a squat	Squat with thighs parallel to floor (or as close as possible to this) and rise without support
10	Carrying small objects (1 hand)	Carrying a 0.5 kg item to front and side, e.g., a cup/mug

the completed tasks, the AnyBody Modelling System generates an array of biomechanical data, such as individual muscle forces, joint contact forces, metabolism and so on. In this part of the study, the primary interested is to obtain joint position data (ROM) and joint torque data for the major upper and lower limb joints of the human body. These data were used to inform the ROM and torque requirements of the main joints of the AXO-SUIT upper body and lower body subsystems. The results for the upper body from the overhead reach task are shown in Fig. 1.8(a) and 1.8(b).



(a)



(b)

Fig. 1.8: Range-of-motion (a) and joint torque (b) during the overhead reach task at the major joints of the right upper limb. The boxes indicate the mean range (i.e., mean maximum ROM/joint torque to mean minimum ROM/joint torque) observed across all participants ($n=8$). Error bars mark the standard deviations of the means.

A focus group was carried out at Aalborg University, Denmark, to obtain end-user feedback on the vision for AXO-SUIT, including its functions, design and commercialisation potential. Seven older adults participated in



Fig. 1.9: Member of the Focus Group wearing the UB-AXO.

the focus group; four females and three males. Participants were older adults from the region near Aalborg. Four researchers implemented the focus group: one moderator, one technical facilitator/demonstrator and two assistants. Two sessions were completed with the focus group. In the sessions, AXO-SUIT was presented as a full-body modular exoskeleton, aimed primarily towards older adults, and with activities like cooking and shopping as potential areas of use. The focus group schedule included an introduction to the AXO-SUIT concept and vision, a demonstration of the SEMTM Glove (Bioservo) [129], a demonstration of the AXO-SUIT prototype and a group discussion of participants' impressions of the AXO-SUIT. The results of the focus group had implications for both AXO-SUIT design and commercialisation planning, including motor sizing, material selection, etc.

1.5 Musculoskeletal Modelling in Exoskeleton Design

Simulation-based design, where mathematical models are used to form and access the design performance, is a strong tool to greatly reduce the number of design iterations and thus, reduce the costs of physical prototypes. In exoskeleton design, multi-body dynamic modelling composed by both a musculoskeletal system and exoskeleton dynamics (illustrated in Fig. 1.10), has been used to analyse and optimise the design of the exoskeleton [130–132].

The AnyBody Modeling System [133] and OpenSIM [134] are examples of the available musculoskeletal modelling software³. Musculoskeletal models consist of a virtual human model that is treated as mechanical multi-body system with anthropometric properties, such as bone geometries and inertial properties, mechanical joints, muscle anchor points and route, muscle actuation models, etc. The models are capable of outputting a range of bio-mechanical data, such as individual muscle forces, reaction forces in the joint and metabolism. Hence, the musculoskeletal models can provide valuable insight to the physical interaction between human body and exoskeletons [130, 135]. In the literature, musculoskeletal models have been used to analyse the physical interaction between the coupled human-exoskeleton systems [57, 130, 135].

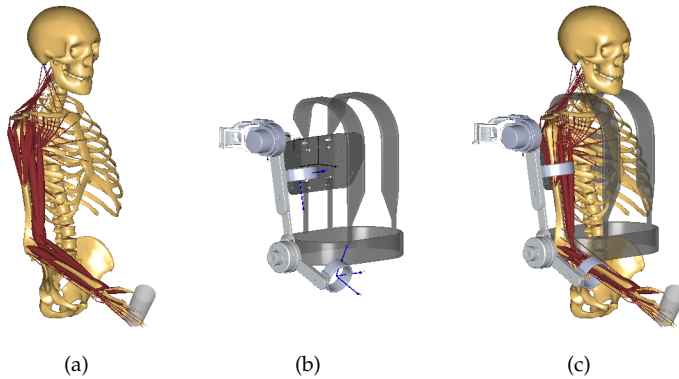


Fig. 1.10: Human-Exoskeleton Model in AnyBody Modelling System: (a) the human biomechanics, (b) the exoskeleton model, (c) the cooperative human-exoskeleton system

Bai et al. [130] presented a human-robot model, which integrated the musculoskeletal model of the human upper body and an exoskeleton arm for shoulder and elbow flexion/extension support. The model was presented as an approach to design and optimise the design of the exoskeleton through biomechanical studies.

Agarwal et al. [135] presented a framework for virtual prototyping of robotic exoskeletons, which was exemplified with a design of an index finger exoskeleton. The framework consisted of six steps: 1) Initial modelling, 2) Performance measure identification, 3) Model fidelity 4) Virtual design, 5) Virtual control and 6) Virtual experimentation. In the framework, biomechanical measures (e.g., joint reaction and metabolic power consumption) were used to access the performance of the exoskeleton.

³Other multi-body dynamics software or tools, such as ADAMS from MSC Software and SimMechanics from Mathworks, have also been used for simulation-based design of exoskeletons [132]

Zhou et al. [57] presented a simulation platform to model the physical human-exoskeleton interaction using the AnyBody Modeling System. The developed biomechanical model provided the designers an insight into the mechanics of the dual human-exoskeleton system when, e.g., paralysing certain muscle [57]. The AAU Cable-Driven Exoskeleton was designed for proof-of-concept and has not yet been further matured for actual patient use [57].

Notably, in the models reported, the coupled human-exoskeleton system is usually assumed to be rigidly connected to the human. This is a simplified contact problem, as it cannot simulate human contact with different attachments. Moreover, the simulations mainly addressed the interaction forces; the power flow is rarely considered.

Chapter 2

Research Challenges and Objectives

2.1 Objectives of the PhD Project

Based on the state-of-the-art presented in the previous sections, a number of challenges have been identified in the design of assistive upper-body exoskeletons that are portable and comfortable to use, while supplying comprehensive support at joint level.

One key challenge is to obtain a good kinematic and kinetic interaction, i.e., physical interaction, between the assistive exoskeleton and human body. Musculoskeletal simulation can assist in several stages of the exoskeleton design, to analyse, evaluate and possibly optimise their design. However, it can be challenging to develop models for co-simulation and set up realistic kinematic and kinetic connections between the human and exoskeleton models. Any type of assistive force or torque from an exoskeleton is transferred to the human by means of contact forces. The behaviour of contact is highly non-linear and complex as it depends on the exoskeleton design and movement of the human body.

An exoskeleton should not only supply the human with additional strength when needed, but it should also move naturally with the human in “free motion”. The mechanical impedance from the exoskeleton can be compensated at a certain level using passive joints. A more effective way to compensate for the mechanical impedance is through active joints and an interaction control strategy. The cost of using active joints is the additional weight, compared to the passive actuation.

Hence, the aim of this PhD study is to design and control a modular assistive upper body exoskeleton capable of supporting occasional activities of daily living following an user-centered design approach, where musculoskeletal modelling is used to aid the development.

More specifically, the objectives of Ph.D. research are:

- to define the physical human-robot interface between the human upper-body and an exoskeleton required for modular motion assistance of healthy elderly users
- to investigate the physical human-robot interaction using musculoskeletal modelling
- to develop a lightweight, wearable and portable exoskeleton capable of motion assistance
- to develop an interaction control strategy that comfortably supplies the user with assistance
- to validate the useability and performance of the exoskeleton with end-user testing.

To fulfil the objectives listed above, the following research questions were formulated and are addressed in this research work:

- Q1** How can an exoskeleton be designed for effective assistance through in-cooperating end-user involvement?
- Q2** How can musculoskeletal modelling be used to aid design and control of the exoskeleton by exploring the physical human-robot interaction?
- Q3** What interaction control strategy is suitable for joint level motion assistance of upper body exoskeletons?
- Q4** How can the usability and performance of the exoskeleton be tested with the end-users?

2.2 Scope of Work and Project Methodology

The overall scope of work is illustrated in Fig. 2.1. The research activities were conducted in parallel and iteratively with the AXO-SUIT project and end-user involvement. The literature study provided a fundamental understanding of the design and control challenges with upper body exoskeletons. From the knowledge obtained from the literature study and initial end-user involvement, conceptual designs were investigated using musculoskeletal co-simulations. A first prototype was manufactured to develop a suitable control strategy for the exoskeleton and to get feedback on the design vision and system functionalities from the end-users via the Focus Group. The detailed design was created using vital feedback from the end-users and musculoskeletal co-simulations for the exoskeleton and human systems to access the physical interaction between the two systems. The final designs were subsequently manufactured and tested on end-users to access the useability and performance of the design and control strategy.

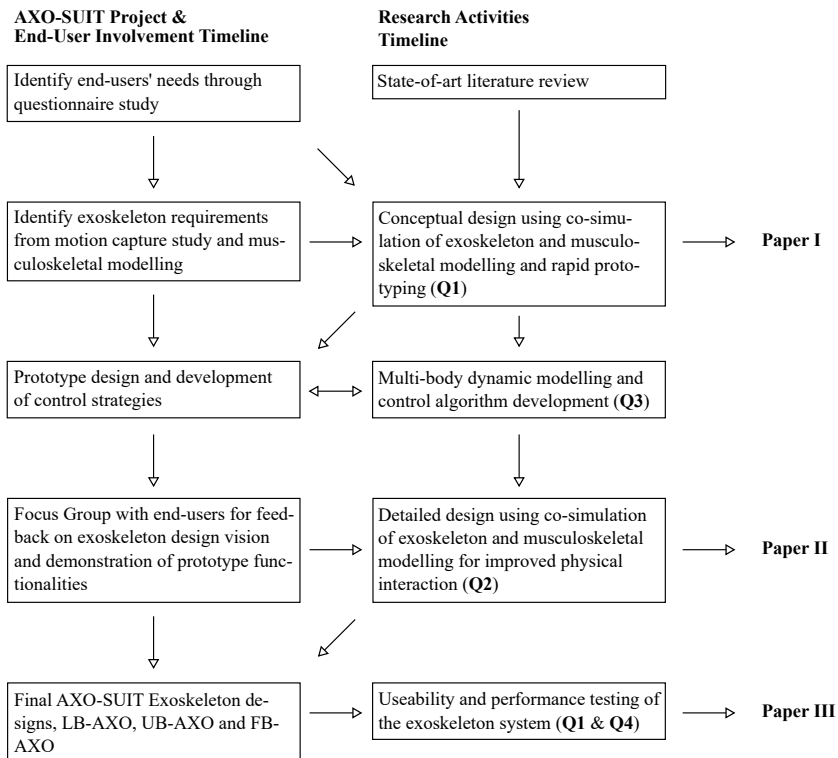


Fig. 2.1: Scope of work for the PhD study.

2.3 Thesis Outline

The present chapter introduces the background and motivation of this PhD study, including a literature review of the current state-of-the-art of both passive and active upper-body exoskeletons, musculoskeletal modelling and the user-centered design approach adapted to the study. The subsequent chapters present the results from the objectives outlined in this chapter, which is organised as a collection of the three scientific journal publications in this thesis. Each chapter is described as follow.

Chapter 3 presents the design of a remote centre of rotation spherical mechanism composed by a double parallelogram linkage (DPL) connecting two revolute joints. The kinematics and singularities are analysed for the spherical mechanism and double parallelogram linkage and a dimensional analysis is carried out to find the design with maximum ROM. The final design of mechanism is constructed and integrated in a four-DOF wearable upper-body exoskeleton.

Chapter 4 presents a human-exoskeleton model comprising the biomechanics of the human upper body and the dynamics of a four-DOF exoskeleton, named UB-AXO. The human-exoskeleton model is used to estimate the effect of physical human-exoskeleton interaction, such as muscle activity, energy consumption and human joint reaction forces, when performing cooperative motions with the exoskeleton. The model development is described, which includes the formulation of kinematic and kinetic constraints between the human and exoskeleton. Subsequently, two simulation studies of typical activities of daily living are conducted to analyse and evaluate the performance of the UB-AXO.

Chapter 5 presents the overall design and development of the powered full-body exoskeleton, named FB-AXO, which is composed by two main subsystems, a lower-body, (LB-AXO) and an upper-body (UP-AXO) subsystem connected together through waist and spine modules. The user-centered design approach adopted at the onset of the project led to the realising of the FB-AXO. The final FB-AXO design comprises of 27 DOFs of which 10 are electrically powered and the 17 are passively supported or truly passive. The design, construction and preliminary testing of the FB-AXO are elaborated, which addresses the design challenges including kinematic compatibility and modularity with innovative solutions. Furthermore, details are provided of the two systems mechanics, sensors and electronics along with specifics of human-exoskeleton interfaces and ranges of motion. Preliminary tests demonstrates that the FB-AXO and its subsystems are able to assist

full-body motions to meet the daily living demands of older users, such as sit-to-stand, reaching overhead and carrying while walking.

Chapter 6 summarises the key findings of the thesis and how this work contributes and impacts the research within the area of wearable robotics. Additional ideas and suggestions for future research and work are discussed.

Chapter 3

Paper I

Kinematic Analysis and Design of a Novel Shoulder Exoskeleton Using a Double Parallelogram Linkage

Simon Christensen, Shaoping Bai

The paper has been published in
Journal of Mechanisms and Robotics Vol. 10(4), pp. pp. 041008-1–041008-10,
2018.
doi:10.1115/1.4040132

The included paper has been approved for redistribution by the publisher.
Copyright ©2018

Kinematic Analysis and Design of a Novel Shoulder Exoskeleton Using a Double Parallelogram Linkage

Simon Christensen

Department of Material and Production,
Aalborg University,
Aalborg 9220, Denmark
e-mail: sic@mp.aau.dk

Shaoping Bai

Department of Material and Production,
Aalborg University,
Aalborg 9220, Denmark
e-mail: shb@mp.aau.dk

The design of an innovative spherical mechanism with three degrees-of-freedom (DOFs) for a shoulder joint exoskeleton is presented in this paper. The spherical mechanism is designed with a double parallelogram linkage (DPL), which connects two revolute joints to implement the motion as a spherical joint, while maintaining the remote center (RC) of rotation. The design has several new features compared to the current state-of-the-art: (1) a relative large range of motion (RoM) free of singularity, (2) high overall stiffness, (3) lightweight, and (4) compact, which make it suitable for assistive exoskeletons. In this paper, the kinematics and singularities are analyzed for the spherical mechanism and DPL. Dimensional analysis is carried out to find the design with maximum RoM. The new shoulder joint is finally designed, constructed, and integrated in a four degree-of-freedom wearable upper-body exoskeleton. A finite element analysis (FEA) study is used to assess the structural stiffness of the proposed design in comparison to the conventional 3R mechanism. [DOI: 10.1115/1.4040132]

1 Introduction

An exoskeleton is a robotic suit that is capable of producing supplementary muscular functions of a wearer. Robotic exoskeletons enable the wearer to lift a greater load or compensate for a lack of strength. They have the potential to be applied in industry and health service such as automotive [1], agriculture [2], nursing [3], and rehabilitation [4]. Depending on the limbs of attachment, exoskeletons can be classified into upper- or lower-body systems. The design challenges with powered assistive upper-body exoskeletons are mainly related to the complexity of the human body, especially the shoulder complex, which is one of the most anatomically complex region in the human body [5,6]. The human upper-body has a large dexterity in order to perform its broad variety of activities. Hence, an optimal exoskeleton design should comply with the full natural range of motion (RoM) of the wearer. Moreover, the RoM has to be achieved without the exoskeleton colliding with the wearer or itself or being satisfactorily far from kinematic singularities. Furthermore, for portable exoskeletons, a small protrusion of the device from the wearer is desirable.

The existing design solutions of shoulder exoskeletons are limited to meet these requirements. Traditional designs of shoulder exoskeletons use a serial linkage system with three-revolute (3R) joints [7–10] to generate the spherical motion of the human shoulder joint (see Fig. 1(a)). A problem with a serial structure is its workspace limit. The wearer of the exoskeleton can only raise the upper arm a small angle in the frontal plane before the shoulder mechanism collides with his/her shoulder, neck, or head. To avoid this problem, some alternative designs have been proposed. The design in Ref. [7] minimized the effect of these problems by designing the 3R mechanism so that the singular configurations and collision problem occur at postures that are less likely for the wearer to reach. Another approach, reported in Refs. [11–13], one of the links in the 3R mechanism is replaced with a circular guide to further avoid collision with the wearer

(see Fig. 1(b)). In another design [14], the circular guide, which often has a heavy and complicated construction, is avoided by moving one of the degrees-of-freedom (DOFs) of the shoulder to the elbow (see Fig. 1(c)). A problem with this solution is the added mass at the elbow due to the additional actuator/joint. There is also a design where an extra link is added to the 3R mechanism making it a 4R mechanism [15] (see Fig. 1(d)). Because of the redundancy of the mechanism, the exoskeleton can avoid singular configurations and collisions with the wearer. For portable exoskeletons, however, adding an active redundant degree-of-freedom causes a concern on both the weight and the occupied space of the exoskeleton.

Parallel linkage systems have also been proposed for shoulder exoskeletons [16–18]. The design in [17] uses a three linear actuation acting in parallel to realize the spherical motion of the shoulder glenohumeral joint. The design offers a low inertia and high stiffness solution due to the parallel structure. However, the linear actuators require a large stroke length in order to match the large range of motion of the shoulder glenohumeral joint, which results in a protruding design. In Ref. [18], two 3R spherical mechanisms are driven by two linear actuators and two crank-slider mechanisms. Because of the crank-slider mechanisms, the actuators can be placed side-by-side and parallel to the human torso, which minimizes the protrusion of the linear actuators. Nevertheless, the workspace is limited by the aforementioned collision problem of 3R mechanism.

In addition, solutions using a flexible structure are presented in Refs. [19] and [20]. Both designs adopt cable-driven transmissions, which are routed through cuffs attached to the human limbs.

In this paper, a novel shoulder mechanism, namely, double-parallelogram spherical mechanism (DPM), is presented. The mechanism is featured with a compact structure, light-weight yet rigid design, and a large range of motion free of singularity. The proposed mechanism is to be used as a novel shoulder joint mechanism for an upper-body exoskeleton. This work is based on the authors' previous work [21], where the overall design of upper-body exoskeleton is presented. In this paper, the kinematics and the mechanism design of the shoulder exoskeleton are duly

Contributed by the Mechanisms and Robotics Committee of ASME for publication in the JOURNAL OF MECHANISMS AND ROBOTICS. Manuscript received July 3, 2017; final manuscript received April 20, 2018; published online May 31, 2018. Assoc. Editor: Robert J. Wood.

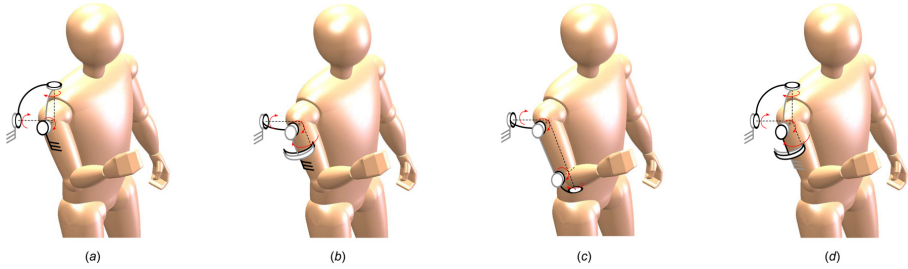


Fig. 1 Illustration of shoulder joint mechanisms using (a) three-revolute joints, (b) two-revolute joints and a circular guide, (c) three-revolute joints with one placed at the elbow, and (d) a redundant joint

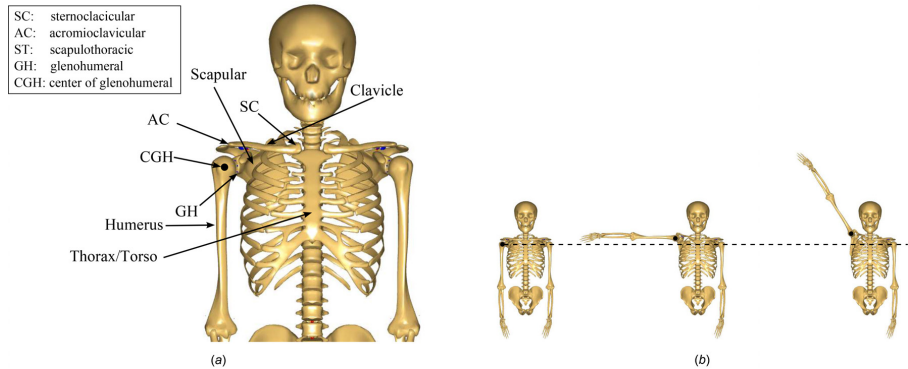


Fig. 2 The shoulder complex: (a) segments and joints and (b) scapulohumeral rhythm

considered with details. A simple biomechanical model that describes the range of motion of the human shoulder is used to assess the performance of the exoskeleton along with a kinematic analysis including a singularity analysis and a manipulability analysis. Dimensional analysis is carried out to find the design with the maximum range of motion. Mechanism design of the shoulder exoskeleton is described, with a FEM analysis to assess the structural stiffness. Finally, prototypes and testing results are presented.

2 Kinematics and Range of Motion of the Human Shoulder

The shoulder complex connects the humerus bone to the thorax through the glenohumeral joint (or shoulder joint) and the shoulder girdle (see Fig. 2(a)).

The glenohumeral joint can be described as a ball-and-socket joint with three degrees-of-freedom that describes the orientation of the humerus relative to the scapula. These three consecutive rotations are noted in Fig. 3 as flexion/extension, abduction/adduction, and internal/external rotation. For a variety of arm activities, where the elevation of the arm is below 90 deg (see Fig. 2(a)), the motions of the shoulder complex can be represented solely by the glenohumeral joint [11]. When the shoulder is fully flexed or abducted, the rotation of the humerus, with respect to the torso, will be a combination of movements in the shoulder girdle and flexion or abduction in the glenohumeral joint. The shoulder girdle is made up of the sternoclavicular joint, the acromioclavicular joint, and the scapulothoracic joint. These three joints form a closed kinematic chain with the thorax, scapular, and clavicle and

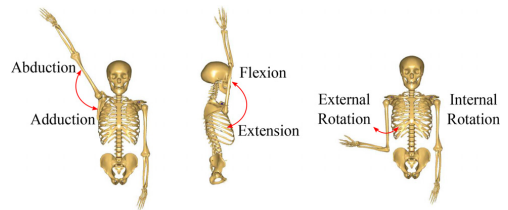


Fig. 3 RoM of the shoulder complex

are therefore unable to move independently [22,23]. Movements of the humerus also cause movements of the scapular. This joint movement relationship is called the scapulohumeral rhythm and is illustrated in Fig. 2(b). As a result, the position of center of the glenohumeral joint shifts. The dominant motions of the shoulder girdle are the two rotational motions: elevation/depression and protraction/retraction. The novel shoulder joint presented in this paper can mimic the three rotations of the glenohumeral joint, which are the dominant movements of the shoulder complex. The anatomical terms of the motions associated with these degrees-of-freedom are illustrated in Fig. 3.

It is noted that the range of motion of the shoulder complex described in the literature differs slightly from each other, so in this work, we take some commonly used values [9–13]. The range of motion of the glenohumeral joint is listed in Table 1 and is given with respect to the anatomical position.

Table 1 Ranges of motion of the glenohumeral joint found in the literature

Movement	Notation	Limits (deg)
Abduction/adduction	ϕ_{Amin}	-20
	ϕ_{Amax}	120
Extension/flexion	ϕ_{Fmin}	-60
	ϕ_{Fmax}	170
Internal/external rotation	ϕ_{Rmin}	-60
	ϕ_{Rmax}	90

3 Kinematic Design of Novel Spherical Shoulder Joint

The proposed design, illustrated in Fig. 4, is a hybrid mechanism that consists of two revolute joints connected together via six links that form a DPL [24], which under the given configuration form a remote center (RC) of motion mechanism, as illustrated in Fig. 5. The mechanism works kinematically equivalent to the 3R mechanisms, meaning that it can rotate about three independent axes that all coincide in one point, namely, the RC. The design parameters of the DPL, as illustrated in Fig. 4, include two offset angles ϕ_1 and ϕ_2 and four link lengths $L_i, i = 1, \dots, 4$ for the two parallelograms A-B-C-D and D-E-F-G. As the two parallelograms are serially connected, they form a third virtual parallelogram between points B-D-E-RC. The range of motion of the DPL is determined from this virtual parallelogram.

It is noted that there are other concepts of DPL mechanisms proposed. A wrist mechanism of minimally invasive surgery robot, where the remote center is generated by DPL to serve as the incision point for the surgery, was reported in Refs. [25] and [26]. In Ref. [27], the DPL is used as a part of a force-reflective master robot of haptic tele-surgery system. Finally, in Ref. [28], the DPL is used in a design synthesis of a mechanism with multiple remote centers of motion, exemplified with the design of a foldable stage.

3.1 Kinematics of the Shoulder Joint. A spherical mechanism is constructed by mounting two revolute joints to the DPL,

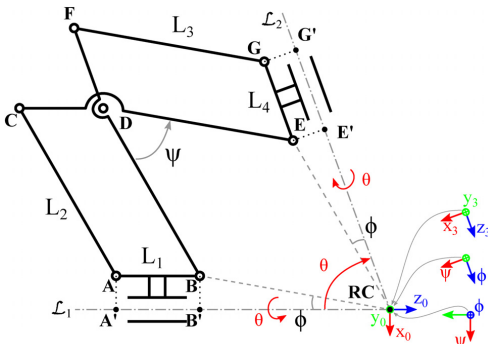


Fig. 4 Kinematic model of the shoulder mechanism

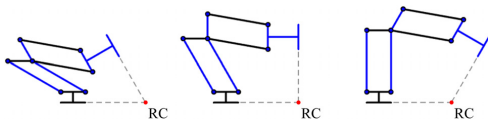


Fig. 5 Working principle of DPL in the shoulder mechanism

Table 2 Denavit–Hartenberg parameters of the proposed mechanism following notation given in Ref. [29]

Link, i	a_i	α_i	d_i	θ_i
1	0	$-\pi/2$	0	θ_1
2	0	$\pi/2$	0	θ_2
3	0	0	0	θ_3

as demonstrated in Fig. 4, where L_1 and L_2 are lines of joint axes. A kinematic model of this mechanism is developed with Denavit–Hartenberg parameters, which are listed in Table 2. For this spherical joint, the kinematics of the DPM is expressed solely by rotations. The rotation matrix is given as

$${}^0\mathbf{R}_3 = \begin{bmatrix} c\theta_1 c\theta_3 c\theta_2 - s\theta_1 s\theta_3 & -c\theta_3 s\theta_1 - c\theta_1 c\theta_2 s\theta_3 & c\theta_1 s\theta_2 \\ c\theta_1 s\theta_3 + c\theta_3 c\theta_2 s\theta_1 & c\theta_1 c\theta_3 - c\theta_2 s\theta_1 s\theta_3 & s\theta_1 s\theta_2 \\ -c\theta_3 s\theta_2 & s\theta_3 s\theta_2 & c\theta_2 \end{bmatrix} \quad (1)$$

where c and s stand for harmonic functions cosine and sine, respectively.

The inverse kinematics is readily solved from the rotation matrix in Eq. (1), where

$$r_{33} = c\theta_2 \quad (2)$$

where r_{33} is the element (3,3) in the rotation matrix. From Eq. (2), the two possible solutions for θ_2 are found as

$$\theta_2 = \pm \arccos(r_{33}) \quad (3)$$

Moreover

$$\theta_1 = \arctan2(-r_{23}/s\theta_2, -r_{13}/s\theta_2) \quad (4)$$

Similarly, using elements r_{31} and r_{32} and the result from Eq. (3) and solving for $s\theta_1$ and $c\theta_1$ leads to

$$\theta_3 = \arctan2(-r_{32}/s\theta_2, r_{31}/s\theta_2) \quad (5)$$

Through the rotation matrix, the velocity equation is obtained as

$$\dot{\theta} = \mathbf{J}_o^{-1} \omega_e \quad (6)$$

where $\dot{\theta} = [\dot{\theta}_1 \ \dot{\theta}_2 \ \dot{\theta}_3]^T$ is a vector with the joint angular velocities, \mathbf{J}_o is the Jacobian, and $\omega_e = [\omega_x \ \omega_y \ \omega_z]^T$ is the end-effector angular velocities. The Jacobian is found as

$$\mathbf{J}_o = \begin{bmatrix} 0 & s\theta_1 & -s\theta_2 c\theta_1 \\ 0 & -c\theta_1 & -s\theta_2 s\theta_1 \\ 1 & 0 & c\theta_2 \end{bmatrix} \quad (7)$$

4 Singularities of the Shoulder Joint

As the mechanism has a hybrid structure, namely, a planar linkage connecting two revolute joints for a spherical mechanism, the singularity analysis is conducted for both the planar linkage and the spherical mechanism, which represents the singularities at local and global levels.

4.1 Global Singularities of the Shoulder Joint. Singularities occur when the Jacobian matrix loses rank, i.e., when the determinant is 0

$$\det(\mathbf{J}) = -\sin \theta_2 = 0 \quad (8)$$

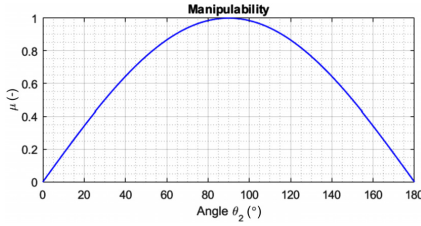


Fig. 6 The manipulability index of the DPM

Equation (8) shows that the DPM becomes singular, when $\theta_2 = 0$ or π , which corresponds the case where the joint axes of the first and third joints constitute a common line.

The kinematic performance of the spherical mechanism is evaluated by the manipulability. The manipulability index μ is determined as

$$\mu(\mathbf{J}) = \sqrt{|\mathbf{J}\mathbf{J}^T|} = |\sin \theta_2| \quad (9)$$

From Eq. (9), it is clear that the manipulability of the DPM depends solely on the second joint rotation and it has an isotropic configuration for $\theta_2 = 90$ deg. The varying performance is displayed in Fig. 6.

4.2 Singularities of the Double Parallelogram Linkage. We look further into the singularity of the parallelogram. In Fig. 4, a coordinate system $x_1 - y_1 - z_1$ is fixed to the DPL, where the y_1 -axis is parallel to line \mathcal{L}_1 and point RC is the origin. In the DPL, AC is the input link and EG is the output link. A total of 15 equations are established to describe the position and orientation constraints of the links in DPL

$$\Phi(q(t), t) = 0 \quad (10)$$

where Φ is the set of constraint equations, q is the generalized coordinates of the links, and t is the time. Differentiating the constraint equations yields

$$\dot{\Phi}(q(t), t) = \Phi_q \dot{q} + \Phi_t = 0 \quad (11)$$

where Φ_q is the constraint Jacobian, Φ_t is the partial derivative of Φ with respect to t , and \dot{q} is the generalized velocity. The singular configuration can be found from the case where the determinant of the Constraint Jacobian is zero

$$\det(\Phi_q) = 0 \quad (12)$$

which yields

$$\psi = -\phi_2 \quad (13a)$$

$$\psi = \pi - \phi_2 \quad (13b)$$

$$\psi = -\phi_1 \quad (13c)$$

$$\psi = \pi - \phi_1 \quad (13d)$$

As seen from the result above, the DPL has four singular configurations, which are linked to the closed loop kinematic chain of the DPL. When one of the parallelograms is collapsed, i.e., ABCD or DEFG constitutes a straight line, the DPL gains a freedom and has two instantaneous degrees-of-freedom. At this configuration, an instantaneous change of θ_2 can lead to the parallelogram switching into an anti-parallelogram. As a result, the

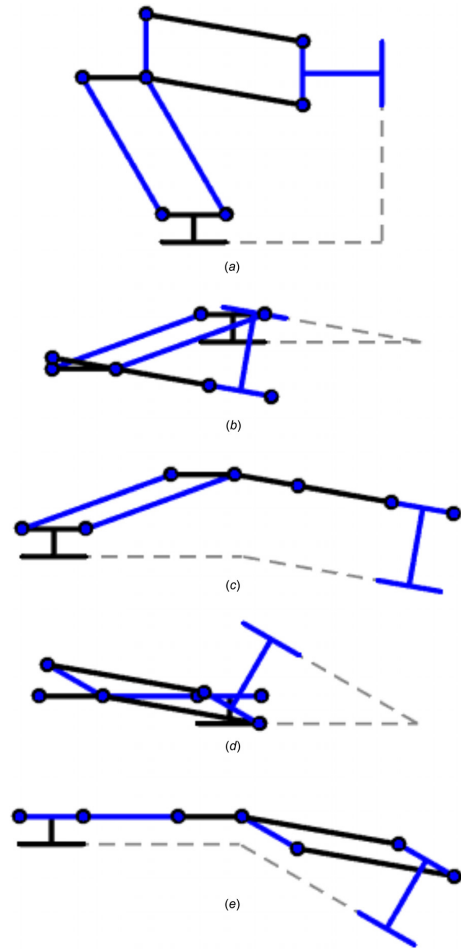


Fig. 7 The DPL with $\phi_1 = 30$ deg and $\phi_2 = 10$ deg in a kinematic configuration with (a) $\psi = 50$ deg, (b) $\psi = -\phi_1$, (c) $\psi = 180$ deg $-\phi_1$, (d) $\psi = -\phi_2$, and (e) $\psi = 180$ deg $-\phi_2$

three axes of rotation of the shoulder mechanism no longer coincide in a fixed remote center. The four singularity configurations of Eq. (12) are demonstrated in Fig. 7 and described subsequently:

- (1) Figure 7(b) shows the singular configuration of Eq. (13a), where the second parallelogram is collapsed at a small angle of θ_2 .
- (2) Figure 7(c) shows the singular configuration of Eq. (13b), where the second parallelogram is collapsed at a large angle of θ_2 .
- (3) Figure 7(d) displays the singular configuration of Eq. (13c), where the first parallelogram is collapsed at a small angle of θ_2 .
- (4) Figure 7(e) displays the singular configuration of Eq. (13d), where the first parallelogram is collapsed at a small angle of θ_2 .

The singular configuration in Eq. (12) reveals that the DPL cannot have a range of motion above 180 deg without having a singularity within its range of motion, since a singularity for both

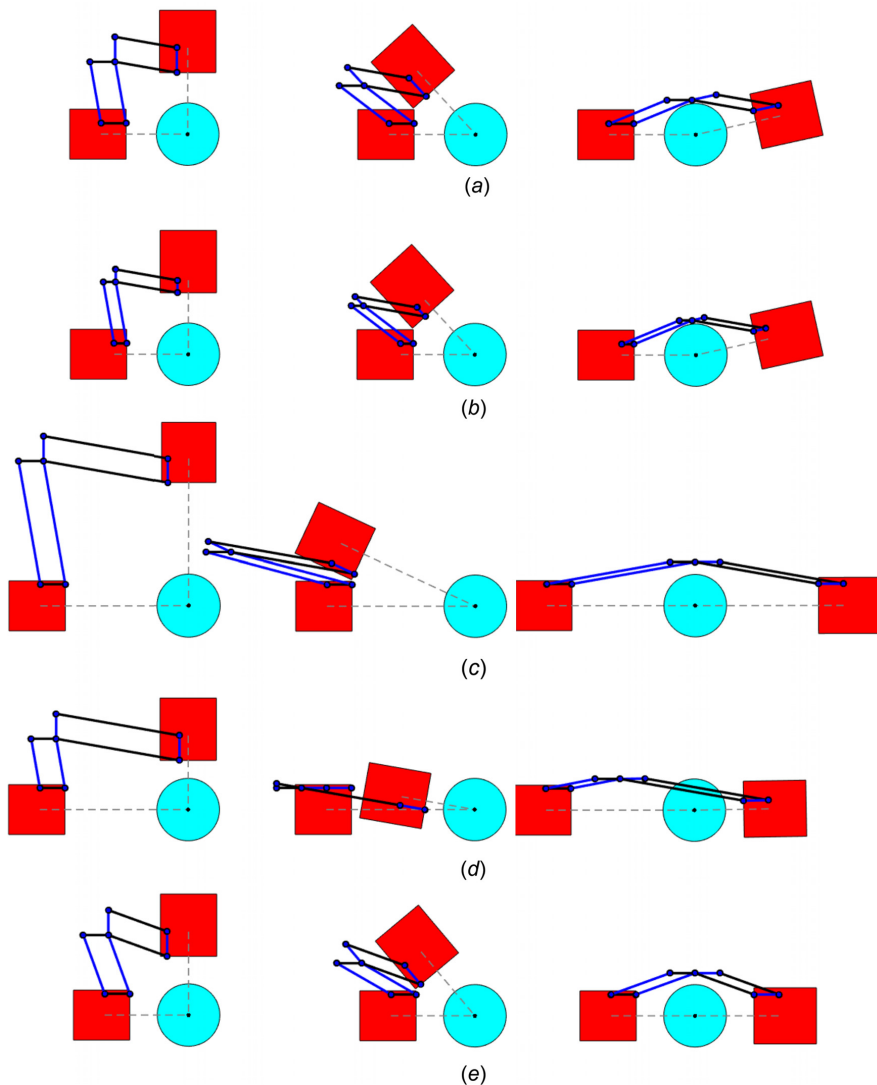


Fig. 8 Maximum and minimum internal/external rotation of the shoulder mechanism for (a) baseline design, (b) variation of lengths of L_1 and L_4 , (c) variation of lengths of L_2 and L_3 , (d) variation of length relation between L_2 and L_3 , and (e) variation of offset angles ϕ_1 and ϕ_2

ϕ_1 and ϕ_2 is repeated after 180 deg. Therefore, to maximize the range of motion the DPL free of singularities, the two offset angles must be as close to each other in size as possible.

5 Dimensioning of Double Parallelogram Linkage

The four link lengths $L_i, i = 1, \dots, 4$ are not included in the Jacobian, hence, these parameters do not affect the manipulability of the mechanism. However, they affect the feasible workspace and the compactness of the shoulder joint. The feasible workspace, or range of motion, of a physical embodiment is smaller

than the ideal workspace due to self-collision of the mechanism and collision with the human. Self-collision depends on the shape and size of the actuation of the shoulder mechanism, while the linkage of the DPL can be constructed such that it does not interfere with the rest of the mechanism.

Collision between the exoskeleton and the wearer is difficult to check accurately, as it highly depends on the shape and size of the wearers shoulder, arm, neck, and back. In this paper, we simplify the problem by using a sphere that represents the human shoulder with its center at the glenohumeral joint. If the shoulder mechanism enters this sphere, the exoskeleton has collided with the wearer. From anthropometric measurements listed in Ref. [30],

Table 3 Minimum and maximum angles and RoM of the five design cases

Design case	Minimum angle (deg)	Maximum angle (deg)	RoM (deg)
Baseline	55	170	125
Case 1	55	170	125
Case 2	25	180	155
Case 3	10	180	170
Case 4	55	180	135

the shoulder diameter is estimated to be 100mm, which fits the 50th% of the population.

5.1 Variations of Link Lengths and Offset Angles on Double Parallelogram Linkage Design. Four design cases of link length variation are considered, namely (1) variation of lengths of L_1 and L_4 , (2) variation of lengths of L_2 and L_3 , (3) variation of length relation between L_2 and L_3 , and (4) variation of offset angles ϕ_1 and ϕ_2 . They have different influence on the practical range of motion, as described presently. Figure 8 illustrates the influence variations of the link lengths and offset angles has on the range of motion of the shoulder exoskeleton in the DPL plane, where the actuators are marked as rectangles and the shoulder sphere as a circle. In Fig. 8(a), a baseline design displays its isotropic, minimum, and maximum configuration. The baseline design has an isometric design, where $L_1=L_4$, $L_2=L_3$, and

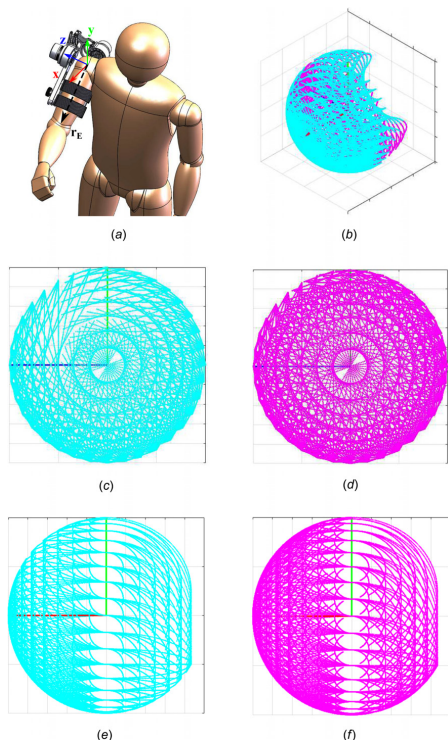


Fig. 9 Workspace analysis of the DPM (cyan) within the human arm workspace (magenta): (a) coordinate setup, (b) isotropic view, (c) front plane view human workspace, (d) front plane view of DPM workspace, (e) sagittal plane view of human workspace, and (f) sagittal plane view of DPM workspace

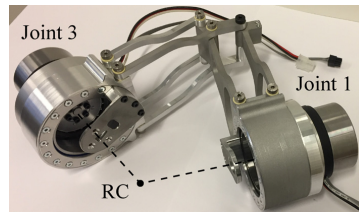


Fig. 10 Spherical shoulder joint built with parallelogram mechanism

$\phi_1 = \phi_2$. The minimum angle is bounded by the footprint of the two actuators, while the maximum angle is bounded by the DPL colliding with the shoulder sphere. Throughout the workspace, the mechanism does not enter a singularity, as none of the axis constitute a common planer (i.e., global singularity) nor does either of the parallelograms collapse (i.e., local singularity). Hence, it is possible to increase the range of motion of the baseline design without compromising singularity restrictions.

5.1.1 Design Case 1—Variation of Lengths of L_1 and L_4 . In Fig. 8(b), the link lengths L_1 and L_4 are halved compared to the baseline design, which clearly does not affect the range of motion, but the protrusion of the DPL is smaller, especially at the minimum angle. However, the stiffness of the DPL is also decreased, which is undesirable.

5.1.2 Design Case 2—Variation of Lengths of L_2 and L_3 . In Fig. 8(c), link lengths L_2 and L_3 are doubled in comparison to the baseline design, which result in a larger range of motion. Similar to the baseline design, the minimum angle is bounded by the footprint of the two actuators, but the maximum angle is now bounded by the global singularity. Nonetheless, the enlarged workspace compromises compactness and stiffness of the design, as protrusion of the DPL is significantly larger.

5.1.3 Design Case 3—Variation of Length Ratio between L_2 and L_3 . In Fig. 8(d), the ratio between the link lengths L_2 and L_3 is changed, where L_2 is the same as that for the baseline design and L_3 is twice as long. As a result, the minimum angle is now limited

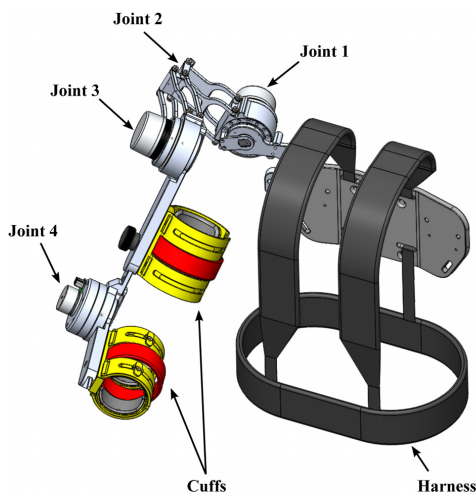


Fig. 11 The shoulder joint mechanism in the 4DOF AAU exoskeleton, with joints 1, 3, and 4 active and joint 2 passive

Table 4 Design parameters of the proposed mechanism

Design parameter	Final design
L_1	30 mm
L_2	100 mm
L_3	100 mm
L_4	20 mm
ϕ_1	25 deg
ϕ_2	22 deg

Table 5 Actuation of the upper-body exoskeleton. Joints 1 and 3 are the active joints in the shoulder mechanism and joint 4 is the elbow joint. Joint 2 is the passive degree-of-freedom of the DPL

	Joint 1	Joint 2	Joint 3	Joint 4
Motor	EC-60	—	EC-60	EC-45
Gear	LCS-17-80	—	CSD-25-50	CSD-25-50

by the local singularity of the parallelograms and the maximum angle of the global singularity. In Fig. 8(d), the links of the DPL enter the human shoulder sphere, however the links can be designed with a curved shape, while maintaining joint placement of the parallelograms. Compared with the design in Fig. 8(c), compactness is only compromised for one of the revolute joints. On the other hand, the design is more complicated than both the baseline design and the design in Fig. 8(c).

5.1.4 Design Case 4—Variation of Offset Angles ϕ_1 and ϕ_2 . In Fig. 8(e), the offset angles ϕ_1 and ϕ_2 are increased compared to the baseline design. From the kinematic analysis, it is seen that the offset angles should be close to each other in size to minimize the sensitivity to singularities. In Fig. 8(e), the offset angles are increased to fit the minimum angle of the baseline

design, i.e., the angle where the actuators collide. This relation can be expressed as

$$\phi_1 = \arcsin\left(\frac{R_{A1}}{L_2}\right) \quad \phi_2 = \arcsin\left(\frac{R_{A3}}{L_3}\right) \quad (14)$$

where R_{A1} and R_{A3} are the radii of the actuator in joints 1 and 3, respectively. The maximum angle is limited by the global singularity. As a result, the design has a relative large range of motion, while only slightly compromising the compactness (compared to the design in Figs. 8(c) and 8(d)).

The minimum and maximum angles and RoM of different designs are listed in Table 3. The result shows that design case 3 has the optimum RoM followed by design case 2. Common for the two design cases is that they significantly improve the reachable minimum angle compared to the other design cases. However, both of these designs have a high protrusion. Design case 2 has the lowest protrusion, but does not improve the RoM compared to the baseline design. A compromise between good RoM and a compact design is found in design case 4.

The reachable workspace of the design case 4, as selected, is further analyzed, with constraint of possible collision between the exoskeleton and the wearer. Figure 9(a) shows the attachment of the DPM on a human dummy, along with the coordinate setup, where the DPL angle, θ_2 , is associated with the human shoulder internal/external rotation. The reachable workspace of the DPM and human glenohumeral joint is shown in Figs. 9(b)–9(f). It can be seen that the majority of the human arm workspace can be reached by the DPM without collision between human and exoskeleton, especially in the front of the human. In total, 90% of the human glenohumeral RoM can be reached by DPM.

6 The Novel Shoulder Mechanism in an Upper-Body Exoskeleton

The shoulder joint has been built, as shown in Fig. 10, and integrated in an upper-body exoskeleton (see Fig. 11) at Aalborg University, Denmark. The upper-body exoskeleton has total of

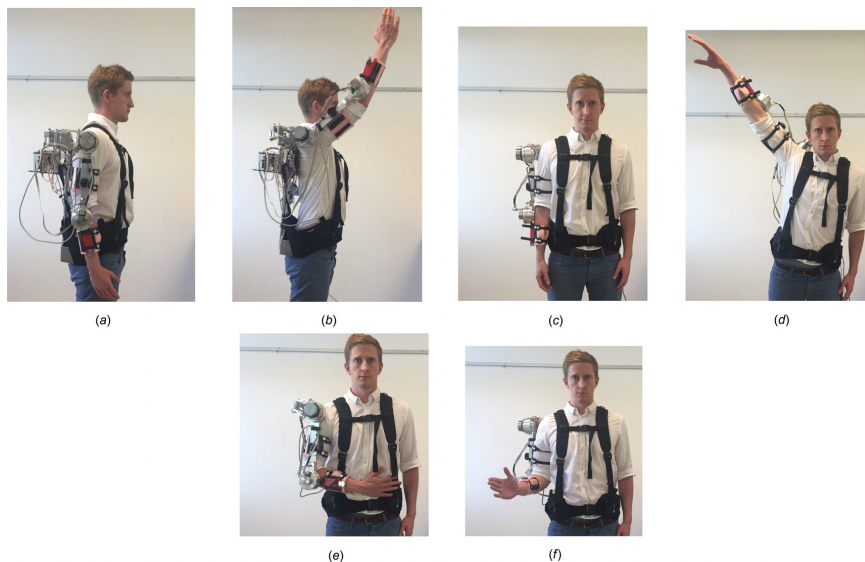


Fig. 12 The shoulder joint mechanism in the AAU exoskeleton in (a) 0 deg shoulder extension, (b) 170 deg shoulder flexion, (c) 0 deg shoulder adduction, (d) 120 deg shoulder abduction, (e) 90 deg shoulder internal rotation, and (f) 20 deg shoulder external rotation

four degrees-of-freedom constituted by the three degrees-of-freedom of the shoulder joint and one additional degree-of-freedom of an elbow joint. The design parameters for the DPL in the shoulder joint are listed in Table 4. The shoulder joint and the rest of the exoskeleton are made from 7075 Aluminum Alloy. The total weight of the shoulder joint is 2650 g of which approximately 200 g is for the DPL.

In the shoulder exoskeleton design, the two revolute joints are actuated by brushless DC-motors in combination with harmonic drives. The harmonic drive was selected for its high efficiency and back-drivability, which allows the user to move even if the motors are powered off without using a clutch. The driving speed and torques are specified based on a series of musculoskeletal simulation of a human doing different activities of daily living with payloads as high as 5 kg. In all studies, the exoskeleton will provide a maximum of 50% of physical assistance for reasons of safety. The DPL is left unactuated, since the musculoskeletal simulation showed low assistance requirements for the internal/external rotation of the shoulder. In Table 5, the shoulder abduction/adduction actuation is listed as joints 1 and 3 are shoulder flexion/extension actuation.

The shoulder joint and the elbow joint are connected of links with length adjustable to fit into wearers of different sizes. The exoskeleton is strapped to the wearer through three attachments: (1) torso harness, (2) upper arm cuff, and (3) forearm cuff. The torso harness consists of a hard back (the shoulder exoskeleton base) with shoulder straps and snap buckle belt for rapidly fitting and easy tightening. The upper arm and forearm cuffs both consist of a flexible plastics material and Velcro straps. Both cuffs are lined with a foam and force sensitive resistor (FSR) sensors, which are used to measure the interaction forces between the exoskeleton and the wearer.

The shoulder joint is able to realize nearly the full range of motion of shoulder flexion/extension 0–170 deg (see Figs. 12(b) and 12(a)) and approximately 0–120 deg shoulder abduction before colliding with the wearer (see Figs. 12(d) and 12(c)). It is noted that our upper-body design does not address the movements of the shoulder girdle, which shifts the center of the glenohumeral joint and as a result creates misalignment between the wearer and the exoskeleton. Nonetheless, the movements are possible due to passive compliance between the robot and the wearer, via the torso harness, which accommodated the misalignment.

Finally, the shoulder joint is able to realize 20 deg of external rotation to 90 deg shoulder internal rotation, which is sufficient to enable the wearer to scratch him/her self on the opposite side of the abdomen (see Figs. 12(e) and 12(f)). While, the shoulder joint is only able to realize 20 deg external rotation, the priority is given to internal rotation of the shoulder, considering that most of our lifting and carrying activities are done in front of our body.

7 Structural Stiffness of the Novel Shoulder Joint

The structural stiffness of the novel shoulder joint is analyzed through finite element analysis (FEA). In different configurations of the DPL, ranging from the minimum angle to the maximum angle with a 5 deg interval, a force of 10 N is applied at the end effector (see Fig. 13). The force is applied in three different cases along the x -, y -, and z -axis of the end effector frame, respectively. For each load case, the displacement of the end effector and the displacement of the remote center of rotation (henceforth RC-displacement) are calculated. For comparison purpose, a FEA study is conducted for a 3R mechanism. The 3R mechanism is designed with similar mechanical and kinematic properties as the DPM, i.e., the total weight is 200 g, the three axes are orthogonal to each other and both the radii of links 1 and 2 are 65 mm. Figure 13 shows the setup for the FEA studies of the two mechanisms. The base is rigidly fixed to a global reference frame, while connections between links are modeled as revolute joints. The elements used are tetrahedral solid elements, where the DPM study has 111,235 elements and the 3R study has 61,525 elements. The DPM study

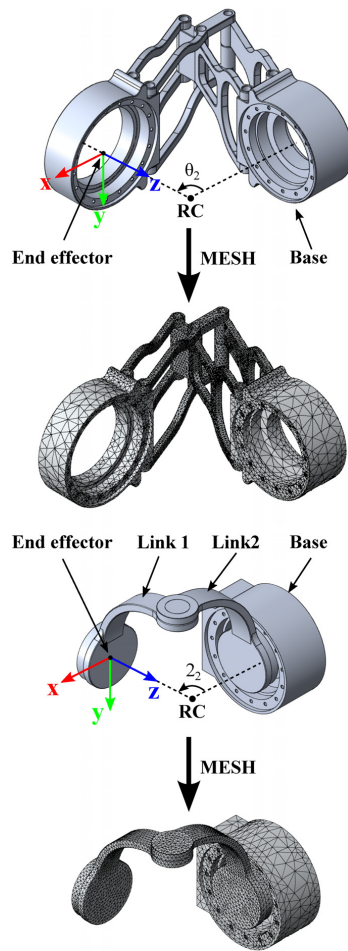


Fig. 13 Structural stiffness analysis of DPM and 3R spherical mechanisms

required a higher number of elements for the result to converge. The mesh of the two studies is illustrated in Fig. 13.

The RC-displacements of the two studies are shown in Fig. 14. For all load cases, the 3R mechanism has a larger RC-displacement, and thus a lower stiffness, compared to the DPM. In other words, the DPM performs generally better than the 3R mechanism in terms of structural stiffness. For the load case along the z -axis, both mechanisms have a nearly constant RC-displacement in the full range of θ_2 . However, magnitude of the RC-displacement of the 3R mechanism is around four times that of the DPM, which is also seen in the equivalent mean stiffnesses in Table 6. For the load case along the x - and y -axis, the displacement for the 3R varies similar to sinusoidal curve that has its extremes at the minimum and maximum angles of θ_2 . In the x -axis load case, the magnitude of the displacement more than doubles, while it triples for the y -axis load case. For the DPM, the change in displacement of the range of motion does not have the same magnitude change or behavior. The dependency of the two parallelograms configuration is most obvious for the load case in the x -axis, while the load cases in the y - and z -axis are

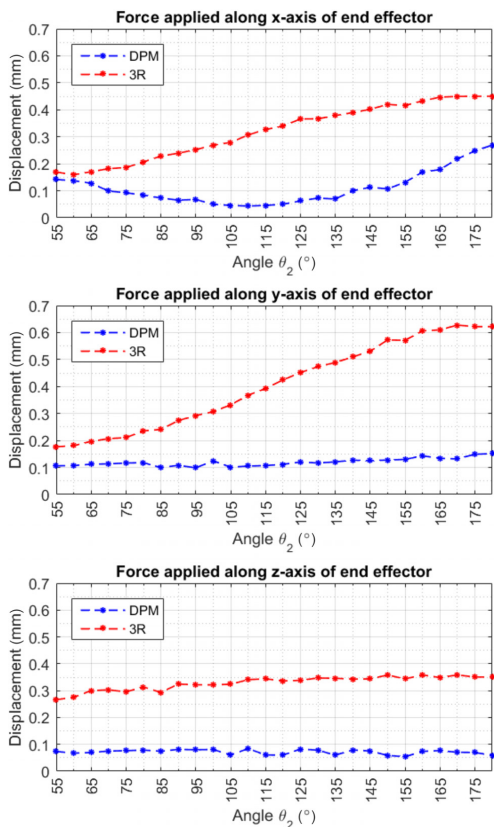


Fig. 14 Displacement of the RC of rotation (RC-displacement) of the DPM and 3R spherical mechanisms, under a force of 10 N along the x -, y -, and z -axis of the end effector frame

insignificantly. In the y -axis load case, the RC-displacement has a slight linear increase, while the RC-displacement in the x -axis load case has a quadratic shape with a minimum around $\theta_2 = 110$ deg. At this angle, the two parallelograms are approximately rectangular, which fits well with the good structural stiffness properties. The largest RC-displacement is found at $\theta_2 = 180$ deg, where the two adjacent sides of the both parallelograms are closest to each other. In the y -axis load case, the change from minimum to maximum RC-displacement is by a factor of 1.5, while for the x -axis load case it is 6.2.

In Table 6, the equivalent minimum, maximum, and mean stiffnesses for the two studies are listed. The mean stiffness of the DPM in the x -axis is 320% greater than that of the 3R and 277%

Table 6 Minimum, maximum, and mean equivalent stiffnesses of the DPM and 3R spherical mechanisms

	Load case	Minimum (N/mm)	Maximum (N/mm)	Mean (N/mm)
DPM	X	37.16	230.41	117.29
	Y	66.14	101.32	85.21
3R	Z	118.62	185.53	141.78
	X	22.17	64.47	36.66
	Y	15.93	58.17	30.73
	Z	27.90	43.18	31.29

and 453% for the y - and z -axis, respectively. Also, for both the load cases in the y - and z -axis, the minimum stiffness of the DPM is higher than the maximum stiffness of the 3R. Hence, this study shows that the DPM has improved stiffness properties compared to the 3R.

It should be noted that the comparison was made for the given design in Fig. 13. Given many variations of the 3R serial shoulder exoskeleton, the stiffness properties of these depend on the geometry link shape and material properties [31]. Hence, our stiffness analysis results do not support and applicable to all designs of 3R mechanism and DPM. Instead, the study just shows the potential of the stiffness improvement with the DPM over the 3R mechanism. It is also noted that the stiffness analysis can be done analytically by assuming that the links are regular shapes [32].

8 Conclusion

This paper presents a novel spherical mechanism for a shoulder exoskeleton joint composed of two revolute joints connected by a double parallelogram linkage. The proposed design has a relative large range of motion free of singularity and good manipulability properties. Compared to the conventional 3R mechanism, the proposed design has a high overall stiffness. FEA simulations show that the DPM has mean stiffness significantly greater than the 3R mechanism.

In the paper, both global and local singularities are analyzed. In the local singularity analysis, four singularities were identified for the DPM.

Dimensional analysis was carried out with different configurations and dimensions of the DPM upon which the design with largest range of motion is identified.

A prototype of the novel design was developed and installed in an upper-body exoskeleton. The real workspace of the shoulder joint was experimentally investigated. The results show that the proposed design is able to general rotations in a large range of motion without interference with the user of the exoskeleton. As a result, the design is well suited for portable upper-body exoskeletons.

References

- [1] Sylla, N., Bonnet, V., Colledani, F., and Fraisse, P., 2014, "Ergonomic Contribution of ABLE Exoskeleton in Automotive Industry," *Int. J. Ind. Ergonom.*, **44**(4), pp. 475–481.
- [2] Bogue, R., 2009, "Exoskeletons and Robotic Prosthetics: A Review of Recent Developments," *Ind. Robot: An Int. J.*, **36**(5), pp. 421–427.
- [3] Yamamoto, K., Hyodo, K., Ishii, M., and Matsuo, T., 2001, "Development of Power Assisting Suit for Assisting Nurse Labor," *Trans. Jpn. Soc. Mech. Eng. Ser. C*, **67**(657), pp. 1499–1506.
- [4] Lo, H. S., and Xie, S. Q., 2012, "Exoskeleton Robots for Upper-Limb Rehabilitation: State of the Art and Future Prospects," *Med. Eng. Phys.*, **34**(3), pp. 261–268.
- [5] Gopura, R., Bandara, D., Kiguchi, K., and Man, G., 2015, "Developments in Hardware Systems of Active Upper-Limb Exoskeleton Robots: A Review," *Rob. Auton. Syst.*, **75**(Pt. B), pp. 203–220.
- [6] Engin, A. E., 1980, "On the Biomechanics of the Shoulder Complex," *J. Biomech.*, **13**(7), pp. 575–590.
- [7] Naidu, D., Stopforth, R., Bright, G., and Davrajh, S., 2011, "A 7 DOF Exoskeleton Arm: Shoulder, Elbow, Wrist and Hand Mechanism for Assistance to Upper Limb Disabled Individuals," *IEEE AFRICON Conference*, Livingstone, Zambia, Sept. 13–15, pp. 13–15.
- [8] Ball, S. J., Brown, I. E., and Scott, S. H., 2007, "MEDARM: A Rehabilitation Robot With 5DOF at the Shoulder Complex," *IEEE/ASME International Conference on Advanced Intelligent Mechatronics (AIM)*, Zurich, Switzerland, Sept. 4–7.
- [9] Nef, T., Guidali, M., and Riener, R., 2009, "ARMin III Arm Therapy Exoskeleton With an Ergonomic Shoulder Actuation," *Appl. Bionics Biomech.*, **6**(2), pp. 127–142.
- [10] Carmichael, M. G., and Liu, D. K., 2015, "Human Biomechanical Model Based Optimal Design of Assistive Shoulder Exoskeleton," *Field and Service Robotics: Results of the 9th International Conference*, L. Mejias, P. Corke, and J. Roberts, eds., Springer International, Cham, Switzerland, pp. 245–258.
- [11] Perry, J. C., Rosen, J., and Burns, S., 2007, "Upper-Limb Powered Exoskeleton Design," *IEEE/ASME Trans. Mechatronics*, **12**(4), pp. 408–417.
- [12] Jung, Y., and Bae, J., 2013, "Kinematic Analysis of a 5 DOF Upper-Limb Exoskeleton With a Tilted and Vertically Translating Shoulder Joint," *IEEE/ASME International Conference on Advanced Intelligent Mechatronics (AIM)*, Wollongong, Australia, July 9–12, pp. 1643–1648.

- [13] Yan, H., Yang, C., Zhang, Y., and Wang, Y., 2014, "Design and Validation of a Compatible 3-Degrees of Freedom Shoulder Exoskeleton With an Adaptive Center of Rotation," *ASME J. Mech. Des.*, **136**(7), p. 071006.
- [14] Chakarov, D., Veneva, I., Tsveov, M., and Tiankov, T., 2014, "New Exoskeleton Arm Concept Design and Actuation for Haptic Interaction With Virtual Objects," *J. Theor. Appl. Mech.*, **44**(4), pp. 3–14.
- [15] Lo, H. S., and Xie, S., 2014, "Optimization and Analysis of a Redundant 4R Spherical Wrist Mechanism for a Shoulder Exoskeleton," *Robotica*, **32**(8), pp. 1191–1211.
- [16] Klein, J., Spencer, S., Allington, J., Bobrow, J. E., and Reinkensmeyer, D. J., 2010, "Optimization of a Parallel Shoulder Mechanism to Achieve a High-Force, Low-Mass, Robotic-Arm Exoskeleton," *IEEE Trans. Rob.*, **26**(4), pp. 710–715.
- [17] Hunt, J., Lee, H., and Artemiadis, P., 2016, "A Novel Shoulder Exoskeleton Robot Using Parallel Actuation and a Passive Slip Interface," *ASME J. Mech. Rob.*, **9**(1), p. 011002.
- [18] Hsieh, H. C., Chen, D. F., Chien, L., and Lan, C. C., 2017, "Design of a Parallel Actuated Exoskeleton for Adaptive and Safe Robotic Shoulder Rehabilitation," *IEEE/ASME Trans. Mechatronics*, **22**(5), pp. 2034–2045.
- [19] Cui, X., Chen, W., Jin, X., and Agrawal, S. K., 2017, "Design of a 7-DOF Cable-Driven Arm Exoskeleton (CAREX-7) and a Controller for Dexterous Motion Training or Assistance," *IEEE/ASME Trans. Mechatronics*, **22**(1), pp. 161–172.
- [20] Xu, K., Zhao, J., Qiu, D., and Wang, Y., 2014, "A Pilot Study of a Continuum Shoulder Exoskeleton for Anatomy Adaptive Assistances," *ASME J. Mech. Rob.*, **6**(4), p. 041011.
- [21] Bai, S., Christensen, S., and Islam, M. R. U., 2017, "An Upper-Body Exoskeleton With a Novel Shoulder Mechanism for Assistive Applications," *IEEE/ASME International Conference on Advanced Intelligent Mechatronics (AIM)*, Munich, Germany, July 3–7, pp. 1041–1046.
- [22] Koo, D., Chang, P.-H., Sohn, M. K., and Shin, J. H., 2011, "Shoulder Mechanism Design of an Exoskeleton Robot for Stroke Patient Rehabilitation," *IEEE International Conference on Rehabilitation Robotics (ICORR)*, Zurich, Switzerland, June 29–July 1, pp. 8–13.
- [23] Culham, E., and Peat, M., 1993, "Functional Anatomy of the Shoulder Complex," *J. Orthopaedic Sports Phys. Ther.*, **18**(1), pp. 342–350.
- [24] Christensen, S., and Bai, S., 2017, "A Novel Shoulder Mechanism With a Double Parallelogram Linkage for Upper-Body Exoskeletons," *Second International Symposium on Wearable Robotics (WeRob)*, Segovia, Spain, Oct. 18–21, pp. 51–56.
- [25] Li, J., Zhang, G., Xing, Y., Liu, H., and Wang, S., 2014, "A Class of 2-Degree-of-Freedom Planar Remote Center-of-Motion Mechanisms Based on Virtual Parallelograms," *ASME J. Mech. Rob.*, **6**(3), p. 031014.
- [26] Li, J., Xing, Y., Liang, K., and Wang, S., 2015, "Kinematic Design of a Novel Spatial Remote Center-of-Motion Mechanism for Minimally Invasive Surgical Robot," *J. Med. Dev.*, **9**(1), p. 011003.
- [27] Hadavand, M., Mirbagheri, A., Behzadipour, S., and Farahmand, F., 2014, "A Novel Remote Center of Motion Mechanism for the Force-Reflective Master Robot of Haptic Tele-Surgery Systems," *Int. J. Med. Rob. Comput. Assisted Surg.*, **10**(2), pp. 129–139.
- [28] Bai, G., Li, D., Wei, S., and Liao, Q., 2014, "Kinematics and Synthesis of a Type of Mechanisms With Multiple Remote Centers of Motion," *J. Mech. Eng. Sci.*, **228**(18), pp. 3430–3440.
- [29] Spong, M. W., Hutchinson, S., and Vidyasagar, M., 2005, *Robot Modeling and Control*, Wiley, Hoboken, NJ.
- [30] Peebles, L., Norris, B., and Trade, G. B. D., 1998, *Adultdata: The Handbook of Adult Anthropometric and Strength Measurements: Data for Design Safety*, Government Consumer Safety Research, Nottingham, UK.
- [31] Teng, C. P., Bai, S., and Angeles, J., 2007, "Shape Synthesis in Mechanical Design," *Acta Polytechnica, Czech Tech. Univ. Prague*, **47**(6), pp. 56–62.
- [32] Wu, G., Bai, S., and Kepler, J., 2014, "Mobile Platform Center Shift in Spherical Parallel Manipulators With Flexible Limbs," *Mech. Mach. Theory*, **75**, pp. 12–26.

Chapter 4

Paper II

Modeling and Analysis of Physical Human-Robot Interaction of an Upper Body Exoskeleton in Assistive Application

Simon Christensen, Xuerong Li, Shaoping Bai

The paper has been published in the
Modeling, Identification and Control Vol. 42(4), pp. 159–172,
doi:2021.10.4173/mic.2021.4.2

The included paper has been approved for redistribution by the publisher.
Copyright ©2021



Modeling and Analysis of Physical Human-Robot Interaction of an Upper Body Exoskeleton in Assistive Applications

Simon Christensen¹ Xuerong Li¹ Shaoping Bai¹

¹Department of Materials and Production, Aalborg University, Aalborg 9220, Denmark. E-mail: {sic,xl,shb}@mp.aau.dk

Abstract

Portable exoskeletons can be used to assist elderly or disabled people in their daily activities. The physical human-robot interaction is a major concern in exoskeleton development for both functioning properly and interacting safely and comfortably. Using a model of the human musculoskeletal system and the exoskeleton can help better understanding, estimating and analyzing the physical human-robot interaction. In this paper, a model comprising the biomechanics of human upper body and the dynamics of a 4-DoF exoskeleton, named UB-AXO, is developed and used to study the physical human-robot interaction. The human-exoskeleton model is able to estimate effect of physical human-exoskeleton interaction, such as muscle activity, and energy consumption and human joint reaction forces, when performing cooperative motions with the exoskeleton. The model development is described and subsequently two simulation studies of typical activities of daily living are conducted to analyze and evaluate the performance of the UB-AXO. The simulation results demonstrate that the UB-AXO is able to reduce muscle loading and energy consumption, while maintaining a safe physical human-exoskeleton interaction.

Keywords: Physical Human-Robot Interaction, Biomechanical Modeling, Assistive Exoskeleton, Energy Exchange in pHRI, Overhead Reaching Tasks

1. Introduction

In the field of wearable robotics, exoskeletons are becoming more and more relevant in domains such as healthcare and industry Sylla et al. (2014); Bai et al. (2018). An exoskeleton is a robotic suit that is capable of producing supplementary muscular functions to its user, by either powered elements (e.g. electric motors) or passive elements (e.g. springs). The exoskeleton enables the user to lift a greater load or compensate for a lack of strength Bock et al. (2021); Gull et al. (2020); Pacifico et al. (2020). In general, exoskeletons are designed to transfer mechanical power to a specific set of human joints, e.g. elbow flexion/extension, by imitating the kinematics of the given body limbs.

Hence, assisting human movements using exoskeletons requires consideration of the contribution of both the human biomechanics and exoskeleton mechanics to the assisted joint. While exoskeletons have the potential to improve the users functionalities and strength, a safe and comfortable interaction with human limbs is a major design and control challenge. The operations of the exoskeleton must be properly coordinated and adapted to the human since unintended interaction can lead to injuries on the human.

Many factors affect the physical human-robot interaction (pHRI) Bicchi et al. (2008); De Santis et al. (2008); Heinzmann and Zelinsky (2003); Davis et al. (2020). One is the transfer of force from an exoskeleton to the human body and consequentially the energy

flow. The forces or torques exerted by the robot onto the human should be delivered as needed. This means that the magnitude of the assistive force/torque has to be specified properly from the perspective of control. Moreover, the interaction should be soft and compliant and most importantly must never exceed the human pressure tolerance.

Another issue in the pHRI is the alignment between human joints and the counterparts of an exoskeleton. Ideally, the exoskeleton should be well aligned with human limbs, but this is quite difficult to achieve, especially for the upper-body exoskeletons [Gopura et al. \(2016\)](#); [Schiele and van der Helm \(2006\)](#); [Zhou et al. \(2015\)](#); [Nf et al. \(2019\)](#). One reason is that the exact location of the human joint axes is not possible to know, simply because they are covered up by human skin, muscles and tissue. Moreover, biological joints are not ideal mechanical joints (like hinge or ball and socket joints), but are rather complex joints' surface geometries (bone on bone joints). As a result, the equivalent rotational joint axes tend to shift during motion. In addition, attachments of exoskeletons on human limbs are not rigid, meaning that slippage between the exoskeleton and the human limb can occur during operation. Consequently, these issues are likely to cause misalignment between the exoskeleton joint and the human joint in the order of a few centimeters [Schiele and van der Helm \(2006\)](#), which can generate undesired reaction forces in the human joint, leading to uncomfortable and possibly painful interaction with the exoskeleton [Schiele \(2008\)](#).

Biomechanical modeling of human-exoskeleton systems is an effective approach to address the aforementioned issues in pHRI. In previous works, musculoskeletal models have been used to analyze the physical interaction between the coupled human-exoskeleton systems [Agarwal et al. \(2016\)](#); [Zhou et al. \(2017\)](#); [Bai and Rasmussen \(2011\)](#); [Narayanan et al. \(2009\)](#). Using advanced musculoskeletal models can gain insight and predict the human response to assistance from exoskeleton. Moreover, using a virtual prototyping environment is less expensive and time consuming than building mock-up models for physical tests.

It is noticed in the models reported, the coupled human-exoskeleton system is usually assumed rigidly connected to the human. This is an oversimplified contact problem, as it cannot simulate the human contact with different attachment. Moreover, the simulations mainly addressed the interaction forces, the power flow is rarely considered.

In this work, a physical human-robot simulation model is developed for a portable upper-body assistive exoskeleton, named UB-AXO. The model includes a biomechanical human subsystem and a mechanical ex-

oskeleton subsystem, both integrated for physical assistance simulations. A contact model is utilized for an improved physical human-exoskeleton interaction modeling. The model is developed by virtue of an advanced biomechanical model of the upper body, which is developed through the AnyBody Modeling System (AnyBody Technology A/S, Aalborg, Denmark). Six different case studies are considered in order to assess the performance of the UB-AXO in collaboration with the human user. The developed model allows us to understand the mechanics of the cooperative human-exoskeleton system, and finally to design and control exoskeletons with improved physical human-robot interaction.

2. A conceptual design of an upper-body assistive exoskeleton (UB-AXO)

Our interest is the pHRI in assistive exoskeletons, which work cooperatively with human to perform a certain limb movement. Our model is developed for an assistive exoskeleton named UB-AXO. The UB-AXO is an upper-body exoskeleton developed at Aalborg University, Denmark, see [Fig. 1](#). It is designed to assist the user at joint level with activities such as lifting and carrying objects. The UB-AXO has a total of four degrees of freedom, three at the shoulder and one at the elbow joint.

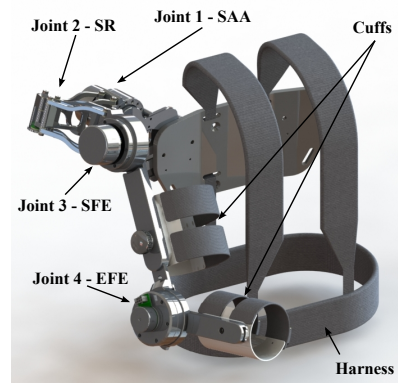


Figure 1: Conceptual design of the UB-AXO

The shoulder mechanism is designed to match the three degrees of freedom of human glenohumeral joint. The shoulder abduction/adduction (SAA) and flexion/extension (SFE) joints are powered, while shoulder internal/external rotation (SR) joint is passively

supported by a double parallelogram linkage (DPL) [Christensen and Bai \(2018\)](#). The elbow mechanism is a single powered joint that supports flexion/extension of the human elbow (EFE). All active joints are composed by a harmonic gear and brushless DC-motor. The harmonic gear is selected for its back-drivability, which allows the user to move even if the motors are powered off.

The UB-AXO is worn by the user through a torso harness, an upper arm cuff and a forearm cuff. The torso harness is composed by a hard back plate fitted with shoulder straps and snap buckle belt for rapidly fitting and easy tightening to the user. Both the upper arm and forearm cuffs consist of a flexible plastics material and are tighten to the limb using velcro straps.

The base of the shoulder mechanism, i.e. the shoulder abduction/adduction joint, and the upper arm link are adjustable to fit the user’s body size.

3. Biomechanical model of the human-exoskeleton system

The human-exoskeleton system is a cooperative system of the exoskeleton mechanics and the human biomechanics, see [Fig. 2](#). Thus, the model is built with two subsystems, namely, the human and the exoskeleton. The biomechanics of the human upper body is considered through a musculoskeletal model by simulating the movements of the arm and the required muscle activations, while the exoskeleton model incorporates the dynamics and control of the exoskeleton.

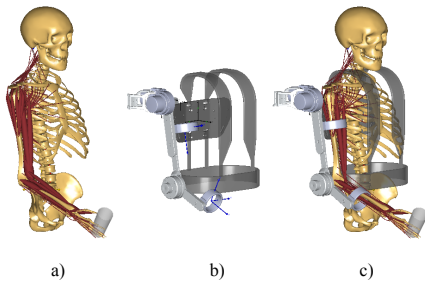


Figure 2: Model of the human-exoskeleton system: a) the human biomechanics, b) the exoskeleton model, c) the cooperative human-exoskeleton system

3.1. Musculoskeletal model of the human upper body

The musculoskeletal model of the human upper body is modeled as a multi-body system, where human bones and joints are considered as mechanical links and ideal joints. Muscles are unidirectional actuators that exert forces on the system. Because of the redundancy of muscles in the system, the system is statically indeterminate. Therefore, the muscle recruitment is formulated as an optimization problem, named direct muscle recruitment [Rasmussen et al. \(2001\)](#):

$$\begin{aligned} \min G(\mathbf{f}^M) \\ \text{s.t. } \mathbf{C}\mathbf{f} = \mathbf{d} \end{aligned} \quad (1)$$

Here $\mathbf{f} = [\mathbf{f}^M \ \mathbf{f}^R]$ is a vector with all unknown forces, where \mathbf{f}^M is an array of the muscle forces and \mathbf{f}^R is the reaction forces in the joints. The matrix \mathbf{C} is a coefficient matrix formed from the human anatomy and muscle attachments and finally, the vector \mathbf{d} is an array of the external forces acting on the human. The objective function $\min G(\mathbf{f}^M)$ is the muscle recruitment criterion and is usually a polynomial criterion, but soft saturation and min/max criterion are also feasible [Rasmussen et al. \(2001\)](#). In this paper, the polynomial criterion is applied:

$$\min G(\mathbf{f}^M) = \sum_i \left(\frac{f_i^M}{N_i^M} \right)^p \quad (2)$$

The term f_i^M/N_i^M is referred to as muscle activity. Here N_i^M is a normalization factor or function for the i -th muscle, which represents the strength of the muscle. Hence, the stronger the muscle, the larger the normalization factor. The power p represents the synergism between the muscles. In this work, the power of $p = 3$ is used, as numerical experiments with it yield good results for submaximal loads. The muscle activities range from 0 to 1, where 0 is an unloaded muscle and 1 is a fully loaded muscle. The muscle forces are calculated using a three-element Hill-type muscle model, which consists of a contractile element (CE), a parallel elastic element (PE) and a serial elastic element (SE) [Winter \(2008\)](#).

In addition to the muscle activities, we are also interested to find the metabolic cost. The metabolic energy is a common evaluation measure for assistive devices and is often experimentally determined by a VO2 mask, which measures the volume of oxygen consumption by the test subject [Rowe \(2020\)](#). While modeling the individual muscle metabolic energy requires complex formulas [Bhargava et al. \(2004\)](#), which includes

information on heat dissipation of the muscle, we calculate in this work the human energy consumption from the mechanical work produced by the contractile element of the muscle model, i.e. the active element of the muscle model. The muscle work rate \dot{W} is calculated as:

$$\dot{W} = f_{CE}(l_{CE}, v_{CE}, s) v_{CE} \quad (3)$$

where f_{CE} is the force produced by the contractile muscle element, which is a function of the length l_{CE} and velocity v_{CE} of the element along with the muscle activity s . For the muscles, both positive and negative works are possible. When a muscle produces positive work, or concentric work, energy is fed to the musculoskeletal system. On the other hand, when a muscle produces negative work, or eccentric work, energy is extracted from the musculoskeletal system. The contractile element of the muscle cannot store energy, instead the energy is dissipated as heat. Hence, the total human energy consumption is estimated as the absolute value of the external work done on the human bodies:

$$E = \sum_{i=1}^N \int_{t_i}^{t_f} |\dot{W}_i| dt \quad (4)$$

where N is the total number of muscles in the model.

3.2. Exoskeleton model

The configuration of the UB-AXO is illustrated in Fig. 3. The shoulder mechanism is composed by the first three revolute joints, which together form a spherical joint, equivalent to the glenohumeral joint of the human shoulder. The fourth revolute joint makes up the elbow mechanism. The Denavit-Hartenberg parameters for the UB-AXO are listed in Table 1, where L_u is the length of the upper arm and L_f is the length of the forearm.

Table 1: Denavit-Hartenberg parameters of the UB-AXO

Link, i	a_i	α_i	d_i	θ_i
1	0	$-\pi/2$	0	θ_1
2	0	$\pi/2$	0	θ_2
3	L_u	0	0	θ_3
4	L_f	0	0	θ_4

The Jacobian of the exoskeleton can be calculated through the velocity propagation from link to link,

which yields:

$$\mathbf{J} = \begin{bmatrix} J_{11} & J_{12} & J_{13} & J_{14} \\ J_{21} & J_{22} & J_{23} & J_{24} \\ 0 & J_{32} & J_{33} & J_{34} \\ 0 & J_{42} & J_{43} & J_{44} \\ 0 & J_{52} & J_{53} & J_{54} \\ 1 & 0 & J_{63} & J_{64} \end{bmatrix} \quad (5)$$

where the elements of the Jacobian are listed in the Appendix A.

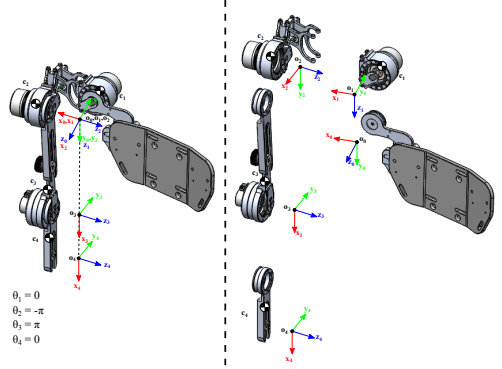


Figure 3: The coordinate systems of the UB-AXO

The inverse dynamics of the exoskeleton is derived using the Euler-Lagrange equation and expressed as:

$$\mathbf{M}(\boldsymbol{\theta}) \ddot{\boldsymbol{\theta}} + \mathbf{c}(\boldsymbol{\theta}, \dot{\boldsymbol{\theta}}) + \mathbf{g}(\boldsymbol{\theta}) = \boldsymbol{\tau} \quad (6)$$

where \mathbf{M} is the mass matrix, \mathbf{c} is a vector with the Coriolis and centrifugal forces, \mathbf{g} is the vector of gravitational forces, $\boldsymbol{\tau}$ is the vector with joint torques and $\boldsymbol{\theta}$ is a vector with the joint angles, as illustrated in Fig. 3.

3.3. Assistance from exoskeleton

The UB-AXO is designed to assist the human body at joint levels, i.e. shoulder abduction/adduction and flexion/extension and elbow flexion/extension, while shoulder internal/external rotation is left passive and unassisted. In assistive applications of active joints, the assistive torques are determined through a control strategy that uses inputs from the system.

In this work, a static-load compensation strategy is adopted, as illustrated in Fig. 4. The assistive torque of each active joint $\boldsymbol{\tau}_{ass}$ is calculated with three parts; an exoskeleton gravity compensation torque $\boldsymbol{\tau}_{exo}$, a human gravity compensation torque $\boldsymbol{\tau}_g$ and torque for external loads $\boldsymbol{\tau}_l$.

$$\boldsymbol{\tau}_{ass} = \boldsymbol{\tau}_{exo} + \mathbf{K}(\boldsymbol{\tau}_g + \boldsymbol{\tau}_l) \quad (7)$$

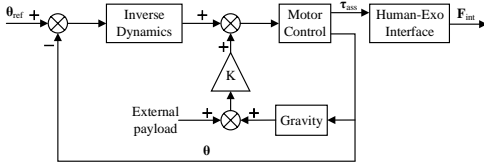


Figure 4: Implementation of the control strategy in the human-exoskeleton model, \mathbf{F}_{int} standing for assistive interaction force to human limb

where $\mathbf{K} = \text{diag}(k_1, k_2, k_3, k_4)$ is the assistance levels at all joints. It should be noted that k_2 and the second entry of $\boldsymbol{\tau}_{exo}$ are equal to zero, as joint 2 in our exoskeleton is a passive joint.

Typically, the mechanical interaction between the human and exoskeleton is addressed through interaction control, such as impedance or admittance control (L. Pons (2008)). Because accelerations and velocities of the human movement are assumed small, the interaction between the human and exoskeleton can be considered quasi-static and the mechanical interaction is simplified to a gravity compensation of the exoskeleton. Hence, the exoskeleton gravity compensation torque is calculated as:

$$\boldsymbol{\tau}_{exo} = \mathbf{g}(\boldsymbol{\theta}) \quad (8)$$

The human gravity compensation torque is based on estimated mass properties of the human. In Winter (2008), the mass of individual body limbs are linked to the total weight of the body, namely, the mass of the upper arm is approximately 2.8% of the total body mass, while the forearm makes up 1.6% of the total body mass Winter (2008), that is:

$$m_u = 0.028m_b, \quad m_f = 0.016m_b \quad (9)$$

As the exoskeleton is presumably kinematically compatible with the human kinematics, the human gravity compensation torques can be calculated from the exoskeleton joint angles.

$$\boldsymbol{\tau}_g = \mathbf{g}_h(\boldsymbol{\theta}) \quad (10)$$

where \mathbf{g}_h is a vector with the estimated human gravitational forces.

The external load is not directly attached to the exoskeleton, but at the hand of the human. The nature of the external load can be quite complex for a variety of tasks where the human interacts with the environment, e.g. opening a door or pushing an object on a table. Regardless of the complexity of the external load, the Jacobian in Eq. (5) can be used to link the

external load at the human hand with the exoskeleton joint torques.

$$\boldsymbol{\tau}_l = \mathbf{J}^T \mathbf{F}_{ext} \quad (11)$$

where \mathbf{F}_{ext} is a vector with the external load expressed with respect to the global reference frame.

3.4. Human-exoskeleton model

The two subsystems, i.e. the musculoskeletal model of human body and the CAD model of the exoskeleton, are implemented in the AnyBody Modeling System, see Fig. 2. AnyBody Modeling System in its essence is an inverse dynamics simulation software that uses a generic musculoskeletal model of human body to study the internal body loads, i.e. muscle, ligament and joint forces, under different motions and external loads. In this study, the musculoskeletal model is comprised of a human torso and right arm, which is derived from the repository in AnyBody. The exoskeleton model is built in SolidWorks and exported to AnyBody. The motion of the musculoskeletal arm is used to drive the cooperative system. The arm motion is generated from motion capture data of people doing the specific task or set of tasks. For simple tasks, such as an arm curl, the model can be driven by explicit functions for each joint.

As the human musculoskeletal and exoskeleton subsystems are connected via attachments, additional kinematic constraints and a contact model need to be defined for the whole system, as described presently.

3.5. Kinematic constraints

The exoskeleton model is connected to the musculoskeletal model at the three ports of power transfer, namely the torso harness, upper arm and forearm cuff. The torso harness is fixed to the torso of the musculoskeletal model by six kinematic constraints, such that the shoulder module is aligned with the human glenohumeral joint. The upper arm and forearm cuffs are attached at the mid point of the upper arm and forearm, respectively. Both cuffs are modeled as cylindrical joints, which add additional eight kinematic constraints. Hence, in total 18 kinematic constraints are used to connect the exoskeleton model to the musculoskeletal model. The UB-AXO has a total of ten degrees of freedom, before it is mounted to human body. The additional 18 kinematic constraints make the whole system kinematically over-determined and there is no unique solution to the kinematics. This problem is solved as an optimization problem, where the constraints are divided into 'hard' and 'soft' constraints. Hard constraints are constraints in the kinematic analysis, which must be fulfilled, while soft constraints are constraints that should be fulfilled as well

as possible by the optimization algorithm. As a result, small kinematic errors are introduced to the model. Similar effect can be experienced in a ‘real’ application, where the human and exoskeleton exhibit small relative motions because of the wearer’s skin or clothes. All kinematic constraints, in this work, are defined as soft constraints, where the allowable kinematic error for the solver is set to 0.1%.

3.6. Contact modeling

The physical interaction between the human and exoskeleton is a contact problem. The assisting torques from the exoskeleton are transmitted to the human musculoskeletal system via contact forces acting between the exoskeleton cuffs and the skin of the human.

The contact forces are determined by calculating the reaction forces between two nodes, a base and a target node, one on the human musculoskeletal body and the other on the exoskeleton. A cylindrical space is defined around the base node. When the target node enters the cylindrical space of the base node, contact is established between the two objects, see Fig. 5. The contact forces are modeled as unilateral normal force and a perpendicular friction force. The friction force is limited by the size of the normal force and the friction coefficient. A set of base nodes are defined on the exoskeleton at the upper arm and forearm cuffs. The nodes form a circular arc with a radius r upon which a total of 12 base nodes are evenly distributed. From anthropometric measurements listed in Peebles and Norris (1999), the inner diameter of the upper arm is estimated to 103 mm and forearm is estimated to 76 mm, which fits 50% of the population.

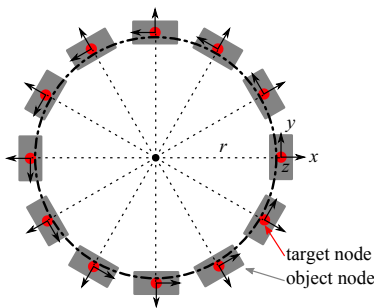


Figure 5: Implementation of contact element for human-exoskeleton interaction forces

Similarly, as for the muscle recruitment, the contact forces have an optimum value, which can be determined through a polynomial criterion. Hence, the

cost function in the direct muscle recruitment Eq. (2) is updated to include the contact forces Skals et al. (2016):

$$\min G(\mathbf{f}^M) = \sum_i \left(\frac{f_i^M}{N_i^M} \right)^3 + \sum_j \left(\frac{f_j^C}{N_i^C} \right)^3 \quad (12)$$

where f_j^C is the contact force and N_i^C is the optimal contact force.

4. Simulation studies

To evaluate the performance of the exoskeleton, two cases are considered. In the first case, the elbow mechanism performs a simple bicep curl, while in the second case, the shoulder mechanism assists an overhead reach task. In both simulations, the motion is generated from explicit functions of the individual joints. The payload in the biceps curl case is 2 kg, while for the overhead reach it is 1 kg. For each case, three studies are simulated. The first study simulates the musculoskeletal model performing the task without the exoskeleton. The second and third studies simulate the musculoskeletal model with the exoskeleton providing 30% and 50% assistance, respectively. The assistance level is controlled through the assistance matrix, \mathbf{K} , from Eq. (7), where the 30% (low-level) assistance implies $k_1 = k_3 = k_4 = 0.3$ and 50% (high-level) assistance implies $k_1 = k_3 = k_4 = 0.5$.

4.1. Case 1 - Bicep curl

In the bicep curl case, the elbow is flexed from 120° to 30° and back again over a period of 3s, see Fig. 6. Furthermore, the shoulder is slightly flexed to an angle of 5° to keep the load free from the body.

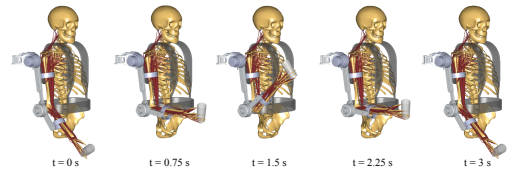


Figure 6: Simulation study of the human-exoskeleton system during the bicep curl

The equivalent human joint torque for each of the degrees of freedom in the arm, are shown in Figs. 7(a)-7(d). As expected, the most loaded joints are shoulder flex/ext (SFE) and elbow flex/ext (EFE), while shoulder abd/add (SAA) and int/ext rotation (SR) are less loaded. Adding the exoskeleton to the simulation leads

Table 2: Mean muscle activation expressed with equivalent joint torques and maximum muscle activity during biceps curl

Motion	Mean muscle activation	Level of assistance		
		w/o Exo	30%	50%
SAA	Torque [Nm]	3.44	0.65	-0.53
	Reduction [%]	-	81	84
SR	Torque [Nm]	0.42	0.22	0.12
	Reduction [%]	-	49	71
SFE	Torque [Nm]	10.62	6.36	4.41
	Reduction [%]	-	40	58
EFE	Torque [Nm]	8.75	4.76	3.0
	Reduction [%]	-	46	66
MMA	[-]	0.38	0.26	0.25
	Reduction [%]	-	30	33

to a reduction in all equivalent human joint torques throughout the entire motion. The internal/external rotation of the shoulder experiences a reduction in load, though it is left passive in the exoskeleton. This is caused by the way the human joint torques are calculated, which includes numerous muscle forces surrounding the shoulder glenohumeral joint. Hence, the assistance supplied by the exoskeleton shoulder abd/abd and flex/ext joint indirectly affects the equivalent human joint torque at the shoulder int/ext rotation.

Table 2 lists the mean equivalent human joint torques during the bicep curl. For the low-level assistance, i.e. 30% assistance, the reduction in muscle activity is in the range of 40-81%, while for the high-level assistance 45-84%. In both cases, the largest reduction is observed at the shoulder abd/add, where the low-level assistance reduced magnitude of the equivalent human joint torque by 81% and the high-level assistance (50%) by 84%.

The maximum muscle activity (MMA) of the muscles in the arm is shown in Fig. 8. The MMA is reduced for both assistance levels, where the largest reduction is seen in the peak value of the MMA. However, the minimum MMA is nearly unaffected. As a result, the mean MMA during the simulation is only slightly reduced from 30% for the low-level assistance to 33% for the high-level assistance, respectively.

The energy flow between the human and exoskeleton during the bicep curl is depicted by the muscle work rate of the human arm, as defined in Eq. (3), the power consumption of the active joints in the exoskeleton and the total human energy consumption, as defined in Eq. (4). The human energy consumptions for the three studies are listed in Table 3. The results show that the exoskeleton is able to reduce the energy consumptions with 45% and 64% for the low- and

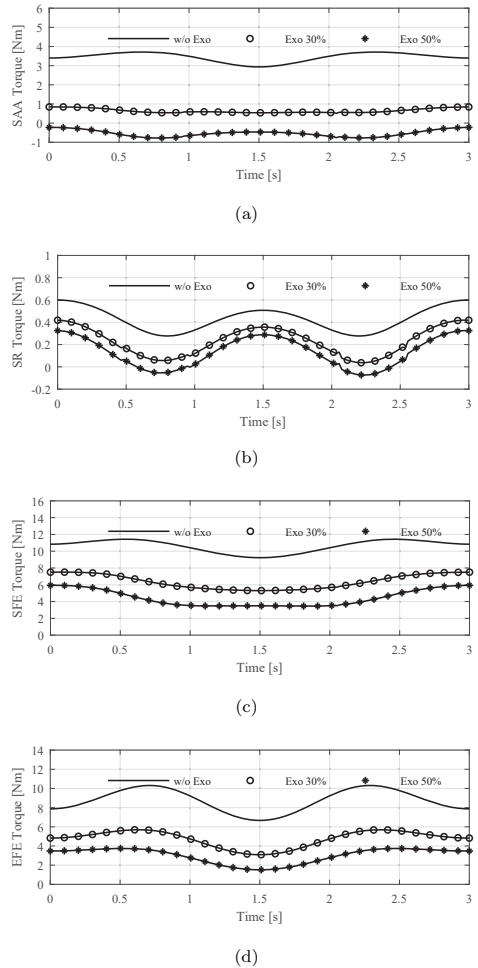


Figure 7: Equivalent joint torques in the human musculoskeletal system during the bicep curl; (a) shoulder abduction/adduction, (b) shoulder internal/external rotation, (c) shoulder flexion/extension, (d) elbow flexion/extension

high-level assistance, respectively. Hence, the exoskeleton is able to reduce energy consumption satisfactorily according to the control strategy.

In the first half of the simulation, from 0 to 1.5s, the collective muscles of the upper body carry out concentric work to lift the load, while for the second half of the simulation, from 1.5 to 3s, the muscles carry out eccentric work to lower the load, see Fig. 9(a). The power consumption of the exoskeleton is mostly related

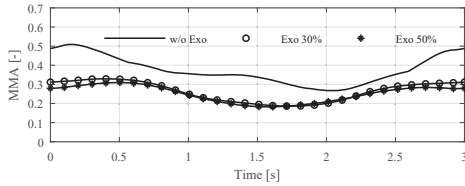


Figure 8: Maximum muscle activity (MMA) in the collective muscles of the upper body during bicep curl

Table 3: Human energy consumption during bicep curl

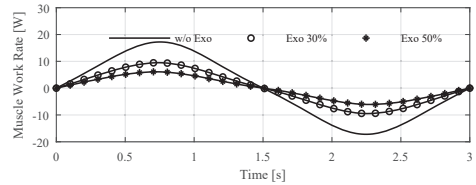
Energy consumption	Level of assistance		
	w/o Exo	30%	50%
Human energy consumption [J]	29.7	16.4	10.6
Reduction in energy consumption [%]	-	45	64

to the elbow joint, since both shoulder joints are static, see Figs. 9(b)-9(d). Similarly, as for muscles, the elbow produces positive work in the first half of the simulation and negative work in the second half. Hence, energy is extracted from the human through the exoskeleton electric motors. The design of the electronics of the exoskeleton must be able to handle the excessive energy by either storing it or having it dissipated.

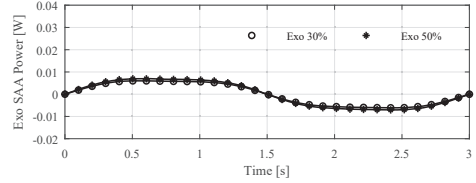
Like the muscle activity, the magnitude of reaction forces in both the shoulder glenohumeral and the elbow joints are reduced when the exoskeleton is assisting the human motion, see Figs. 10(a) and 10(b), with results summarized in Table 4. The mean reaction force in the shoulder is reduced with 45% and 64% for the low- and high-level assistance, respectively, and the mean reaction force in the elbow is reduced with 25% and 29%, respectively.

Table 4: Magnitude of the mean joint reaction forces during biceps curl

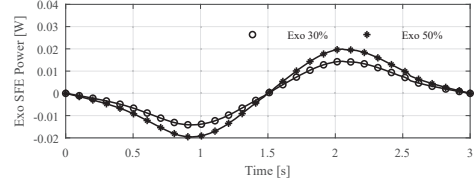
Joint	Mean joint reaction force	Level of assistance		
		w/o Exo	30%	50%
Shoulder	Force [N]	413.3	223.6	149.2
	Reduction [%]	-	45	64
Elbow	Force [N]	171.0	127.8	121.1
	Reduction [%]	-	25	29



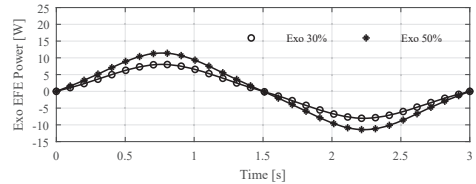
(a)



(b)



(c)

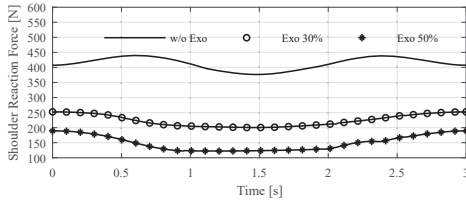


(d)

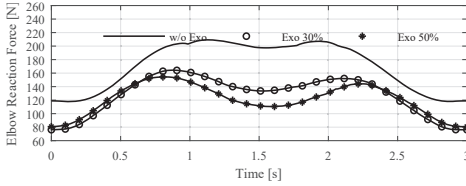
Figure 9: Energy flow in between the human and exoskeleton during the bicep curl depicted by: (a) the total muscle work rate, (b) the power consumption of the shoulder abb/abd, (c) the power consumption of the shoulder flex/ext, (d) the power consumption of the elbow flex/ext

4.2. Case 2 - Overhead reach

In the overhead reach study, a load is lifted from a table to a shelf above shoulder height over a period of 2s. During the lift, the load moved from the outside of the body and across the body, see Fig. 11. This motion requires all degrees of freedom in the shoulder engaged.



(a)



(b)

Figure 10: Magnitude of joint reaction forces in the human musculoskeletal system during the bicep curl; (a) shoulder glenohumeral joint, (b) elbow joint

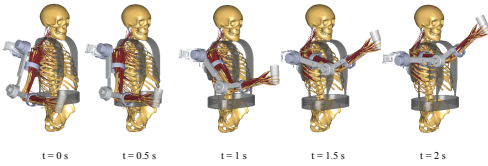
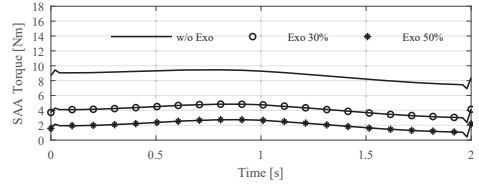


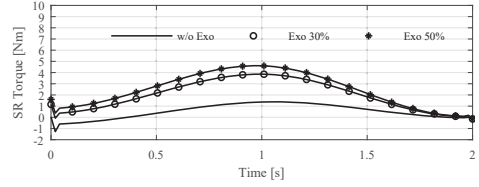
Figure 11: Simulation study of the human-exoskeleton system during the overhead reach

The human joint torques are shown in Figs. 12(a)-12(d) and the results are summarized in Table 5. The most loaded motions are shoulder flex/ext, shoulder abb/abd and elbow flex/ext, while shoulder int/ext rotation is nearly unloaded. Adding the exoskeleton to the simulation leads to a reduction in all assisted human joint torques throughout the entire motion.

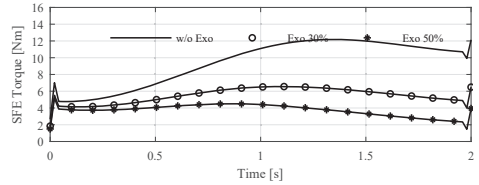
The mean muscle activity is reduced with 42% to 56% for the low-level assistance case and 61% to 78% for the high-level assistance case, respectively. Hence, the mean muscle activity is reduced with slightly more than intended, i.e. 30% and 50%, respectively. It is also noticed that the mean muscle activity for the shoulder internal/external rotation is increased significantly, with 281% and 372%, respectively. On the other hand, the torques are still small, which implies that a passive shoulder internal/external rotation is feasible for the



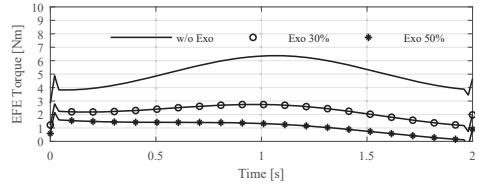
(a)



(b)



(c)



(d)

Figure 12: Equivalent joint torques in the human musculoskeletal system during the overhead reach, (a) shoulder abduction/adduction, (b) shoulder internal/external rotation, (c) shoulder flexion/extension, (d) elbow flexion/extension

assistance of the overhead reach.

The MMA of the muscles in the arm is shown in Fig. 13. The MMA is reduced with the aid of the exoskeleton for both the low-level and high-level assistance. The mean MMA during the simulations, listed in Table 5, is reduced with 45% in the low-level assistance and 62% for the high-level assistance.

The human energy consumption for the three sim-

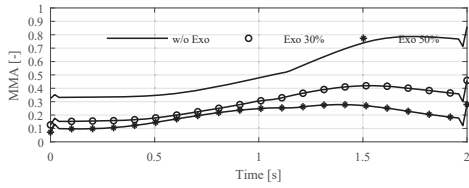


Figure 13: Maximum muscle activity (MMA) in the collective muscles of the upper body during the overhead reach

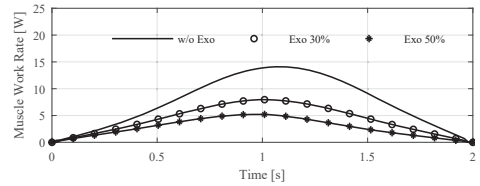
Table 5: Mean muscle activation expressed with equivalent joint torques and maximum muscle activity during overhead reach

Motion	Mean muscle activation	Level of assistance		
		w/o Exo	30%	50%
SAA	Torque [Nm]	8.76	4.12	2.05
	Reduction [%]	-	53	77
SR	Torque [Nm]	0.52	1.99	2.47
	Reduction [%]	-	-281	-372
SFE	Torque [Nm]	9.41	5.48	3.71
	Reduction [%]	-	42	61
EFE	Torque [Nm]	5.09	2.21	1.08
	Reduction [%]	-	56	78
MMA	[-]	0.53	0.29	0.20
	Reduction [%]	-	45	62

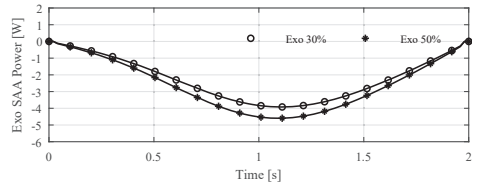
ulations are listed in Table 6. The results show that the exoskeleton is able to reduce the energy consumption with 43% and 63% for the low- and high-level assistance, respectively. Hence, the reduction in human energy consumption has a good consistency with the goal of the control strategy.

Throughout the entire overhead reach simulation, the collective muscles of the upper body are carrying out concentric work to lift the load, as shown in Fig. 14(a). Powers associated to motions at each joints are shown in Figs. 14(b)-14(d). It is noted that there exist both positive and negative powers, which imply that energy is both fed and extracted from the exoskeleton to the human. The shoulder and elbow flexion/extension joints both produced positive work to lift the load, while the shoulder abduction/adduction produced negative work to dampen the cross body movement.

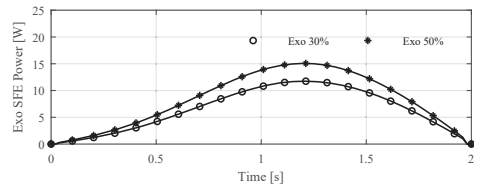
The magnitudes of reaction forces in both the shoulder glenohumeral and elbow joint are reduced when the exoskeleton is assisting the human motion, see Figs. 15(a) and 15(b). The magnitude of the mean reaction force in the shoulder is reduced by 36% and 47% for the low- and high-level assistance, respectively.



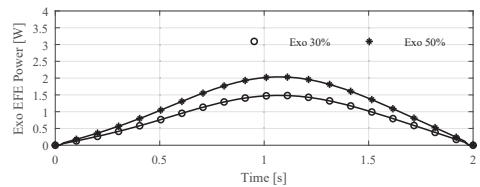
(a)



(b)



(c)



(d)

Figure 14: Energy flow in between the human and exoskeleton during the overhead reach depicted by: (a) the total muscle work rate, (b) the power consumption of the shoulder abb/abd, (c) the power consumption of the shoulder flex/ext, (d) the power consumption of the elbow flex/ext

For the elbow joint, the reduction of the mean reaction force is 53% and 52% for the low- and high-level assistance, respectively, as listed in Table 7.

Table 6: Human energy consumption during overhead reach

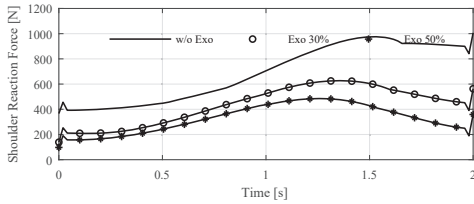
Energy consumption	Level of assistance		
	w/o Exo	30%	50%
Human energy consumption [J]	15.3	8.7	5.6
Reduction in energy consumption [%]	-	43	63

Table 7: Magnitude of the mean joint reaction forces during overhead reach

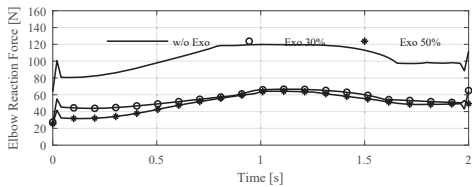
Joint	Mean joint reaction force	Level of assistance		
		w/o Exo	30%	50%
Shoulder	Force [N]	690.3	436.0	327.1
	Reduction [%]	-	36	53
Elbow	Force [N]	104.2	54.9	49.8
	Reduction [%]	-	47	52

5. Physical construction of UB-AXO

A prototype of the UB-AXO is built, as shown in Fig. 17 with the design specifications for the upper-body exoskeleton listed in Table 8. The total weight



(a)



(b)

Figure 15: Magnitude of joint reaction forces in the human musculoskeletal system during the overhead reach, (a) shoulder glenohumeral joint, (b) elbow joint

of the UB-AXO is 10 kg and includes a 3 kg Li-ion battery, which can power the suit continuously for approximately 4 hours. The prototype will be utilized to test in the physical human-exoskeleton interaction.

Table 8: Actuation of the UB-AXO. Joints 1 and 3 are the active joints in the shoulder mechanism and joint 4 is the elbow joint. Joint 2 is the passive degree of freedom of the DPL

	Joint 1	Joint 2	Joint 3	Joint 4
Motor Type	EC-60	-	EC-60	EC-45
Gear Type	LCS-17-80	-	CSD-25-50	CSD-25-50

The upper arm and forearm cuffs are designed based on the simulated contact forces, which must be less than a safe limit. If the contact forces are too high, the use of an exoskeleton may lead to skin irritation and even pressure ulcers Lyder (2003). Excessive skin pressure can compromise both safety and comfort. Regarding safety, the common guideline is to avoid pressures above the ischemic level Lyder (2003); L. Pons (2008), which is the level at which the capillary vessels are no longer able to conduct blood. On the other hand, a comfortable pressure is more complex to define, since it is a highly subjective measure. In Farasyn and Meeusen (2003), a study was conducted on 34 healthy adults to determine the pressure pain threshold (PPT) on selected points on the upper body. The PPT is a measure for the minimum pressure that induces pain or discomfort of human, which can be used to justify whether or not the exoskeleton is comfortable to wear. The PPT of the upper arm is in the range of 83.5 to 96.6 kPa Farasyn and Meeusen (2003). The contact forces in the simulations are linked to contact pressure by estimating the equivalent area that the contact force acts on.

$$p_j^C = \frac{f_j^C}{A_j^C} \quad A_j^C = \frac{d\pi w}{12} \quad j = 1, 2, \dots, 12 \quad (13)$$

where p_j^C is the contact pressure of the j -th node, A_j^C is the equivalent area, and d and w are the diameter and width of the cuff, respectively. The diameter of the two cuffs are determined in Section 3.6 as 103 mm for the upper arm and 76 mm for forearm. The cuffs are designed to have a width of 150 mm, thus the minimum discomfort pressure force can be determined from Eq. (13) as 337-390 N for the upper arm and 249-288 N for the forearm. The contact forces in both the biceps curl and overhead reach simulations are shown in Figs. 16(a) to 16(d). The maximum contact forces

for both upper arm and forearm are below the minimum discomfort pressure forces, which indicates that the exoskeleton is comfortable to wear.

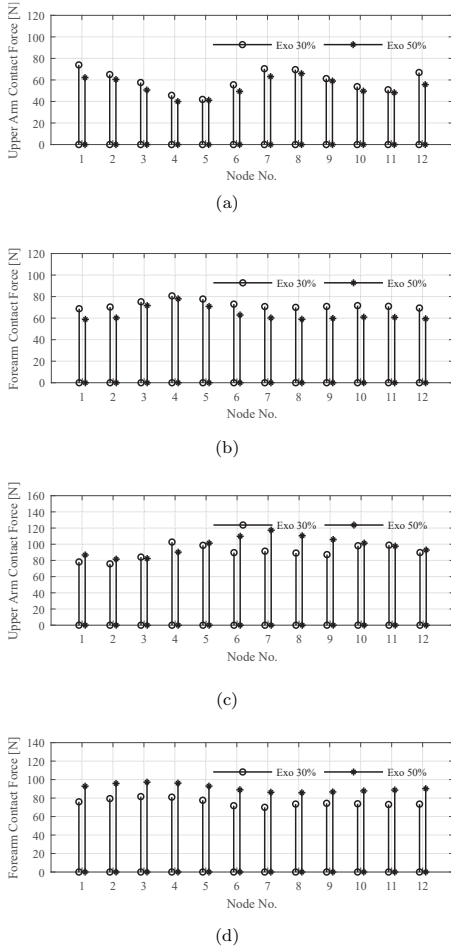


Figure 16: Maximum normal forces of the contact model nodes in: (a) upper arm cuff in biceps curl study, (b) forearm cuff in biceps curl study, (c) upper arm cuff in overhead study, (d) forearm cuff in overhead study

6. Discussion and conclusions

In this paper, a human-exoskeleton model is developed for modeling and analyzing the physical interaction between a human arm and a 4-DoF upper-body ex-



Figure 17: The built prototype of the UB-AXO

oskeleton named UB-AXO. In the model, major factors that affect the physical human-robot interaction are duly considered. They cover the torques and reaction forces at the human joints and the power and energy consumption in the motion assistance. Moreover, the problem of physical contact between the exoskeleton and the human limb is addressed. The model allows us to estimate the dynamic behavior of the human-exoskeleton system and conduct comprehensive simulations to improve our understanding on the pHRI and to finally design an exoskeleton with optimized pHRI.

Two cases were simulated, one for a bicep curl and the other for an overhead reach. The simulation results show that the use of the proposed exoskeleton can significantly reduce both the required maximum muscle activity, targeted human joint torques and muscle energy consumption in the human arm. In our simulated study, the mean maximum muscle activity during the motions was reduced by 30% to 45% with the low-level assistance control and 33% to 62% for the high-level assistance control. The targeted joint torques, i.e. shoulder abduction/adduction and flexion/extension and elbow flexion/extension, were reduced by 40% to 81% with the low-level assistance control and 58% to 84% for the high-level assistance control. The largest reductions in joint torques and maximum muscle activity were achieved in static postures, which is in good agreement with the selected control strategy.

The simulation reveals also energy exchange between human and exoskeleton during the physical human-robot interaction. The energy exchange was studied in terms of instantaneous exoskeleton joint powers and human muscle work rate along with the overall energy

consumption. In the simulated cases, the human energy consumption was reduced with 45% and 43% for the low-level assistance control and 64% and 63% for the high-level assistance control in the bicep curl and overhead reach simulation, respectively. The study of energy exchange in pHRI is useful for the development of control strategy and also for the optimum design of the exoskeleton systems.

The simulated cases in this paper include only a bicep curl and overhead reach. With the developed model, more cases of daily activities can be conducted, for example, hand lifting, arm carrying, side reach, etc. On the other hand, experiments of physical human-robot interaction with the physical exoskeleton system are desirable for comparison with the simulation results. Extra cases of study and experimental investigation are tasks considered in the future.

References

- Agarwal, P., Neptune, R. R., and Deshpande, A. D. A simulation framework for virtual prototyping of robotic exoskeletons. *Journal of Biomechanical Engineering*, 2016. 138(6):061004. doi:[10.1115/1.4033177](https://doi.org/10.1115/1.4033177).
- Bai, S. and Rasmussen, J. Modelling of physical human-robot interaction for exoskeleton designs. *Proc. of Multibody Dynamics 2011, ECCOMAS Thematic Conference*, 2011. (July):1–7.
- Bai, S., Virk, G. S., and Sugar, T. G. *Wearable exoskeleton systems: Design, control and applications*, volume 108. Control, Robotics and Sensors, 2018.
- Bhargava, L. J., Pandey, M. G., and Anderson, F. C. A phenomenological model for estimating metabolic energy consumption in muscle contraction. *Journal of Biomechanics*, 2004. 37(1):81–88. doi:[10.1016/S0021-9290\(03\)00239-2](https://doi.org/10.1016/S0021-9290(03)00239-2).
- Bicchi, A., Peshkin, M. A., and Colgate, J. E. *Safety for physical human-robot interaction*. Springer Berlin Heidelberg, Berlin, Heidelberg, 2008. doi:[10.1007/978-3-540-30301-5_58](https://doi.org/10.1007/978-3-540-30301-5_58).
- Bock, S. D., Ghillebert, J., Govaerts, R., Elprama, S. A., Marusic, U., Serrien, B., Jacobs, A., Geeroms, J., Meeusen, R., and Pauw, K. D. Passive shoulder exoskeletons: more effective in the lab than in the field? *IEEE Transactions on Neural Systems and Rehabilitation Engineering*, 2021. 29:173–183. doi:[10.1109/TNSRE.2020.3041906](https://doi.org/10.1109/TNSRE.2020.3041906).
- Christensen, S. and Bai, S. Kinematic analysis and design of a novel shoulder exoskeleton using a double parallelogram linkage. *Journal of Mechanisms and Robotics*, 2018. 10(4). doi:[10.1115/1.4040132](https://doi.org/10.1115/1.4040132).
- Davis, K. G., Reid, C. R., Rempel, D. D., and Treaster, D. Introduction to the human factors special issue on user-centered design for exoskeleton. *Human Factors*, 2020. 62(3):333–336. doi:[10.1177/0018720820914312](https://doi.org/10.1177/0018720820914312).
- De Santis, A., Siciliano, B., De Luca, A., and Bicchi, A. An atlas of physical humanrobot interaction. *Mechanism and Machine Theory*, 2008. 43(3):253–270. doi:[10.1016/j.mechmachtheory.2007.03.003](https://doi.org/10.1016/j.mechmachtheory.2007.03.003).
- Farasyn, A. and Meeusen, R. Pressure pain thresholds in healthy subjects: influence of physical activity, history of lower back pain factors and the use of endermology as a placebo-like treatment. *Journal of Bodywork and Movement Therapies*, 2003. 7(1):53–61. doi:[10.1016/S1360-8592\(02\)00050-5](https://doi.org/10.1016/S1360-8592(02)00050-5).
- Gopura, R., Bandara, D., Kiguchi, K., and Mann, G. Developments in hardware systems of active upper-limb exoskeleton robots: A review. *Robotics and Autonomous Systems*, 2016. 75:203–220. doi:[10.1016/j.robot.2015.10.001](https://doi.org/10.1016/j.robot.2015.10.001).
- Gull, M. A., Bai, S., and Bak, T. A review on design of upper limb exoskeletons. *Robotics*, 2020. 9(1). doi:[10.3390/robotics9010016](https://doi.org/10.3390/robotics9010016).
- Heinzmann, J. and Zelinsky, A. Quantitative safety guarantees for physical human-robot interaction. *The International Journal of Robotics Research*, 2003. 22(7-8):479–504. doi:[10.1177/02783649030227004](https://doi.org/10.1177/02783649030227004).
- L. Pons, J. *Wearable robots: biomechatronic exoskeletons*. Wiley, 2008.
- Lyder, C. H. Pressure ulcer prevention and management. *JAMA*, 2003. 289(2):223–226. doi:[10.1001/jama.289.2.223](https://doi.org/10.1001/jama.289.2.223).
- Narayanan, M., Kannan, S., Mendel, F., and Krovi, V. Case studies of musculoskeletal-simulation-based rehabilitation program evaluation. *IEEE Transactions on Robotics*, 2009. 25(3):634–638. doi:[10.1109/TRO.2009.2019780](https://doi.org/10.1109/TRO.2009.2019780).
- Nf, M. B., Junius, K., Rossini, M., Rodriguez-Guerrero, C., Vanderborght, B., and Lefeber, D. Misalignment compensation for full human-exoskeleton kinematic compatibility: State of the art and evaluation. *Applied Mechanics Reviews*, 2019. 70(5). doi:[10.1115/1.4042523](https://doi.org/10.1115/1.4042523).

- Pacifico, I., Scano, A., Guanziroli, E., Moise, M., Morelli, L., Chiavenna, A., Romo, D., Spada, S., Colombina, G., Molteni, F., Giovacchini, F., Vitiello, N., and Crea, S. An experimental evaluation of the proto-MATE: A novel ergonomic upper-limb exoskeleton to reduce workers' physical strain. *IEEE Robotics Automation Magazine*, 2020. 27(1):54–65. doi:[10.1109/MRA.2019.2954105](https://doi.org/10.1109/MRA.2019.2954105).
- Peebles, L. and Norris, B. *Adultdata: The handbook of adult anthropometric and strength measurements: Data for design safety*. Government consumer safety research. Department of Trade and Industry, 1999. doi:[10.1177/106480469900700310](https://doi.org/10.1177/106480469900700310).
- Rasmussen, J., Damsgaard, M., and Voigt, M. Muscle recruitment by the min/max criterion a comparative numerical study. *Journal of Biomechanics*, 2001. 34(3):409–415. doi:[10.1016/S0021-9290\(00\)00191-3](https://doi.org/10.1016/S0021-9290(00)00191-3).
- Rowe, M. F. Safety measures for conducting exercise oxygen consumption, VO₂, tests in developing countries. *Tropical Doctor*, 2020. 50(3):280–281. doi:[10.1177/0049475520918033](https://doi.org/10.1177/0049475520918033).
- Schiele, A. An explicit model to predict and interpret constraint force creation in pHRI with exoskeletons. In *2008 IEEE International Conference on Robotics and Automation*. pages 1324–1330, 2008. doi:[10.1109/ROBOT.2008.4543387](https://doi.org/10.1109/ROBOT.2008.4543387).
- Schiele, A. and van der Helm, F. C. T. Kinematic design to improve ergonomics in human machine interaction. *IEEE Transactions on Neural Systems and Rehabilitation Engineering*, 2006. 14(4):456–469. doi:[10.1109/TNSRE.2006.881565](https://doi.org/10.1109/TNSRE.2006.881565).
- Skals, S., Jung, M. K., Damsgaard, M., and Andersen, M. S. Prediction of ground reaction forces and moments during sports-related movements. *Multibody System Dynamics*, 2016. 39(3):175–195. doi:[10.1007/s11044-016-9537-4](https://doi.org/10.1007/s11044-016-9537-4).
- Sylla, N., Bonnet, V., Colledani, F., and Fraise, P. Ergonomic contribution of ABLE exoskeleton in automotive industry. *International Journal of Industrial Ergonomics*, 2014. 44(4):475–481. doi:[10.1016/j.ergon.2014.03.008](https://doi.org/10.1016/j.ergon.2014.03.008).
- Winter, D. A. *Biomechanics and Motor Control of Human Movement*. JOHN WILEY & SONS, INC., Hoboken, New Jersey, 2008. doi:[10.1002/9780470549148](https://doi.org/10.1002/9780470549148).
- Zhou, L., Bai, S., Andersen, M. S., and Rasmussen, J. Modeling and design of a spring-loaded, cable-driven, wearable exoskeleton for the upper extremity. *Modeling, Identification and Control*, 2015. 36(3):167–177. doi:[10.4173/mic.2015.3.4](https://doi.org/10.4173/mic.2015.3.4).
- Zhou, L., Li, Y., and Bai, S. A human-centered design optimization approach for robotic exoskeletons through biomechanical simulation. *Robotics and Autonomous Systems*, 2017. 91:337–347. doi:[10.1016/j.robot.2016.12.012](https://doi.org/10.1016/j.robot.2016.12.012).

Appendix A

Entries of the Jacobian matrix of Eq. (5):

$$\begin{aligned}
 J_{11} &= -L_f s\theta_4 (c\theta_1 c\theta_3 - c\theta_2 s\theta_1 s\theta_3) - L_u c\theta_1 s\theta_3 \\
 &\quad - L_f c\theta_4 (c\theta_1 s\theta_3 + c\theta_2 c\theta_3 s\theta_1) - L_u c\theta_2 c\theta_3 s\theta_1 \\
 J_{12} &= -c\theta_1 s\theta_2 (L_f c(\theta_3 + \theta_4) + L_u c\theta_3) \\
 J_{13} &= L_f s\theta_1 s\theta_3 s\theta_4 - L_f c\theta_3 c\theta_4 s\theta_1 - L_u c\theta_1 c\theta_2 s\theta_3 \\
 &\quad - L_u c\theta_3 s\theta_1 - L_f c\theta_1 c\theta_2 c\theta_3 s\theta_4 - L_f c\theta_1 c\theta_2 c\theta_4 s\theta_3 \\
 J_{14} &= L_f s\theta_1 s\theta_3 s\theta_4 - L_f c\theta_3 c\theta_4 s\theta_1 - L_f c\theta_1 c\theta_2 c\theta_3 s\theta_4 \\
 &\quad - L_f c\theta_1 c\theta_2 c\theta_4 s\theta_3 \\
 J_{21} &= L_u c\theta_1 c\theta_2 c\theta_3 - L_f c\theta_4 (s\theta_1 s\theta_3 - c\theta_1 c\theta_2 c\theta_3) \\
 &\quad - L_u s\theta_1 s\theta_3 - L_f s\theta_4 (c\theta_3 s\theta_1 + c\theta_1 c\theta_2 s\theta_3) \\
 J_{22} &= -s\theta_1 s\theta_2 (L_f c(\theta_3 + \theta_4) + L_u c\theta_3) \\
 J_{23} &= L_u c\theta_1 c\theta_3 + L_f c\theta_1 c\theta_3 c\theta_4 - L_f c\theta_1 s\theta_3 s\theta_4 \\
 &\quad - L_u c\theta_2 s\theta_1 s\theta_3 - L_f c\theta_2 c\theta_3 s\theta_1 s\theta_4 \\
 &\quad - L_f c\theta_2 c\theta_4 s\theta_1 s\theta_3 \\
 J_{24} &= L_f c\theta_1 c\theta_3 c\theta_4 - L_f c\theta_1 s\theta_3 s\theta_4 - L_f c\theta_2 c\theta_3 s\theta_1 s\theta_4 \\
 &\quad - L_f c\theta_2 c\theta_4 s\theta_1 s\theta_3 \\
 J_{31} &= 0 \\
 J_{32} &= -c\theta_2 (L_f c(\theta_3 + \theta_4) + L_u c\theta_3) \\
 J_{33} &= s\theta_2 (L_f s(\theta_3 + \theta_4) + L_u s\theta_3) \\
 J_{34} &= L_f s(\theta_3 + \theta_4) s\theta_2 \\
 J_{41} &= 0 \\
 J_{42} &= -s\theta_1 \\
 J_{43} &= c\theta_1 s\theta_2 \\
 J_{44} &= c\theta_1 s\theta_2 \\
 J_{51} &= 0 \\
 J_{52} &= c\theta_1 \\
 J_{53} &= s\theta_1 s\theta_2 \\
 J_{54} &= s\theta_1 s\theta_2 \\
 J_{61} &= 1 \\
 J_{62} &= 0 \\
 J_{63} &= c\theta_2 \\
 J_{64} &= c\theta_2
 \end{aligned}$$

Chapter 5

Paper III

Design of a Powered Full-Body Exoskeleton for Physical Assistance of Elderly People

Simon Christensen, Sajid Rafique and Shaoping Bai

The paper has been published in the
International Journal of Advanced Robotic Systems Vol. 18(6), pp. 1–15, 2021.
doi:10.1177/17298814211053534

The included paper has been approved for redistribution by the publisher.
Copyright ©2021

Design of a powered full-body exoskeleton for physical assistance of elderly people

*International Journal of Advanced
Robotic Systems*

November-December 2021: 1–15

© The Author(s) 2021

Article reuse guidelines:

sagepub.com/journals-permissions

DOI: 10.1177/17298814211053534

journals.sagepub.com/home/arxSimon Christensen¹, Sajid Rafique²  and Shaoping Bai¹ 

Abstract

The development of full-body exoskeletons has been limited due to design complexities, mechanical integration intricacies, and heavier weight, among others. Consequently, very few full-body powered exoskeletons were developed to address these challenges, in spite of increasing demand for physical assistance at full-body level. This article presents an overall design and development of a powered full-body exoskeleton called “FB-AXO.” Primarily, FB-AXO consists of two main subsystems, a lower-body and an upper-body subsystem connected together through waist and spine modules. FB-AXO is developed for the support of weaker ageing adults so that they can continue functioning their daily activities. At the onset of the project, a set of functional and design requirements has been formulated with an extensive end-user involvement and then used in realizing the FB-AXO. The final FB-AXO design comprises of 27 degrees of freedom, of which 10 are active and 17 are passive, having a total system weight of 25 kg. Overall, the article elaborates comprehensively the design, construction, and preliminary testing of FB-AXO. The work effectively addresses design challenges including kinematic compatibility and modularity with innovative solutions. The details of the mechanics, sensors, and electronics of the two subsystems along with specifics of human-exoskeleton interfaces and ranges of motion are also provided. The FB-AXO exoskeleton effectively demonstrated to assist full-body motions such as normal walking, standing, bending as well as executing lifting and carrying tasks to meet the daily living demands of older users.

Keywords

Assistive exoskeleton, mechanism design, performance assessment, full-body exoskeletons, upper-body exoskeleton, lower-body exoskeleton

Date received: 14 February 2021; accepted: 28 September 2021

Topic: Service Robotics

Topic Editor: Marco Ceccarelli

Associate Editor: Erwin-Christian Lovasz

Introduction

The research in wearable exoskeletons has been increasing over the last few years as the technology advances in personal care robots.^{1–6} Wearable exoskeletons offer useful solutions to the growing needs for assistive technologies.^{7–11} Despite this growth, exoskeleton research has largely been focused on military applications to enhance the load carrying capabilities of soldiers/workers, assisting individuals following trauma and/or spinal cord injury and for rehabilitation needs.¹² Besides military-focused exoskeletons, the majority of research activities

has been focused on medical application.^{1,13} The needs of ageing society for physical assistance are not sufficiently

¹ Department of Materials and Production, Aalborg University, Aalborg, Denmark

² Department of Electronics, Mathematics and Natural Sciences, University of Gavle, Gavle, Sweden

Corresponding author:

Sajid Rafique, Department of Electronics, Mathematics and Natural Sciences, University of Gavle, Gavle 80176, Sweden.

Email: sajid.rafique@hig.se



Creative Commons CC BY: This article is distributed under the terms of the Creative Commons Attribution 4.0 License (<https://creativecommons.org/licenses/by/4.0/>) which permits any use, reproduction and distribution of the work without

further permission provided the original work is attributed as specified on the SAGE and Open Access pages (<https://us.sagepub.com/en-us/nam/open-access-at-sage>).

addressed to utilizing the strong potential in the support of motion.^{11,14} This work addresses the possibility of using wearable exoskeletons for ageing to provide general assistance in a natural manner to support activities in daily living.^{12,15,16}

Full-body (FB) exoskeletons are typically used as human strength amplifiers, where loads are transferred through the exoskeleton, controlled by the human, to the ground. Hence, in the physical interaction with the exoskeleton, only a small part of the load is experienced by the human. As the power is mainly transferred through the mechanical structure of the exoskeleton, the human is able to manipulate loads beyond its natural capabilities. FB exoskeletons are developed to provide comprehensive assistance at body levels, not on single limbs.¹⁷ Examples of such exoskeletons are the Body Extender (BE)¹⁸ or the XOS2.¹⁹ The BE has a quasi-anthropomorphic kinematic structure with a total of 22 degrees of freedom (DoF), all powered by electric motors. Its kinematic structure consists of two identical legs and arms with 6 DoF and 5 DoF, respectively. The BE exoskeleton enables the wearer to manipulate up to 50 kg in each arm and weighs 160 kg excluding the power supply.¹⁸ The system is worn by the user through a set of straps at the feet, two shoulder straps and a belt, and two grippers at the hand. On the other hand, the XOS2 is lighter compared to the BE, with a weight of 95 kg. Like the BE, the kinematic structure of the XOS2 is quasi-anthropomorphic. The system is actuated by 23 hydraulic actuators, where each leg has 6 DoF, each arm has 5 DoF, and the torso has 1 DoF. The system is able to manipulate a payload of 23 kg in each arm. The XOS2 is strapped to the user similarly to the BE, namely, at the feet, waist, upper torso, and with a tool at the hands.¹⁹

Another class of FB exoskeleton is the powered assistive exoskeletons. Instead of transferring the payload from a gripper or tool to the ground, these exoskeletons transfer power between segments of the human limb. Hence, the exoskeleton complements the function of the human musculoskeletal system, where the assistance level is lower than the counterparts for the strength amplifier type exoskeletons. The most well-known power assistive exoskeleton is the Hybrid Assistive Limb, also known as HAL-5, developed at the University of Tsukuba in Japan.^{20,21} HAL-5 is the fifth generation of the HAL exoskeletons and is designed for both rehabilitation and assistive purposes.^{22,23} The exoskeleton system is powered by eight electric motors with a reduction gear in the sagittal plane at the knee, hip, shoulder, and elbow. The exoskeleton was able to maneuver 15 kg in each arm and lift and hold a total payload of 70 kg close to the body.²⁰ Moreover, HAL-5 is fitted with passive joints at each ankle and shoulder. Compared to XOS2 and BE, HAL-5 is much lighter, weighing only 23 kg. HAL-5 has an anthropomorphic kinematic structure and is attached to the user's feet, shank, thigh, waist, upper torso, upper arm, and forearm, which allows the suit to give assistance at a specific joint.

Other powered assistive FB exoskeletons include the KanaGawa Power Assist Suit^{24,25} and Wearable Agri-Robot.²⁶ The KanaGawa Power Assist Suit was designed to aid nurses in their daily work activities. The system has a total weight of 30 kg and is powered by six pneumatic actuators in the sagittal plane at the elbow, waist, and knee. Moreover, two passive joints are included at each ankle and shoulder. Wearable Agri-Robot was designed for agricultural workers with a total of 15 DoF and weight of 30 kg. Wearable Agri-Robot is actuated in the sagittal plane at the hip, knee, shoulder, and elbow using DC motors and a reduction gearing. Moreover, passive joints are included at the ankle, torso, and shoulder. Like HAL-5, both KanaGawa Power Assist Suit and Wearable Agri-Robot have an anthropomorphic kinematic structure and are attached to the wearer at the neighboring limbs of each assisted joint. In a recent work, a FB exoskeleton for enhancing heavy load-carrying capacities was proposed.²⁷ The exoskeleton was designed for a maximum 5 kg payload of the upper body and 40 kg of the lower body.

The design challenges for the powered assistive type of exoskeletons are mainly related to the complexity of the human anatomy,^{15,28–30} particularly the shoulder complex and the spine.⁶ Exoskeletons are mechanical structures that match the structure of the human body. Hence, the exoskeleton should be able to replicate the kinematics of the human anatomy to as large extent as possible without the exoskeleton colliding with the human or itself. This poses problems for assistive exoskeletons that are attached to each limb segment for the human. A common issue is misalignment that occurs between limbs of the two systems. A mismatch in the kinematics between the exoskeleton joint and corresponding human joint can potentially lead to large human–exoskeleton interface forces and damage the human joint in worst cases.³¹ Moreover, it has been shown that the attachment pressure has a large effect on comfort, mental load, physical demand, and effort experienced by subjects.³² One approach to this problem is to use manually adjustable links, which was adopted by HAL-5,²⁰ among others. In this approach, the linkage lengths of the exoskeleton are manually adjusted to align the exoskeleton with the human joint. This approach can give good initial alignment but is unable to adjust for possible misalignment during movements. To solve this problem, researchers suggested to use passive joints in the exoskeleton joint design, which maintain alignment between the exoskeleton and the human joints.^{29,30} The drawback of this approach is a complicated design and increased inertia and mass. Moreover, for assistive portable exoskeletons, a compact design is desirable. Hence, the exoskeleton design solution should be a trade-off between a compact and lightweight structure with sufficient DoF for the user to comfortably complete a given activity.

The design of a spine module that connects lower-limb and upper-limb exoskeletons is another challenge for FB exoskeletons. Existing designs use either fixed connection

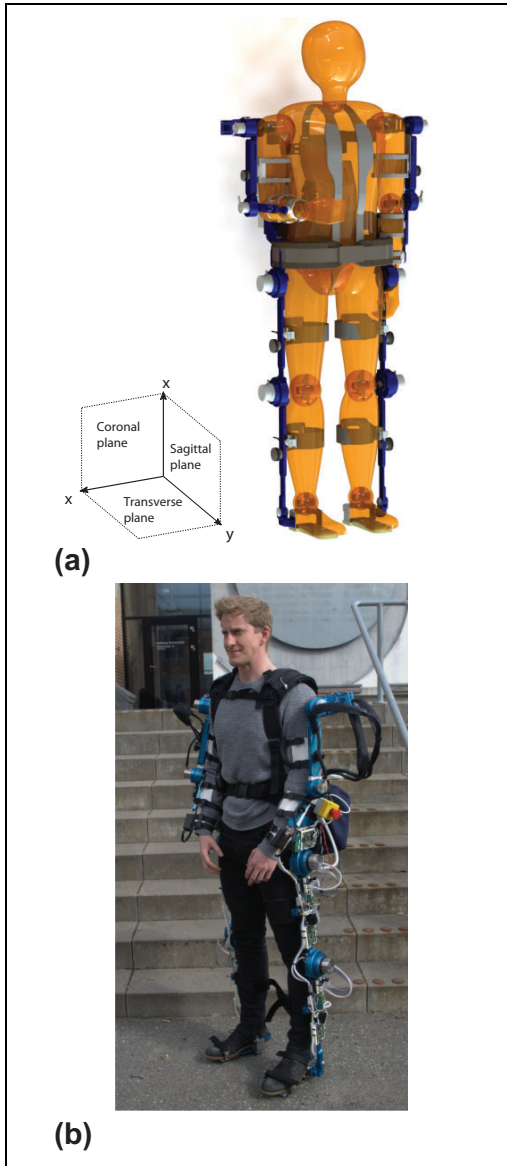


Figure 1. FB-AXO exoskeleton: (a) conceptual design and (b) physical system.

like HAL-5 or only one DoF such as XOS2. The limitation with existing designs is that the range of motion (ROM) is considerably constrained, comparing to a flexible spine of humans, which leads to poor interaction between human and the exoskeleton and increased muscle activities.

This article elaborates the design and development of a FB exoskeleton, called FB-AXO, as shown in Figure 1. This exoskeleton was developed in the AXO-SUIT project (www.axo-suit.eu) to address the aforementioned challenges with innovative solutions. It is a medium-duty exoskeleton, designed to support the user in daily life activities such as walking, squatting, standing, bending as well as performing lifting, holding and carrying tasks with objects weighing 5 kg in each arm. The exoskeleton was developed with novel designs of shoulder joint mechanism and a flexible biomimic spine module, which mitigate the issues of kinematic compatibility.

This work extends the authors' previous work,^{33–35} where the relevant studies and overall FB-AXO concept are presented. In this article, the overall mechanical design is elaborated in details, describing the kinematic compatibility with the human, physical interface design, and force interaction sensor design. A design overview including design requirements is presented in the following section followed by detailed design and construction of the lower-body (LB-AXO) and upper-body exoskeletons (UB-AXO), respectively. Subsequently, initial testing results are described.

Design of FB-AXO from end-user requirements

In AXO-SUIT project, a fully functional prototype of FB exoskeleton namely “FB-SUIT” was designed and developed. The design of FB-AXO has been driven by a high level of end-user involvement. A range of methodologies were used for this to ensure that appropriate end user input was obtained, for example, questionnaires, focus groups, interviews.³⁶ The extensive involvement of end users right from the beginning of AXO-SUIT project provided vital inputs and feedbacks on both functional requirements finalization and product design throughout the development of the prototypes. The most frequent motions of upper body, lower body, and FB described by the participants of this study were considered as the highest priorities for assistance and are presented in Table 1.³³ The inputs of end users were thoroughly discussed among the AXO-SUIT consortium before finalizing the target motions and

Table 1. Highest priority of lower body, upper body, and full body motions, as ranked by questionnaire participants.³⁶

Priority ranking	Lower body	Upper body	Full body
	Sit-to-stand	Lifting/dropping without grasping	Getting up from kneeling
	Walking and turning	Reaching to the side overhead/opposite shoulder	Getting up from squatted position
	Standing	Carrying an object in front with both arms	Carrying small objects with one hand

incorporating them in the design process. To further validate the practicability of the identified motions and also to facilitate the decision-making process, three-dimensional human kinetic and kinematic simulation data were gathered for these tasks to decide the ROM and torque requirements at joints of the FB-AXO.³⁷

A specially designed exoskeleton with angle measurement sensors at the hip, knee, and ankle joints of both legs was designed to experimentally measure human walking gait patterns to acquire accurate kinematic and kinetic data.³⁸ It was found that human biomechanical data of high variability were depended on various internal factors such as age, physical and mental state, and pathological reasons. Therefore, precise sensing and identification of human gait parameters are essential for realizing energy efficient exoskeleton system. The results of the study were used for the design requirements for sizing of the hardware such as link lengths and actuators needed.³⁸

Therefore, questionnaire results combined with biomechanical data and expert discussions were used to inform the functional goals, design, and technical specifications for the FB-AXO prototypes and are presented in more detail.³⁶

The FB-AXO design, illustrated in Figure 1(a) along with the physical system shown in Figure 1(b), is developed to provide a moderate supplement of strength at the joint level and is adaptable to wearers of different weights and heights ranging from 70 kg to 110 kg and 1.55 m to 1.8 m, respectively, based on anthropometric measurements listed in Peebles et al.³⁹ The system has a total of 27 DoFs, of which 17 are passive and 10 active. The ROM of the different DoF is determined based on motion analysis of the movements in Table 1. The active DoFs are linked to movements in the sagittal plane, as the end-user requirements listed in Table 1 are mainly related to motion in this plane.³⁶ The passive DoFs are introduced to replicate the key kinematics of the human. Moreover, some of the passive DoFs, namely, the DoFs in the passive spine module, contain elastic elements, which allow a certain ranges of bending and twisting motion and also provide additional support to the body.

To make the system reliable, effective, and flexible, a modular methodology is implemented for FB-AXO. The overall FB system consists of two main subsystems, namely, the lower- and the upper-body subsystems, named LB-AXO and UB-AXO. Each subsystem is capable to work autonomously to provide assistance as required. The assistance is provided at joint level through a number of modules. The LB-AXO subsystem consists of two identical legs (left and right legs), each with a hip, knee, and ankle module. It connects to the human via straps at the foot, shank, thigh, and waist. A waist plate, located above the hip joint, physically and functionally joins the two legs. Similarly, the UB-AXO subsystem consists of left and right arms, each comprising of a shoulder and elbow module. UB-AXO also connects to the human via straps at the forearm, upper arm, and torso and

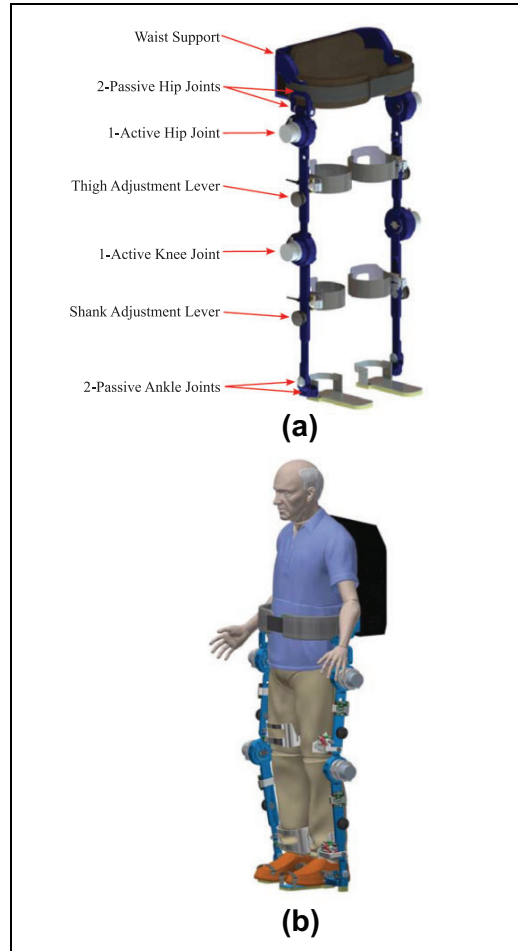


Figure 2. Conceptual design: (a) CAD model, (b) LB-AXO in simulation software.

waist. The two arms are joined through the torso, which also contains a spine module. The FB-AXO has a total weight of 25 kg, of which UB-AXO weighs 12 kg and LB-AXO make up 13 kg, respectively. The system is powered by a Li-ion battery that can power the whole FB system uninterruptedly for approximately 1 h.

The lower-body subsystem—LB-AXO

The LB-AXO subsystem, referring to Figure 2(a), is designed to support the weight of the wearer and UB-AXO and to provide supplementary assistance to perform a range of basic motions for daily living. The design of LB-AXO is mainly focused to improve modularity, adjustability, ergonomics, and affordability aspects. Consequently, a

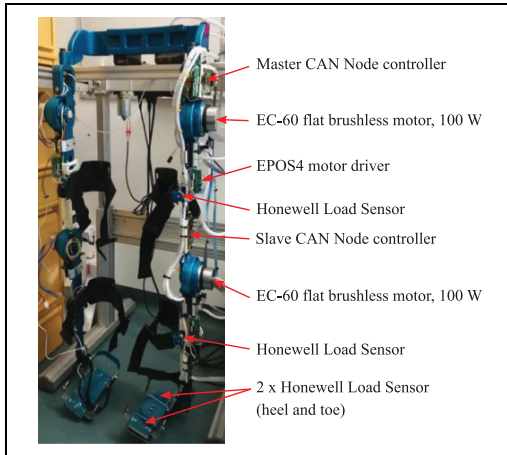


Figure 3. The LB-AXO physical system.

lightweight prototype was realized, as shown in Figure 3, and successfully tested for users of ages between 20 and 62 (elaborated in the section on preliminary tests).

LB-AXO module

LB-AXO has a total 12 DoF (4 active and 8 passive). All the active joints are in sagittal plane at the hip and knee modules. Furthermore, the hip module has a passive abduction/adduction and a rotation DoF. The knee module is completely active and has no passive movement DOF, whereas the ankle module is fully passive and has one dorsi/plantar flexion and an inversion/eversion passive DoF. Both of the passive joints of ankle consist of specially designed bolts which have threads at the tip sides to fasten the joint through nuts to allow desired rotation.

From the prioritized list of motions in Table 1, it can be seen that the majority of movement for the LB system is linked to the sagittal plane. Hence, the DoFs in the LB-AXO are primarily related to movements in this plane. As mentioned in the introduction section, a large number of DoFs provides flexibility in motion but introduces complexity in the system. In this regard, motion study was conducted with commercially available 3D modeling software Inventor and Matlab during the design phase of the LB-AXO. The kinematic compatibility between a human model and LB-AXO, illustrated in Figure 2(b), was studied. In the study, the motion pattern is sent from Matlab to the human model, and the exoskeleton model moves along the human model via the kinematic constraints between the two models. In the testing, the load sensors, mounted at the interfaces of thigh and shank, detect the human intention for mobility and the controller power on the actuators accordingly. Therefore, the exoskeleton system moves along human with synchronization.

Table 2. LB-AXO details for hip, knee, and ankle joints.³³

Module	Joint	RoM	Actuation
Hip	flex./ext.	122°/–122°	EC-60 and HAINA XSF (125:1 ratio)
	medial/lateral rot. abd./add.	45°/–45° 80°/–80°	Passive joint
Knee	flex./ext	122°/0°	EC-60 and HAINA XSF (60:1 ratio)
Ankle	dorsi/plantar flex.	25°/–30°	Passive joint
	inversion/eversion	35°/–35°	Passive joint

LB-AXO model from CAD, which includes mass, inertia, joint constraints, and 3D geometry, was imported into Mechanics toolbox of Matlab. SimMechanics toolbox provides a multi-body simulation environment for 3D LB-AXO system. Three cuff-straps were provided on each leg, to hold the LB-AXO with the human leg, at thigh, shank, and foot. The locations of the cuffs and straps can be adjusted vertically and horizontally so that a comfortable fit can be achieved for every individual user. The knee joint was modelled as a single revolute joint allowing flexion/extension motion of the leg in the sagittal plane. The details of the study can be seen in Virk et al.³⁸ It is noted that the knee joint can also be modelled as a joint involving both rotating and sliding motions,⁴⁰ but this also implies a complicated design of joints.⁴¹ We thus consider the knee as a revolute joint to make the design simple and compact.

The selection of active and passive DoF of LB-AXO is determined based on the motion analysis and the results from the previous project EXO-LEGS.⁴² As the torque assistance in sagittal plane is dominant, flexion/extension joints of hip and knee are powered by actuators. Table 2 lists the RoM of all joints, which is sufficient to cover the target motion of normal human walking, standing, sitting on a chair, squatting, or kneeling. The medial/lateral rotation DOFs of hip, knee, and ankle joints have a possibility of being passive to improve the performance. Moreover, the dorsiflexion/plantar flexion joint at the ankle can be passive to improve mobility, wearability, and controllability while drastically reducing weight and complexity of the system.

The specifications of the hip, knee, and ankle modules in terms of their actuation and the range of movements are listed in Table 2. The EC series DC motors from Maxon Motor Inc. and the XFS harmonic drive from HAINA are used for active actuation. This drive performs similar to Harmonic Drive but costs only one-third of the latter. The active joints are able to assist with up to 50% of the power required for a target motion, which complies with the low-risk physical assistive robots as defined in EN ISO 13482. The electric motors are mounted with harmonic gear sets with suitable reduction ratio that balances the required assistance torque and human movement speed. Table 3 lists the power, torque, and velocity specifications of the LB-AXO.

Table 3. Power, torque, and velocity details for LB-AXO active joints.

Module	Joint	Power	Cont./max torque	Vel.
Hip	flex./ext.	100 W	28/440 Nm	28 rpm
Knee	flex./ext	100 W	14/212 Nm	58 rpm

LB-AXO adjustments and attachments

The LB-AXO subsystem is fitted with wearers using length and width adjustments at the waist, thighs, shanks, and feet, see Figures 2 and 3. The waist support comprises adjustable fastening mechanism around the waist, containing interfaces for the mounting of left and right legs and also provides interfaces to integrate with the UB-AXO through the spine module. The thigh and shank links are adjustable in lengths to fit different heights of the wearers and housing the motors and gear assemblies for the hip and knee joints. The lengths of the links can be adjusted by using sliding links, as shown in Figure 4(a). The foot section is adjustable in length to fit different sizes of feet of wearers. The foot design includes sensors for detecting ground reaction forces. It also comprises of a Velcro belt for attaching the exoskeleton to the shoe of the wearer as shown in Figure 4(b).

Another vital aspect in the design of the LB-AXO is the method for effectively mounting the exoskeleton onto the human's lower extremities with comfort. The appropriate selection of human attachment is vital not only for its wearability but also for the performance of LB-AXO subsystem. LB-AXO directly attaches to the wearer at the waist/upper body, thighs, shanks, and feet. The attachment of LB-AXO and UB-AXO is achieved through the waist support, on which the spine module is mounted. A blast-belt harness, which is normally used for extreme sports and backpacking, is adopted to maximize the adherence level of waist attachment. The blast-belt harness is composed by a soft back with Velcro straps and snap buckle belt for rapidly fitting and easy tightening. This ensures a firm yet comfortable attachment interface.

At the thighs and shanks, an adjustable aluminum strip (front and back) is provided to integrate force sensors. A Velcro belt is used for rapid tightening. The aluminum strip is designed to be adjustable by sliding and locking with a cam slider lever-bolt device as shown in Figure 4(a). It is manufactured by Misumi Inc. and provides comfortable way of adjusting the location of strips with the human body according to the size of the wearer. When the lever is pulled up, it allows movement of the aluminum strip until the user feels comfortable. The lever is then pushed down to lock that position. Furthermore, a soft strip is attached inside of the aluminum strip to improve the comfort and flexibility.

LB-AXO uses a set of different sensors for measuring the state of the system. All active joints are fitted with absolute encoders to obtain the joint angles and thus the

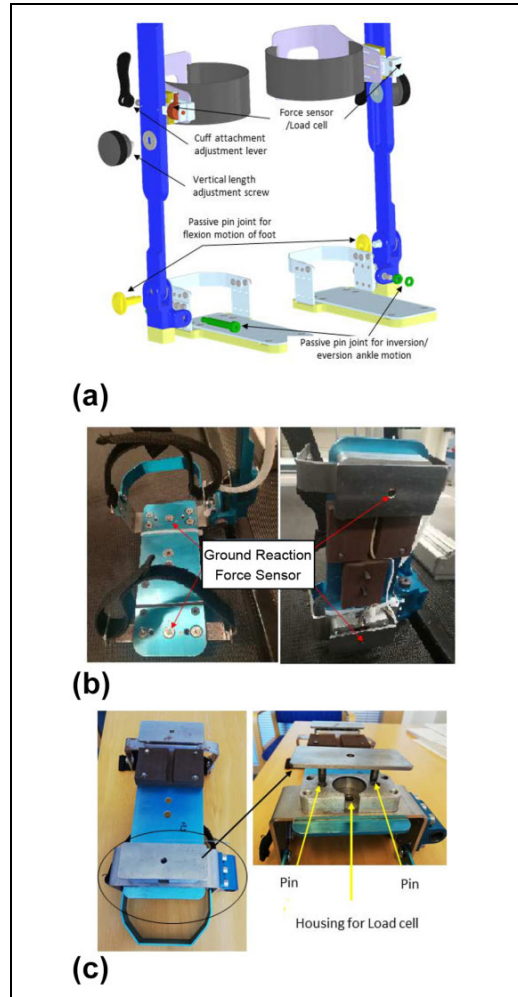


Figure 4. Attachments and force sensors in LB-AXO: (a) CAD model of thigh cuff with integrated minor adjustment and interaction force sensor, (b) foot attachment with integrated ground reaction force sensors, and (c) the pressure plate showing with details.

system configuration. The active joints are also fitted with angular speed sensors for motor control purposes. There are many different sensors available for measuring force between the mechanical components. In this work, load cells are used to measure the force. Load cells are preferred over other methods to measure ground reaction forces and heel strikes because the other methods (force sensitive resistors, etc.) cannot measure heavy loads. In LB-AXO, load cells (AL31-MM-1C) manufactured by Honeywell Inc. are used to measure the ground reaction force through

the foot module. It is important to note that to properly assist the human during each phase of the walking cycle (stance phase, single support phase, and double support phase), each phase's start and end must be appropriately measured. Therefore, a foot assembly is designed for each leg of the exoskeleton with two load cells as illustrated in Figure 4(b), one at the toe to detect toe-off and the other at the heel to detect heel strike. The load cells are mounted through a separate pressure plate with sliding steel pins to allow proper force application and sensing.

Load cell is sandwiched between the plate and the foot side assembly as shown in Figure 4(c). Two pins are provided on the plate which are located on either side of the load cell housing to ensure vertical alignment as well as to eliminate any motion in the lateral direction. It is noted that the vertical direction component is dominant in calculating the ground reaction force, hence, the lateral direction force component is negligible and was not used in the control system.

The two-plate assembly, on the other hand, provides the necessary freedom to the human for proper walking. Furthermore, the load cells allow proper measurement of the ground reaction forces at each foot of the exoskeleton to estimate the center of pressure which is important in applying advanced stability-control techniques to the exoskeleton. Moreover, the thigh and shank cuffs are also fitted with the load cells to measure interaction forces between the wearer and LB-AXO.

The upper-body subsystem—UB-AXO

The UB-AXO, shown in Figure 5, is designed to support the wearer in activities that require lifting and holding/carrying objects below and above shoulder height, mainly in the sagittal plane. However, these motions also include reaching to the opposite shoulder. Due to these requirements and the large dexterity of the human upper body, the UB-AXO has a total of 15 DoFs, including six DoFs in each upper limb and three DoFs in the spine module. Of them, six DoFs are active and the remaining nine DoFs are passive (Figure 5(a)). Each shoulder module has 2 active and 1 passive DoF, while each elbow module has 1 active DoF. Moreover, the shoulder module is extended with two more passive joints, namely, Joint 1&2-SPR, to account for the shoulder protraction and retraction (SPR). The specifications of shoulder and elbow modules in terms of their actuation and RoM are listed in Table 4, where EC motors from Maxon Motor and harmonic gear from Leaderdrive are used for actuation. The harmonic gear is selected for its back-drivability, which allows the user to move even if the motors are powered off.

The shoulder and elbow modules

The shoulder module has five DoF, where two are used to match the protraction/retraction of the human shoulder

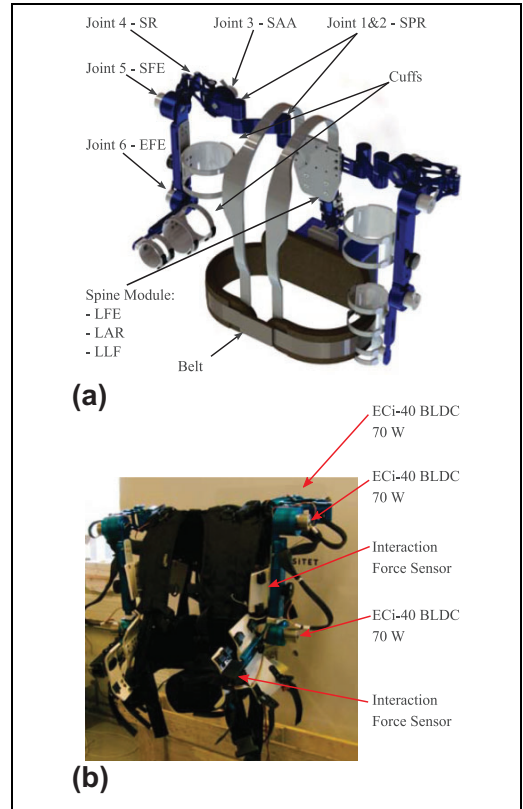


Figure 5. The UB-AXO system: (a) conceptual design of the UB-AXO, where joints 3, 5, and 6 in each arm are active, while other joints are passive and (b) the physical UB-AXO system.

Table 4. UB-AXO specifications for spine, shoulder, and elbow modules.³³

Module	Joint	RoM	Actuation
Spine	lumbar flex./ext.	30°/–30°	Rubber disks
	axial rot.	30°/–30°	Rubber disks
	lateral flex.	30°/–30°	Rubber disks
Shoulder	protra./retraction	122°/–122°	Passive
	abd./add.	120°/–80°	EC-i40 and LCS-17-100
	int./ext. rot.	90°/–50°	Passive joint
	flex./ext.	170°/–10°	EC-i40 and LCS-17-100
Elbow	flex./ext.	145°/0°	EC-i40 and LCS-17-50

girdle and the final three DoFs are used to match the three rotational DoFs of the human glenohumeral joint. The shoulder protraction/retraction is realized by two passive revolute joints in series (see Figure 5), as aforementioned.

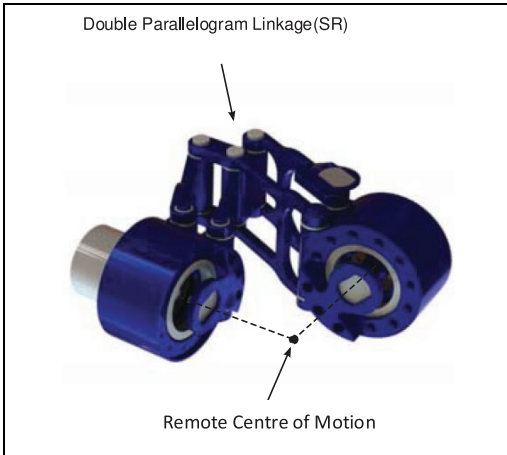


Figure 6. The double parallelagram spherical mechanism.

Table 5. Motor specifications for UB-AXO active joints.

Module	Joint	Cont./max torque	Vel.
Shoulder	abd./add.	10.5/29.8 Nm	41 rpm
	flex./ext.	10.5/29.8 Nm	41 rpm
Elbow	flex./ext	5.3/9.9 Nm	82 rpm

The glenohumeral joint motion is realized by a novel shoulder mechanism composed by two revolute joints connected by a double parallelagram linkage.⁴³ The double parallelagram spherical mechanism (DPM in short), illustrated in Figure 6, is a remote center of motion (RCM) mechanism with a relatively large RoM free of singularity, which is able to map 90% of the human glenohumeral RoM.³⁴ Moreover, the parallel structure of the double parallelagram linkage gives the DPM a high overall stiffness, while remaining lightweight and compact. These features make the DPM suitable for assistive portable exoskeletons. The DPM has two active joints and one passive. The shoulder abduction/adduction (SAA) and flexion/extension (SFE) joints are powered, while shoulder internal/external rotation (SR) joint is passive. The elbow module is a single powered joint that supports flexion/extension of the human elbow (EFE). Table 5 lists the torque and velocity specifications of the UB-AXO active joints. All motors have an output power of 70 W.

The spine module

The UB-AXO includes also a spine module, which has three passive DoF supported by compliant elements. The module is designed to transfer the load of the UB-AXO to

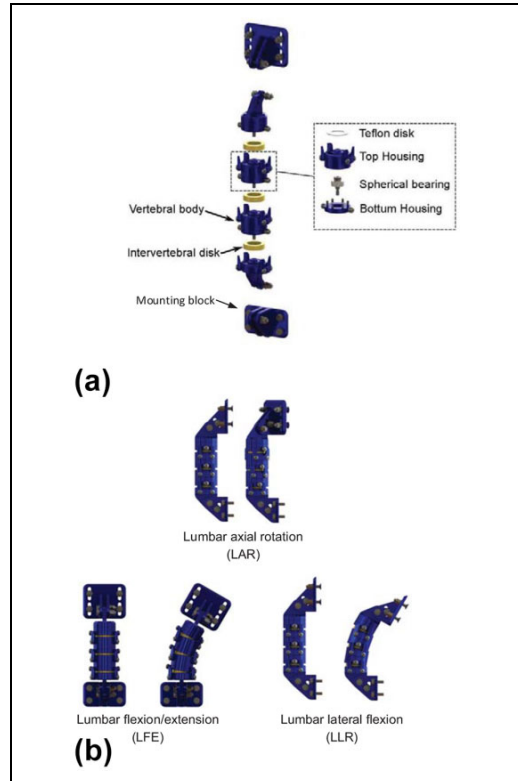


Figure 7. The spine module: (a) conceptual design and (b) flexible motion with the spine module.

the LB-AXO and support human upper body, while matching three DoF of the lumbar spine (Figure 7(a) and (b)). The design adopts biomimic approach, with which the spine module is designed to resemble the human lumbar with a set of vertebral bodies of aluminum and intervertebral disks of rubber. The number of vertebral bodies and intervertebral disks used in the spine module depends on the size of the wearer. For the target user group, the number of disks used in the spine module ranges between 3 and 5.

The vertebral body consists of two housing units enclosing a spherical bearing to realize three rotational DoF for each vertebral disk. A Teflon bushing is inserted between the vertebral body and intervertebral disk to minimize frictional losses during Lumbar axial rotation (LAR). The RoM of LAR is constrained by end-stops on the vertebral bodies. The end-stop consists of a wishbone structure on the top housing and pin on the adjacent bottom housing, see Figure 7(b).

The lumbar flexion/extension and lateral (LFE and LLR) movements have a spring-backed support by the compliance in the intervertebral rubber disks. By selecting

different rubber disks of varying stiffness, the spine module can provide varying supports to users.

The spine module transfers load from the upper body and arms to the legs. Moreover, it provides support to human spine to prevent possible injury caused by extra loads and motion beyond RoM of the spine. Tests were conducted on the bending stiffness of the spine model, as presented in section “Usability testing.”

UB-AXO adjustments and attachments

Similar to the LB-AXO, the UB-AXO is fitted with a set of adjustable links to fit target users. The length of the spine module can be modified by either adding or removing a disk element. Moreover, a sliding adjustment can further be used for fine adjustment. The upper arm and forearm links are both adjustable to fit the wearers arm.

UB-AXO is worn by the user through a set of attachments at the human torso, upper arm, and forearm. A snap buckle belt embedded with a flexible plastics material wraps around the waist of the user and attaches to the base of the spine module. At the top of the spine module, a rigid back plate is fitted with shoulder straps that wrap around the users torso and are attached to the belt. The belt and shoulder straps enable a quick fitting and easy tightening to the user. The upper arm and forearm links are fitted with a set of cuffs consisting of flexible plastics materials tightened to the limb using straps.

UB-AXO uses a number of sensors for measuring both the exoskeleton state and also the human–exoskeleton interaction forces. The SAA, SR, SFE, and EFE joints are fitted with absolute encoders to detect the joint angles and thus the system configuration. The active joints, namely, SAA, SFE, and EFE, are also fitted with angular speed sensors for motor control purposes.

In the design, the upper arm and forearm cuffs are fitted with strain gauge-based force sensors (see Figure 8(a)) to measure interaction forces, noted by F_{int} , between the human and UB-AXO. It is noted that there are many different ways to measure the interaction force, either using commercial standard load cell, such as ATI six-DoF force sensor,⁴⁴ or design special ones to meeting specific requirements.⁴⁵ In this system, we designed our own force measuring device to meet space constraints to achieve a compact and portable system.

The force sensors are designed with two flat beams with an equal distance to the centerline, as illustrated in Figure 8(b). A total of eight strain gauges are configured in two full-bridge configurations that measure bending moment in the two beams. The first full-bridge (SG11, SG12, SG13, and SG14) measures the force applied along the z -axis at the cuff interface, while the second full-bridge (SG21, SG22, SG23, and SG24) measures the force along the y -axis. The Wheatstone bridge configurations for the two force readings are illustrated in Figure 8(c), where V_s is the excitation voltage and V_o is the sensor output voltage.

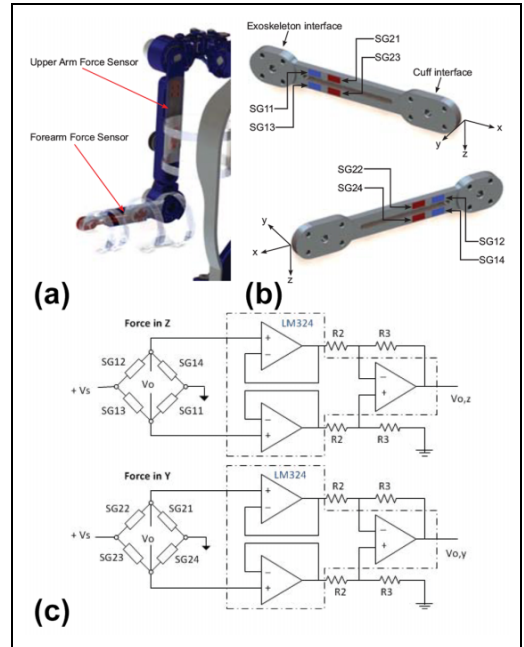


Figure 8. The strain gauge-based interaction force sensors in UB-AXO: (a) force sensors integrated in UB-AXO, (b) strain gauge placement on the UB-AXO force sensors, (c) Wheatstone bridge circuit for the UB-AXO force sensor. $V_{o,y}$ and $V_{o,z}$ are output voltages associated with interaction forces in y and z directions.

Because the sensor output voltage is low (in the size of mV), an amplifier circuit built with an IC chip, namely, LM324, is used to scale the output voltages for better readability, in which the gain of amplification is determined by $R3/R2$.

System development and preliminary testing

The FB-AXO has been constructed, as shown in Figure 1(b), with controllers developed. Upon the system developed, the AXO-SUIT was preliminarily tested.³⁵

Control strategies for the LB-AXO, UB-AXO and FB-AXO in the initial testing

In assistive applications of active joints, the assistive torques are determined through a control strategy that uses inputs from the system, as illustrated in Figure 9.

In UB-AXO, a static load compensation strategy is adopted. The assistive torque of each active joint is calculated with three parts; an exoskeleton gravity compensation torque τ_{exo} , a human gravity compensation torque τ_g and torque for external loads τ_l , namely

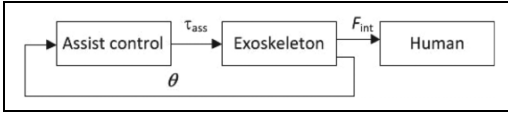


Figure 9. Control strategy, where θ stands for joint variables and F_{int} for interaction force between human and exoskeleton measured through force sensors.

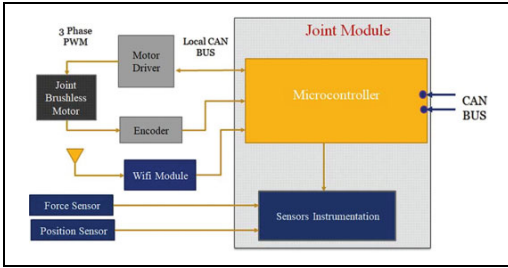


Figure 10. Schematic of joint level control by slave controller.

$$\tau_{ass} = \tau_{exo} + \mathbf{K}(\tau_g + \tau_l) \quad (1)$$

where \mathbf{K} defines the assistance levels of all joints. Moreover, τ_l is dependent on external load \mathbf{F}_p , which can be determined by

$$\tau_l = \mathbf{J}\mathbf{F}_p \quad (2)$$

where \mathbf{J} is the Jacobian of the UB-AXO limb.

Considering that the accelerations and velocities of the human movement are assumed small, the interaction between the human and exoskeleton can be considered quasi static. In this light, a control strategy with gravity compensation is sufficient for the assistance of activities in daily life.

The LB-AXO subsystem adopts a distributed control scheme to take the advantage of separated functionality of each control module. The distributed control can mitigate the computational burden at the specific microprocessor. Therefore, each leg has a powered revolute knee and hip joints which are locally controlled by four CAN-based motor power drives connected to respective slave controllers. All the four slave CAN controllers are connected together through a master CAN controller. Each of the four slave controllers locally handles the sensor input and motor command output and performs data sharing with the master software via CAN bus. Figure 10 shows the joint level control scheme by the slave CAN controller. Each LB-AXO joint assembly primarily consists of a brushless DC-motor as joint actuator, a harmonic drive as gearhead, and an encoder (2 channels MILE 1024) as a joint speed sensor. The inductive MILE encoder ideally complements brushless motors. It offers an impressive resolution and high accuracy. The encoder with inverse signals is very

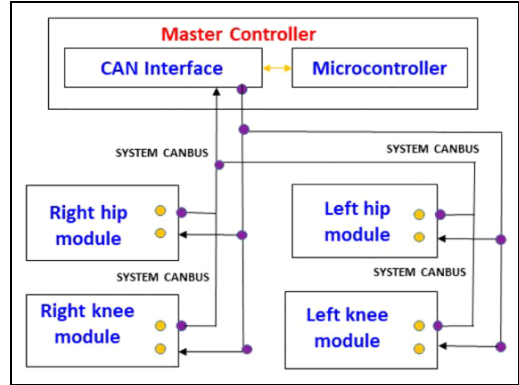


Figure 11. Flow diagram of joint level (Slave)-Master microcontroller system of LB-AXO.

resistant against magnetic and electric fields as well as dirt. It is integrated directly into the motor. The position of each brushless DC motors was locally controlled by EPOS4 Compact 50/15 CAN controller.

The master controller not only connects and processes the data from slave controllers but also provides communication GUI link between human user and the LB-AXO as shown in Figure 11. For the LB-AXO system, a force-based control strategy is used, which functions on human-exoskeleton interaction. The force/torque sensors mounted at the interfaces with the wearer (the thigh, shank, and foot attachments) detect the intentions of the human and communicate this to the control system of LB-AXO which, in turn, provides the desired assistance by running the actuators accordingly.

The ranges of motion of hip, knee, and ankle joints of both legs of the model are constrained according to the counterparts of human segments. To simulate the ground reaction forces, foot is represented as rigid body connected by a pin joint, to allow movement in sagittal plane, and contact forces are used between the foot and the ground at estimated times of the heel strike, the single stance phase, the toe off and over the double stance phase. The master controller connects, synchronizes, and provides a central control of the whole system. The details concerning control equations used in the control system design can be seen in a separate study.³⁸

Usability testing

Tests were conducted to assess the performance of the system. The purpose of usability testing is to examine how usable the FB-AXO is, considering its size adjustability, comfort, and ROM in different poses. Prior to testing at the FB system, each module was tested to function properly. Figure 12 shows the bending curve of the spine with three types of rubber disks, obtained experimentally with a

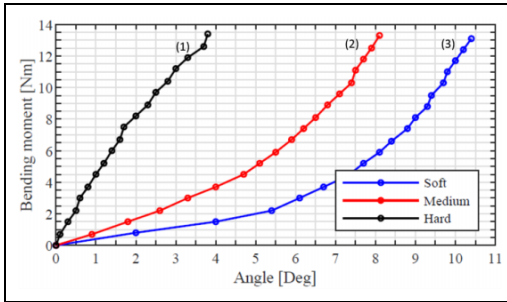


Figure 12. Bending moment/angle curve for the three intervertebral disks of (1) hard, (2) medium, and (3) soft rubber. While all disks show nonlinearity in stiffness, the hard disk displays only its linear part in the range of applied bending torque, due to its high stiffness.

fixed maximum torque. The flexibility of the module enables a natural and comfortable interaction between FB-AXO and human trunk. Meanwhile the stiffness can be adjusted with respect to working conditions. For example, hard rubber disks can be used if the exoskeleton is intended to assist carrying heavy loads.

In usability tests, the participants were asked to complete a set of basic movements related to the prioritized list of motions in Table 1. Tasks for UB-AXO include lifting, lowering, and carrying, while for LB-AXO the task is to walk on treadmill. The tasks for FB-AXO performed include carrying a payload while walking, standing stably in free space, walking up/down stairs, and so on. Figure 13 depicts the usability testing of walking with 6 kg load on a treadmill at a speed of 1.2 m/s. The assistance level was kept constant over the complete interval. A harness on the ceiling was used to protect the user from falling for safety. In total, 24 healthy persons (12 in UB-AXO, 10 in LB-AXO, and 2 in FB-AXO) of ages between 20 and 62 have participated in the usability test separately.

Questions asked include whether they feel comfortable in different poses and also feel support to carry the load. Participants provided positive feedback, which demonstrates FB-AXO's usability to fit and assist users in these tasks. On the other hand, it is also noted that participants feel not easy to put on and take off the exoskeleton and need others' assistance, which could be further improved through engineering design.

Physical assistance testing

Tests were performed for UB-AXO in load carrying assistance, including lifting, lowering a 6 kg payload (Figure 14). In addition, testing includes also a task of carrying the 6 kg payload while walking.

The users are fitted with EMG sensors at the larger muscle groups, including the biceps and deltoid muscles, to record the muscle activities with/without exoskeleton

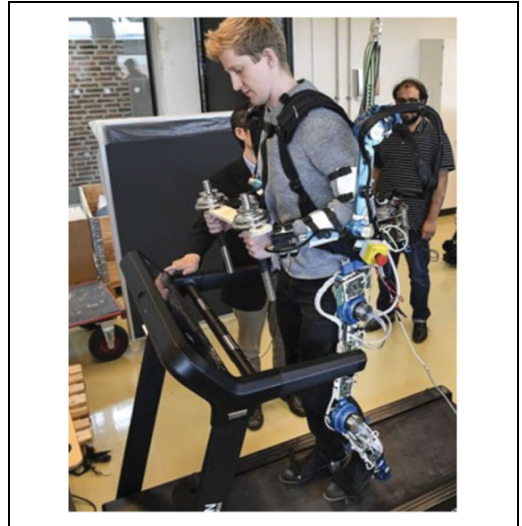


Figure 13. Testing of FB-AXO on carrying payload while walking on treadmill.

assistance. The selection of muscles was made following European recommendations for surface electromyography for the non-invasive assessment of muscles (SENIAM, <http://seniam.org/>). Surface EMG data for all tasks were recorded using the four-channel NeXus-10 MKII hardware and BioTrace+ V2017A software (Mind Media B.V., Netherlands). The EMG data were normalized with respect to maximum voluntary contraction (MVC).

Table 6 presents muscle activities recorded by EMG for two scenarios of the carrying task, one to carry 6 kg payload for 1 min (Carry-M1), the other for 3 min (Carry-M3). The effect of physical assistance can be observed from the data recorded. It is also interesting to notice the difference of assistance effect for the cases of using exoskeleton for 1 min and for 3 min. In the latter case, the assistive effect is more obvious. An explanation to this result is that human users need time to “learn” how to get assistance from exoskeleton. With the current control strategy, the exoskeleton system is not fully adaptive to the given assistive tasks. But once human users learned how to use the system, they can effectively take the advantage of exoskeleton for assistance. This results thus demonstrate also mutual adaptation in the human-exoskeleton interaction.⁴⁶ In general, the test results are mixed, showing an overall positive assistance with most tasks.³⁵ Figure 15 plots variation of interaction force during load carrying. For the 6 kg payload, or 58.8 N, carried by the system, it is observed that roughly 10 N force applied on single human arm, therefore about 20 N force on both arms. In other words, most payload was carried by the exoskeleton, a strong evidence of physical assistance generated.



Figure 14. Test of the UB-AXO with 6 kg payload lifted from the ground to a table.

Table 6. Muscle activities (RMS Amplitude) in load carrying.

Condition	Task	Biceps Brachii (% MVC)			Deltoid(middle)(% MVC)		
		Mean \pm SD	Min	Max	Mean \pm SD	Min	Max
No Exo	Carry-M1	11.78 \pm 5.75	5.36	24.78	2.15 \pm 1.05	0.88	6.32
	Carry-M3	14.17 \pm 8.02	6.72	29.36	2.11 \pm 1.32	0.84	7.16
With Exo	Carry-M1	15.04 \pm 6.15	6.42	37.99	4.65 \pm 2.86	1.48	16.22
	Carry-M3	10.79 \pm 6.81	4.71	28.37	2.35 \pm 2.47	0.90	8.47

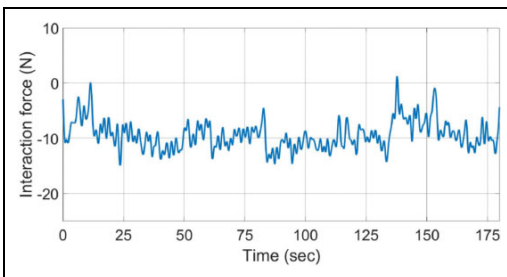


Figure 15. Interaction force during 6 kg load carrying

The performance of the AXO-SUIT was also assessed by Rating of Perceived Exertion (RPE),⁴⁷ which is the numeric estimate of subject's activity intensity. The RPE was measured for participants using a scale from 1 to 10, representing from very light to very heavy perceived exertion. The scores of RPE assessment of UB-AXO module are listed in Table 7, which indicates slightly decreased scores, reflecting the effect of physical assistance by the exoskeleton.

Table 7. Ratings of Perceived Exertion (RPE).

Task	No Exo Median (Min–Max)	with UB-AXO Median (Min–Max)	Med. Difference
Lifting	3.0 (1.0–3.0)	2.0 (1.0–4.0)	–1.0
Lowering	2.0 (1.0–3.0)	2.0 (1.0–4.0)	–0.0
Carrying	4.0 (1.0–5.0)	3.0 (3.0–7.0)	–1.0

It is noted that the performance assessment of exoskeleton systems is a very challenging task, which requires well-defined protocols and assessment criteria, and performance metrics.⁴⁸ While the preliminary tests on FB-AXO show its positive effect on assistance, more study is needed to test the system and assess performance comprehensively.

Conclusions and discussion

In this article, the design of a modular FB powered assistive exoskeleton FB-AXO is presented. The design challenge of kinematic compatibility between user and exoskeleton was addressed through a close end-user involvement.

Table 8. Full-body exoskeletons.

No.	Name	active DoF	Weight(kg)	Main features
1	Body Extender ¹⁸	22	160	DC motors; 50 kg payload
2	XO2 ¹⁹	23	95	Hydraulic powered; 23 kg payload
3	HAL-5 ²⁰	8	23	Battery powered DC motors; 15 kg payload
4	DFKI exoskeleton ⁴⁹	30	41	Battery powered DC motors
5	FB-AXO	10	25	Battery powered DC motors; 5 kg payload

Questionnaires on functional requirements lead to a prioritized list of upper-, lower, and FB motions to assist. A further study of these prioritized motions was done to determine dominating DoFs, the ROM, joint torques and velocities, and so on.

In this work, a novel exoskeleton is designed with two innovative mechanisms: the DPM shoulder joint and biomimetic spine module. The DPM shoulder joint has a high overall stiffness, while being lightweight and compact. The biomimetic spine module transfers loads from the UB-AXO to the LB-AXO with three quasi-passive DoFs. Moreover, it increases the dexterity for upper-body activities allowing the user to complete complex motions, such as reaching to the side overhead/opposite shoulder.

FB-AXO features a high number of DoFs and adjustments to bring higher kinematic compatibility and physical comfort to the user. Compared with other FB exoskeletons, such as HAL-5 and XO2, as shown in Table 8, the FB-AXO has a low weight, while provides mid-duty comprehensive support that are suitable for physical assistance of the elderly.

Results from the preliminary studies, including the usability and functional tests, of the FB-AXO prototype show a good compatibility between the user and exoskeleton and positive effect in physical assistance. On the other hand, the preliminary test reveals also some limitations of the design, which include the considerable weight and also misalignment due to different subject sizes. Moreover, control of human-exoskeleton systems for upper-body exoskeleton applicable for versatile and dexterous arm motion is yet to be developed.

From the preliminary tests, the difference of assistance effects due to variation of using time suggests a strong mutual adaptation between human and exoskeletons. A recent study on wearable robots demonstrates the use of augmentation devices such as exoskeleton relies on our brain's ability to learn, adapt, and interface with the devices.⁵⁰ Further study on the complex kinematic, dynamic, and cognitive synergies between human and exoskeletons could be investigated.

The designed exoskeleton is mainly for light-duty physical assistance of daily activities. The system is also applicable for other purposes, for example, physical training, workplace assistance, and so on. Further investigation on improving the physical assistance and interaction with the LB-AXO, UB-AXO, and FB-AXO is planned.

Acknowledgments

The work reported is supported in part by the EU AAL Programme through project AXO-SUIT (www.axo-suit.eu). MTD Precision Engineering is duly acknowledged for mechanical design and fabrication. The testing results were jointly obtained by participants of the project partners including Aalborg University, University of Gavle, University of Limerick, and Commeto.


Declaration of conflicting interests


The author(s) declared no potential conflicts of interest with respect to the research, authorship, and/or publication of this article.

Funding

The Authors disclosed the receipt of the following financial support for the research, authorship, and/or publication of this article: The EU AAL Joint Programme CALL 6 project 2013-6-042.

ORCID iDs

Sajid Rafique  <https://orcid.org/0000-0002-1813-9030>

Shaoping Bai  <https://orcid.org/0000-0001-5882-9768>

References

- Bogue R. Robotic exoskeletons: a review of recent progress. *Indust Robot: An Int J* 2015; 42(1): 5–10.
- Guizzo E and Goldstein H. The rise of the body bots robotic exoskeletons. *IEEE Spectrum* 2005; 42(10): 50–56.
- Yang CJ, Zhang JF, Chen Y, et al. A review of exoskeleton-type systems and their key technologies. In *Proceedings of the Institution of Mechanical Engineers, Part C: Journal of Mechanical Engineering Science*, vol. 222, pp. 1599–1612.
- Chen B, Ma H, Qin LY, et al. Recent developments and challenges of lower extremity exoskeletons. *J Orthop Translat* 2016; 5: 26–37.
- Lee H, Kim W, Han J, et al. The technical trend of the exoskeleton robot system for human power assistance. *Int J Precis Eng* 2012; 13(8): 1491–1497.
- Gull M, Bai S and Bak T. A review on design of upper limb exoskeletons. *Robotics* 2020; 9: 16.
- Xu K, Zhao J, Qiu D, et al. A pilot study of a continuum shoulder exoskeleton for anatomy adaptive assistances. *ASME J Mech Robot* 2014; 6(4): 041011/1–041011/10.
- Hunt J and Lee H. A new parallel actuated architecture for exoskeleton applications involving multiple degree-of-freedom biological joints. *ASME J Mech Robot* 2018; 5(10): 051017/1–051017/10.

9. Laschowski B, Mcphee J and Andrysek J. Lower-limb prostheses and exoskeletons with energy regeneration: mechatronic design and optimization review. *ASME J Mech Robot* 2019; 11(4): 040801/1–040801/8.
10. Refour E, Sebastian B and Ben-Tzvi P. Two-digit robotic exoskeleton glove mechanism: design and integration. *ASME J Mech Robot* 2018; 10(2): 025002/1–040801/9.
11. Kapsalyamov A, Hussain S and Jamwal PK. State-of-the-art assistive powered upper limb exoskeletons for elderly. *IEEE Access* 2020; 8: 178991–179001.
12. Rupal BS, Rafique S, Singla A, et al. Lower-limb exoskeletons: research trends and regulatory guidelines in medical and non-medical applications. *Int J Adv Robot Sys* 2017; 14(6): 1–27.
13. Lo HS and Xie SQ. Exoskeleton robots for upper-limb rehabilitation: state of the art and future prospects. *Med Eng Phys* 2012; 34(3): 261–268.
14. Sawicki GS, Beck ON, Kang I, et al. The exoskeleton expansion: improving walking and running economy. *J Neuroeng Rehabilitation* 2020; 17(1): 1–9.
15. Herr H. Exoskeletons and orthoses: classification, design challenges and future directions. *J Neuroeng Rehabilitation* 2009; 6(1): 21.
16. Ahmed A, Cheng H, Lin X, et al. Survey of On-line control strategies of human-powered augmentation exoskeleton systems. *Adv Robot Auto* 2016; 05(03): 1–8.
17. Park H, Kim S, Lawton W, et al. Effects of using a whole-body powered exoskeleton on physical demands during manual handling. *Proc Hum Factors Ergon Soc Annu Meet* 2020; 64(1): 888–889.
18. Fontana M, Vertechy R, Marcheschi S, et al. The Body Extender. *IEEE Robot Auto Magazine* 2014; (December): 34–44.
19. Raytheon XOS2 exoskeleton. Available at: <https://www.army-technology.com/projects/raytheon-xos-2-exoskeleton-us/> (2010, accessed 08 February 2019).
20. Sankai Y. HAL: Hybrid assistive limb based on cybernics. *Springer Tracts Adv Robot* 2010; 66: 25–34.
21. Sankai Y. Frame structure of wearable motion assisting device, 2010. WO/2010/035706.
22. Van Der Heide LA, Gelderblom GJ and De Witte LP. Dynamic arm supports: overview and categorization of dynamic arm supports for people with decreased arm function. *IEEE Int Conf Rehabil Robot* 2013; 38(4): 287–302.
23. Kawabata T, Satoh H and Sankai Y. Working posture control of robot suit HAL for reducing structural stress. In *2009 IEEE International Conference on Robotics and Biomimetics, ROBIO 2009*. ISBN 9781424447756, pp. 2013–2018.
24. Yamamoto K, Hyodo K, Ishii M, et al. Development of power assisting suit for assisting nurse labor. *Trans Jpn Soc Mech Eng Series C* 2001; 67: 1499–1506.
25. Yamamoto K, Ishii M, Noborisaka H, et al. Stand alone wearable power assisting suit—sensing and control systems. In *13th IEEE International Workshop on Robot and Human Interactive Communication*. pp. 661–666.
26. Toyama S and Yamamoto G. Development of wearable-agri-robot—mechanism for agricultural work. In *2009 IEEE/RSJ International Conference on Intelligent Robots and Systems, IROS 2009*, St. Louis, USA, 11–15 October 2009, pp. 5801–5806.
27. Vibhute R, Yeole S, Waghmare S, et al. Design, development and analysis of human exoskeleton for enhancing human capabilities. In *IOP Conference Series: Materials Science and Engineering*, volume 1012. p. 012015.
28. Gopura R, Bandara D, Kiguchi K, et al. Developments in hardware systems of active upper-limb exoskeleton robots: a review. *Robot Auto Syst* 2015; 75: 203–220.
29. Schorsch JF, Keemink AQL, Stienen AHA, et al. A novel self-aligning mechanism to decouple force and torques for a planar exoskeleton joint. *Mech Sci* 2014; 5(2): 29–35.
30. Stienen AHA, Hekman EEG, van der Helm FCT, et al. Self-aligning exoskeleton axes through decoupling of joint rotations and translations. *IEEE Trans Robot* 2009; 25(3): 628–633.
31. Sarkisian SV, Ishmael MK and Lenzi T. Self-aligning mechanism improves comfort and performance with a powered knee exoskeleton. *IEEE Trans Neural Syst Rehabilitation Eng* 2021; 29: 629–640.
32. Schiele A. Ergonomics of exoskeletons: subjective performance metrics. In *2009 IEEE/RSJ International Conference on Intelligent Robots and Systems, IROS 2009*, St. Louis, USA, 11–15 October 2009, pp. 480–485.
33. Christensen S, Bai S, Sullivan LO, et al. AXO-SUIT—a modular full-body exoskeleton for physical assistance. In *IFTOMM Symposium on Mechanism Design for Robotics (MEDER)*, volume 4. Springer International Publishing, pp. 443–450.
34. Christensen S and Bai S. Kinematic analysis and design of a novel shoulder exoskeleton using a double parallelogram linkage. *ASME J Mech Robot* 2018; 10(4): 1–27.
35. Bai S, Christensen S, Islam M, et al. Development and testing of full-body exoskeleton AXO-SUIT for physical assistance of the elderly. In: Carrozza MC, Micera S and Pons JL (eds) *Wearable Robotics: Challenges and Trends*. Cham: Springer International Publishing, pp. 180–184.
36. O’Sullivan L, Power V, Virk G, et al. End user needs elicitation for a full-body exoskeleton to assist the elderly. *Procedia Manufac* 2015; 3: 1403–1409.
37. Kruijff BJ, O’Sullivan L, Schmidhauser E, et al. Interaction modelling for wearable assistive devices. In *Proceedings of the 9th ACM International Conference on Pervasive Technologies Related to Assistive Environments*. pp. 1–2.
38. Virk GS, Haider U, Indrawibawa IN, et al. Exo-legs for elderly persons. In: Kozłowski K, Tokhi MO and Virk GS (eds) *Mobile service robotics. Paper presented at 17th International Conference on Climbing and Walking Robots (CLAWAR)*, July 21–23, 2014, Poznan, Poland. Singapore: World Scientific, pp. 85–92.

39. Peebles L and Norris B, of Trade GBD, et al. *Adultdata: The Handbook of Adult Anthropometric and Strength Measurements: Data for Design Safety*. Government consumer safety research, Department of Trade and Industry, 1998.
40. Reichl I, Auzinger W, Schmiedmayer HB, et al. Reconstructing the knee joint mechanism from kinematic data. *Math Comput Model Dyn Syst* 2010; 16: 403–415.
41. Zhou L, Chen W, Wang J, et al. A novel precision measuring parallel mechanism for the closed-loop control of a biologically inspired lower limb exoskeleton. *IEEE/ASME Trans Mech* 2018; 23: 2693–2703.
42. Virk GS, Haider U, Nyoman I, et al. Design of EXO-LEGS exoskeletons. In *Assistive Robotics - Proc. 18th Inter. Conf. On Climbing and Walking Robots and the Support Technologies for Mobile Machines (CLWAR 2015)*. pp. 59–66.
43. Christensen S and Bai S. A novel shoulder mechanism with a double parallelogram linkage for upper-body exoskeletons. In *Wearable Robotics: Challenges and Trends*, volume 16. pp. 51–56.
44. Li J, Zuo S, Xu C, et al. Influence of a compatible design on physical human-robot interaction force: a case study of a self-adapting lower-limb exoskeleton mechanism. *J Intell Robot Syst* 2019; 98(98): 525–538.
45. Grosu V, Grosu S, Vanderborght B, et al. Multi-axis force sensor for human-robot interaction sensing in a rehabilitation robotic device. *Sensors* 2017; 17: 1294.
46. Moreno JC, Brunetti F, Navarro E, et al. Analysis of the human interaction with a wearable lower-limb exoskeleton. *Appl Bionics Biomech* 2009; 6(2): 245–256.
47. Egan A, Winchester J, Foster C, et al. Using session RPE to monitor different methods of resistance exercise. *J Sports Sci Med* 2006; 5: 289–295.
48. Bostelman R, Li-Baboud Y, Virts A, et al. Towards standard exoskeleton test methods for load handling. In *2019 Wearable Robotics Association Conference (WearRAcon)*. pp. 21–27.
49. DFKI GmbH Exoskeleton. Available at: <https://robotik.dfki-bremen.de/en/research/robot-systems/ganzkoerperexoskelett/> (2021, accessed 08 August 2021).
50. Kieliba P, Clode D, Maimon-Mor RO, et al. Robotic hand augmentation drives changes in neural body representation. *Sci Robot* 2021; 6(54): eabd7935.

Chapter 6

Summary of Results and Conclusion

This chapter summarises briefly the included journal papers. Their objectives, methods and the results of the research works in the three papers will be highlighted. The contributions and impact of the work will be presented. Suggestions and recommendations for future work within this field of research are included at the end.

6.1 Summary of Results

Paper I:

Kinematic Analysis and Design of a Novel Shoulder Exoskeleton using a Double Parallelogram Linkage

A novel spherical mechanism for a shoulder exoskeleton joint composed of two revolute joints connected by a double parallelogram linkage (also known as the Double Parallelogram Mechanism) is presented in Paper I. This spatial mechanism has a remote centre-of-rotation that coincides with anatomical shoulder joint centre-of-rotation without interfering with the natural motion of the joint or colliding with the soft tissue of the human body. The forward and inverse kinematics of this mechanism are derived theoretically and an analysis of the manipulability analysis demonstrates that the mechanism is singularity-free within its ROM. This innovative mechanism was designed to overcome the drawbacks of the traditional serial-linkage shoulder mechanisms, which are bulky and kinematically limited. These mechanisms protrude away from the human body and suffer from singular points within its workspace, where the mechanisms lose a DOF and cannot move any further.

Moreover, the bulky design of these mechanisms limit the real workspace of the exoskeleton, due to interference with the human. An analysis of the reachable workspace for the DPM yield that 90% of human glenohumeral joint could be reached without collision between the mechanism and human shoulder. Finally, the real workspace of the DPM was experimentally investigated, yielding a large ROM without interference with the user of the exoskeleton. The weight of the constructed double parallelogram linkage was approx. 200g, hence, the design is deemed well suited for portable upper-body exoskeletons.

Paper II:

Modeling and Analysis of Physical Human-Robot Interaction of an Upper Body Exoskeleton in Assistive Application

To aid the design process of the UB-AXO exoskeleton, a human-exoskeleton co-simulation model, presented in Paper II, is used to analyse the physical interaction between a bio-mechanical model of the human arm and the conceptual design of UB-AXO. The exoskeleton is illustrated in Fig. 6.1, which features the aforementioned Double Parallelogram Mechanism as its shoulder mechanism (Paper I). The exoskeleton is designed to actively support the anatomical shoulder abduction/adduction and flexion/extension along with the elbow flexion, while the shoulder internal/external rotation is added as a passive joint in order to realise the ROM required by the end-users.

The human-exoskeleton system in this work comprises two systems: (1) a musculoskeletal human body and (2) an exoskeleton model. The human-exoskeleton model is implemented in the musculoskeletal modelling software AnyBody Modeling System [128]. The musculoskeletal model is sized as a 50th percentile European male and derived from the repository in AnyBody and the mechanical properties of the exoskeleton are extracted from CAD using SolidWorks. As input to the model artificially generated using kinematic drivers of the elbow and shoulder was used to drive the musculoskeletal arm. The exoskeleton model consists of all links, joints and motors of the exoskeleton in Fig. 6.1. The assistance of the exoskeleton follows an ideal static-load compensation control strategy. In essence, the control is an open loop gravity compensation that neglects effects like friction and interaction control, which must be included in a real system. The control only utilises sensor telemetry from the exoskeleton, thus, the exoskeleton control is decoupled from telemetry from the human model. The two systems are connected at three ports of interaction, namely the trunk, upper arm and forearm in order to supply joint level assistance. A set of kinematic and kinetic constraints are formulated at the three ports to form a single mechanical system in the analysis model and are formulated to give a realistic interaction between the human and exoskeleton.

The kinematic constraints between the two systems make the whole system kinematically over-determined, thus there is no unique solution to the kinematics. The AnyBody software is able to handle a kinematically over-determined system through a nonlinear least-squares optimisation algorithm, where "soft" constraints are allowed small kinematic errors.

The kinetic constraints are formulated as a contact problem using the unilateral contact model in the AnyBody Software, which consists of a unilateral normal force, i.e., pressure forces and friction forces. The contact forces are determined by calculating the reaction forces between a base and a target node, where the base node is attached to the exoskeleton and the target node on the human musculoskeletal body. The base node constitutes a cylindrical space to establish contact between the two nodes, i.e., if the target node enters the cylindrical space, the exoskeleton and human have contact.

The human-exoskeleton model is used to simulate internal body loads, such as muscle activity and joint reaction forces under the influence of the UB-AXO in addition to the power and energy consumption needed for the motion assistance. The model also allows us to estimate the dynamic behaviour of the human-exoskeleton system and conduct comprehensive simulations to improve our understanding of the pHRI and, finally, to design an exoskeleton with improved pHRI. This is demonstrated with two simulation cases; one for a simple bicep curl and the other for an overhead reach related to the ADLs required by the end-users. The simulation results show that the use of the UB-AXO can significantly reduce the required maximum muscle activity, targeted human joint torques and muscle energy consumption in the human arm by 30% to 45% with the low-level assistance control and 33% to 62% for the high-level assistance control.

Paper III:

Design of a powered full-body exoskeleton for physical assistance of elderly people

Paper III presents the design, development, construction and preliminary evaluation of a powered full-body exoskeleton for weaker ageing adults. The development of the entire system is driven by a close interaction with the end-user to derive requirements, assessment of the designs and preliminary test and evaluation of the system performance. To support the development further, three-dimensional human kinetic and kinematic simulation data were gathered for the highest priority tasks to decide the ROM and torque requirements at the joints of the FB-AXO, which were also used in Paper II.

The exoskeleton, named FB-AXO, features a high number of DOFs and adjustments to add a higher level of kinematic compatibility and physical comfort to the user. Compared with other full-body exoskeletons, the FB-AXO has a low weight, while being able to provide medium-duty and com-

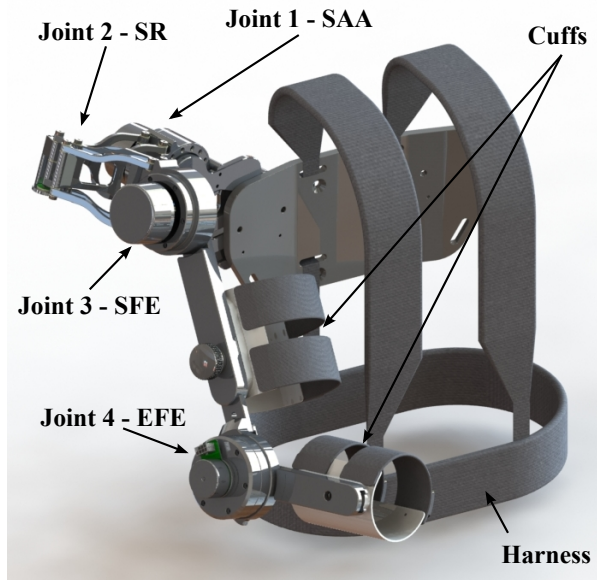


Fig. 6.1: Conceptual design of the UB-AXO

prehensile support, which is suitable for physical assistance of the elderly. FB-AXO is a modular system, comprised by two main subsystems; the lower body exoskeleton LB-AXO and upper body exoskeleton UB-AXO. The UB-AXO is a second iteration of the version presented in Paper II, where a spine module has been added. The spine module is designed to transfer the load from the UB-AXO to the LB-AXO, while matching the three DOFs of the lumbar spine, which are passively supported by rubber disks. The rubber disks come in three different stiffness properties and can be changed pending the use-case of the exoskeleton. The additional DOFs from the spine module increase the dexterity for upper-body activities, thus allowing the user to complete complex motions, such as reaching to the side overhead/opposite shoulder. Each subsystem is capable to work autonomously, as the assistance of the device is provided at joint level. The final design of FB-AXO weighs 25 kg and includes a total of 27 DOFs, of which 10 are active and 17 are passive. All the active DOFs are powered using DC motors and harmonic gears for compact, light and backdrivable actuation. To fit a broader range of users a number of adjustments, e.g. length adjustments of the shank, thigh and upper arm) are included for the FB-AXO to bring a higher kinematic compatibility and physical comfort to the user.

The LB-AXO and UB-AXO follow different control strategies. The LB-AXO uses a force-based control strategy, that functions on human

and exoskeleton interaction from a set of force sensors. This includes load cells in foot module to detect heel strike and "toe-off" and centre of pressure of the system, and load cells in the thigh and shank to anticipate human intention for walking. The high level control strategy for UB-AXO is a static load compensation strategy, which compensates the gravitational load of the human arm τ_g and an external load in the hand of the user reflected in exoskeleton joints τ_l , to deliver a desired assistive joint torque, τ_{ass} , for the different joints. Similar strategy was presented in Paper II. Hence, the high level control can be expressed as:

$$\tau_{ass} = \mathbf{K} (\tau_g + \tau_l) \quad (6.1)$$

where \mathbf{K} defines the assistance levels of all joints.

The assistance contributions τ_g and τ_l are estimated based on inputs from the user, where a control interface is used to enter the weight for the user and the weight of the object to be carried. The individual masses of the upper body limbs, i.e. upper arm and forearm, are calculated based on estimated mass properties from [136]. Since, the exoskeleton presumes it is kinematically compatible with the human kinematics, the exoskeleton joint angles can be used to calculate their contributions to the desired assistive joint torque.

The control can switch between "free motion" and "assistive" mode. In "free motion" the assistance level \mathbf{K} is set to zero, meaning the desired assistive torque is zero. To provide the desired assistance torque, the low level control is implemented, which consists of an admittance control, consisting

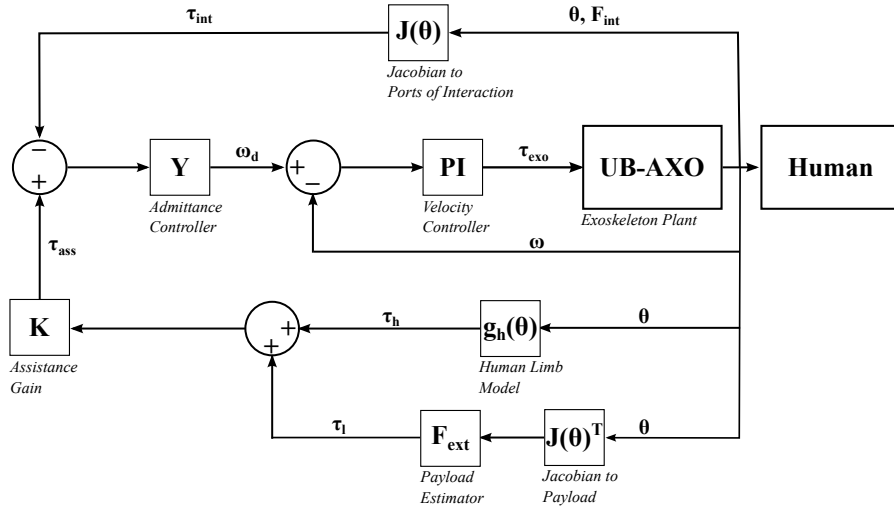


Fig. 6.2: Admittance based control strategy adopted in Paper III for UB-AXO.

of an admittance filter $Y(s)$ and velocity PI-controller. The admittance filter had the following form:

$$Y(s) = \frac{\omega_d}{\tau_{ass}} = \frac{1}{Bs + D} \quad (6.2)$$

where B and D is the desired inertia and dampening, respectively, at the given interaction port. The control strategy is illustrated in Fig. 6.2.

It is noted that the control implementation of the low level control in Paper III was not detailed. However, this has been corrected in later publications of researchers in the AXO-SUIT project [126, 137].

The FB-AXO, UB-AXO and LB-AXO are all subjected to user testing to evaluate the usability of the exoskeletons in terms of user satisfaction and performance. A total of 24 subjects were involved with the testing (12 in UB-AXO, 10 in LB-AXO and 2 in FB-AXO). The test subject were ask to perform tasks derived from the end-user requirements with and without the exoskeletons. Following the tasks, the subject were asked to access the Rating of Perceived Exertion (RPE), which is a numeric estimate of subject's activity intensity. For the UB-AXO, the test subjects were also fitted with EMG sensors on two larger muscle groups in the upper arm, the biceps brachii and middle deltoid muscles, to compare the muscle activity with and without the exoskeleton.

The results show, that the prototypes demonstrates a good compatibility between the user and exoskeleton and positive effect in physical assistance, especially the RPE, while the EMG measurements were more conflicting. The RPE was reduced with nearly 33% for the lifting and carrying tasks, while for the lowering task it was unchanged. The %MVC (Percentage of participant's Maximal Voluntary Contraction from the EMG daga) should effect of assistance the 3 minute carrying task, however, for the 1 minute carrying task did not demonstrate an obvious assistance. For the bicep the %MVC was reduced from 14.17 to 10.78 for the 3 minute carrying task, while for the 1 minute carrying task, the %MVC was increased from 11.78 to 15.04. For the deltoid %MVC all increased when using the exoskeleton.

Hence, it is noted that the performance assessment of the exoskeleton systems is a very challenging task, which requires well-defined protocols and assessment criteria, and performance metrics.

6.2 Contributions

The main contribution presented in this thesis is the development of an upper body exoskeleton through an user-centered design approach supported by a

bio-mechanical simulation to achieve improved physical human-robot interaction. As a result, a novel hybrid upper body exoskeleton, named UB-AXO, was proposed, designed, constructed and tested with potential end-users.

The shoulder module in UB-AXO consists of an innovative spherical mechanism, named DPM (Double Parallelogram Mechanism). The spherical mechanism is designed with a double parallelogram linkage (DPL), which connects two revolute joints to implement the motion as a spherical joint, while maintaining the remote centre-of-rotation. The design has several new features compared to the current state-of-the-art, such as a relative large ROM free of singularity, a high overall stiffness and a lightweight and compact design. These are all features that make it suitable for assistive exoskeletons. This invention resulted in a patent application, *Patent No. WO 2017/167349*

The complex physical interaction between the human body and robotic exoskeleton was addressed with a human-exoskeleton model. The problem of physical contact between the exoskeleton and the human limb was addressed through the kinematic and kinetic connection. The kinematic overdeterminate connection was solved using a nonlinear least-square optimisation algorithm to minimise the kinematic error between the two systems. Unidirectional contact elements were implemented to model the force transmission between the human and exoskeleton. The model was used to not only simulate biomechanical effects of the UB-AXO, such as muscle forces and joint reaction forces, but also the power and energy consumption needed for the motion assistance. For actively actuated exoskeletons, the power exchange is of interest, as power is not only fed to the human, but also extracted. Hence, the excessive energy from the exoskeleton could be converted to electric energy and stored for later use, rather than having it dissipated in the electronics.

A major part of this research is linked to the end-user involvement, which plays a key role in the development for human-robotic systems. For the preliminary testing of the exoskeleton, both objective measures (i.e., electromyography) and subjective measures (i.e., ratings of user exertion and overall user experience) were collected to assess the performance of the system. This provided valuable data on the usability of the system, as well as the user acceptance of the system. The latter has quite often been ignored in the tests conducted on other exoskeleton systems. Hence, the user assessment method of the motion assistance of the exoskeleton is a major contribution of this work.

6.3 Limitation and Future Work

The previous section listed the different contributions made to advance the current state-of-the-art in the field of wearable robotics, however, some limitations were found during this project. Hence, the presented research can be extended and improved in numerous ways. For that purpose, this section lists some limitations of this work and also recommendations for future works.

In Paper I the reachable workspace of the spherical mechanism, DPM, was analysed with a simple sphere to represent the human shoulder geometry. Subsequently, the ROM was assessed in an exoskeleton setup, where only a single DOF was tested at a time, e.g., shoulder flexion/extension. Moreover, the ROM was only tested with the remaining DOFs in their anatomical position. Hence, the reachable workspace was not investigated in full detail. Experimental investigation using motion capture, like the method proposed by Castro et al. [138], could provide more detailed insight into how well the DPM actually covers the anatomical ROM. This also requires a mechanism that can supplement the shoulder girdle movements, due to the scapulo-humeral rhythm.

The human-exoskeleton model presented in Paper II needs validation to verify the modelling approach of the force transfer using contact modelling. This could be achieved by motion capture of simple biceps curls, as one of the simulation cases considered in the paper, combined with EMG measurements of the larger muscle groups and force/pressure sensing of the interaction forces between the human and exoskeleton. Moreover, the model should also be extended to include the entire human musculoskeletal system to study the impact of the weight on the spine and the shifting of centre of mass of the exoskeleton, as it is known from the useability testing to have an influence on the force transfer characteristic between the two systems. Finally, the model should be driven by real motion data to generate more realistic movements of the human limb and exoskeleton for better assessment of the physical interaction and exoskeleton performance.

In Paper III the end-user testing of the full body exoskeleton also revealed some limitations of the system, from which major lessons have been learned for future work. On the design of the exoskeleton, one important limitation of the system performance is linked to the total weight of the system. Although, the weight is low compared to other state-of-the-art full-body exoskeletons, it is still too heavy for user acceptance. Thus, the total weight needs to be improved. One improvement could be to the actuation. In the UB-AXO, the

actuation accounts for more than half of the total weight; hence, alternative high power intensity actuators should be considered or replaced with passive spring supports. Moreover, to reduce the weight further, the structural design could be improved. Currently, the structural design has not been optimised, nor have alternative materials to aluminium been considered. Thus, it is fair to assume that the weight can be reduced substantially by investigating these areas.

The issue of kinematic alignment, i.e., the possible misalignment of human joints and the counterparts of the exoskeleton, still needs further work. The shoulder girdle movements were not supported by the exoskeleton, which for some end-users posed constraint movements and even motion resistance rather than assistance. Finally, the compactness of the exoskeleton design has to be considered further to achieve a higher degree of user acceptance.

The preliminary tests of the UB-AXO involved a total of 12 subjects. Note that the testing was split into two levels, where Level 1 were healthy adults at age 18 years and over, while Level 2 were healthy adults at age 50 years and over, as reported in [126]. Level 1 test subjects (total of eight) participated in a more elaborate test protocol, which included EMG measurements, while Level 2 (total of four) completed a simpler test protocol, which did not include EMG measurements, but only their RPE. As a result, the duration of the test was one hour for Level 1 and only half an hour for Level 2. The split in Level 1 and 2 test subjects was done due to safety consideration of the older adults. Hence, for more complete assessment of user acceptance, a larger pool of Level 2 tests are required.

The results of the objective measures (i.e., EMG measurements) and subjective measures (i.e., RPE and overall user experience) were at times inconsistent. In general, the RPE indicated a positive effect in assistance, while the EMG measurements did not. The risk with subjective measures, such as the RPE, is that the subject might feel they receive assistance even though that is not the case. To improve the credibility of the RPE, a placebo trial could be included in the test protocol, where the exoskeleton is programmed not to assist the subject. This test trial could then be used to cross check the subjects responses, rather than only trust the evaluation of the test subjects. However, it should also be noted that the EMG measurements had a high SD variation among the test subjects. This could be explained by differences of compatibility with the exoskeleton, as this will affect their muscle activities with operating the exoskeleton. Alternatively, cognitive activities could also influence the measurements, as some of the subjects indicated some nervousness about wearing the exoskeleton. Nevertheless, to perform proper statistical analysis on the results, a larger pool of subjects is needed.

The experimental tests only focused on the short-term use of the exoskeletons' systems. The long-term use of the portable assistive devices, like the FB-AXO, LB-AXO and UB-AXO, needs to be studied to determine its impact

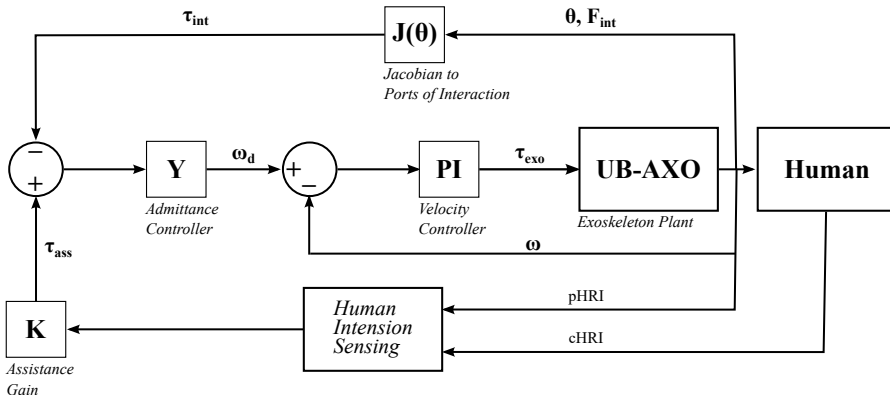


Fig. 6.3: General application of the admittance based control strategy adopted in Paper III.

when performing more realistic movements during ADLs. This could also provide valuable information on if or how the human can adapt to use of the exoskeleton, i.e., is the human able to learn how to utilise the assistance from the exoskeletons better over time?

The control strategy utilised for the testing of the UB-AXO did not include any method for human intention sensing. Instead, a simple static load compensation strategy was adopted, which included gravitational compensation of the human arm and an external load in the hand of the user. Hence, the intention of the human was simply to input the weight of the object to be held. To give more comprehensive support, such as push/pull actions, a better method of acquiring human intention is required. However, the framework of the admittance based control strategy presented can be applied in a general sense, providing that the human intention algorithm can produce a desired joint torque, as illustrated in Fig. 6.3.

References

- [1] AXO-SUIT, "AXO-SUIT Project webpage."
<https://www.axo-suit.eu/>.
Accessed: 2022-08-19.
- [2] K. Wilhelmson, C. Andersson, M. Waern, and P. Allebeck, "Elderly people's perspectives on quality of life," *Ageing Soc.*, vol. 25, no. 2005, pp. 585–600, 2005.
- [3] A. G. Dunning and J. L. Herder, "A review of assistive devices for arm balancing," *IEEE Int. Conf. Rehabil. Robot.*, 2013.
- [4] R. a. R. C. Gopura, K. Kiguchi, and D. S. V. Bandara, "A brief review on upper extremity robotic exoskeleton systems," *2011 6th Int. Conf. Ind. Inf. Syst. ICIIS 2011 - Conf. Proc.*, vol. 8502, pp. 346–351, 2011.
- [5] H. S. Lo and S. Xie, "Optimization and analysis of a redundant 4R spherical wrist mechanism for a shoulder exoskeleton," *Robotica*, vol. 32, no. 08, pp. 1191–1211, 2014.
- [6] D. Hill, C. S. Holloway, D. Z. M. Ramirez, P. Smitham, and Y. Pappas, "What are user perspectives of exoskeleton technology? a literature review," *International journal of technology assessment in health care*, vol. 33, no. 2, pp. 160–167, 2017.
- [7] L. Shore, V. Power, A. De Eyto, and L. W. O'Sullivan, "Technology acceptance and user-centred design of assistive exoskeletons for older adults: A commentary," *Robotics*, vol. 7, no. 1, 2018.
- [8] K. G. Davis, C. R. Reid, D. D. Rempel, and D. Treaster, "Introduction to the human factors special issue on user-centered design for exoskeleton," *Human Factors*, vol. 62, no. 3, pp. 333–336, 2020.
- [9] E. Rocon, A. F. Ruiz, R. Raya, A. Schiele, J. L. Pons, J. M. Belda-Lois, R. Poveda, M. J. Vivas, and J. C. Moreno, *Human-Robot Physical Interaction*. John Wiley & Sons, Ltd, 2008.
- [10] S. Bai and G. S. Virk, *Wearable exoskeleton systems : design, control and applications*. IET control, robotics and sensors series ; 108, London, England: Institution of Engineering and Technology, 2018.
- [11] H. Herr, "Exoskeletons and orthoses: classification, design challenges and future directions," *J. Neuroeng. Rehabil.*, vol. 6, no. 1, p. 21, 2009.
- [12] General Electric, "Hardiman Project."
<https://www.ge.com/news/taxonomy/term/2999>.
Accessed: 2022-08-19.

-
- [13] H. Kazerooni, "Human-Robot Interaction via the Transfer of Power and Information Signals," *IEEE Transactions on Systems, Man and Cybernetics*, vol. 20, no. 2, pp. 450–463, 1990.
- [14] M. Fontana, R. Vertechy, S. Marcheschi, F. Salsedo, and M. Bergamasco, "The Body Extender," *IEEE Robotics & Automation Magazine*, no. December, pp. 34–44, 2014.
- [15] A. B. Zoss, H. Kazerooni, and A. Chu, "Biomechanical Design of the Berkeley Lower Extremity Exoskeleton (BLEEX)," *IEEE/ASME Transactions on Mechatronics*, vol. 11, no. 2, pp. 128–138, 2006.
- [16] Lockheed Martin, "ONXY Exoskeleton."
<https://www.ucf.edu/pegasus/power-move-onyx-exoskeleton/>.
Accessed: 2022-08-19.
- [17] Raytheon, "XOS2 Exoskeleton."
<https://www.army-technology.com/projects/raytheon-xos-2-exoskeleton-us/>.
Accessed: 2022-08-19.
- [18] A. Dollar and H. Herr, "Design of a quasi-passive knee exoskeleton to assist running," in *2008 IEEE/RSJ International Conference on Intelligent Robots and Systems*, pp. 747–754, IEEE, 2008.
- [19] EKSO Bionics, "EKSO Bionics Exoskeleton."
<https://eksobionics.com/ekshealth/>.
Accessed: 2022-08-19.
- [20] Y. Sankai, "HAL: Hybrid assistive limb based on cybernics," *Springer Tracts in Advanced Robotics*, vol. 66, pp. 25–34, 2010.
- [21] A. Schiele and F. C. T. Van Der Helm, "Kinematic design to improve ergonomics in human machine interaction," *IEEE Transactions on Neural Systems and Rehabilitation Engineering*, vol. 14, no. 4, pp. 456–469, 2006.
- [22] A. Schiele, "Ergonomics of exoskeletons: Subjective performance metrics," *2009 IEEE/RSJ International Conference on Intelligent Robots and Systems, IROS 2009*, pp. 480–485, 2009.
- [23] H. Lee, W. Kim, J. Han, and C. Han, "The technical trend of the exoskeleton robot system for human power assistance," *Int. J. Precis. Eng. Manuf.*, vol. 13, no. 8, pp. 1491–1497, 2012.
- [24] T. Nef, M. Guidali, and R. Riener, "ARMin III – arm therapy exoskeleton with an ergonomic shoulder actuation," *Appl. Bionics Biomech.*, vol. 6, no. January 2015, pp. 127–142, 2009.

- [25] J. Rosen, J. Perry, N. Manning, S. Burns, and B. Hannaford, "The human arm kinematics and dynamics during daily activities - toward a 7 dof upper limb powered exoskeleton," in *ICAR '05. Proceedings., 12th International Conference on Advanced Robotics, 2005.*, pp. 532–539, 2005.
- [26] J. C. Perry, J. Rosen, and S. Burns, "Upper-limb powered exoskeleton design," *IEEE/ASME Trans. Mechatronics*, vol. 12, no. 4, pp. 408–417, 2007.
- [27] J. C. Perry, J. M. Powell, and J. Rosen, "Isotropy of an upper limb exoskeleton and the kinematics and dynamics of the human arm," *Appl. Bionics Biomech.*, vol. 6, no. 2, pp. 175–191, 2009.
- [28] S. J. Ball, I. E. Brown, and S. H. Scott, "MEDARM: A rehabilitation robot with 5DOF at the shoulder complex," *IEEE/ASME Int. Conf. Adv. Intell. Mechatronics, AIM*, 2007.
- [29] D. Gijbels, I. Lamers, L. Kerkhofs, G. Alders, E. Knippenberg, and P. Feys, "The Armeo Spring as training tool to improve upper limb functionality in multiple sclerosis: a pilot study," *J. Neuroeng. Rehabil.*, vol. 8, no. 2008, p. 5, 2011.
- [30] M. A. Gull, S. Bai, and T. Bak, "A review on design of upper limb exoskeletons," *Robotics*, vol. 9, no. 1, 2020.
- [31] L. Bishop and J. Stein, "Three upper limb robotic devices for stroke rehabilitation: A review and clinical perspective," *NeuroRehabilitation*, vol. 33, pp. 3–11, 2013.
- [32] H. S. Lo and S. Q. Xie, "Exoskeleton robots for upper-limb rehabilitation: State of the art and future prospects," *Med. Eng. Phys.*, vol. 34, no. 3, pp. 261–268, 2012.
- [33] R. a. R. C. Gopura and K. Kiguchi, "Mechanical designs of active upper-limb exoskeleton robots state-of-the-art and design difficulties," *2009 IEEE Int. Conf. Rehabil. Robot. ICORR 2009*, pp. 178–187, 2009.
- [34] R. Gopura, D. Bandara, K. Kiguchi, and G. Man, "Developments in hardware systems of active upper-limb exoskeleton robots: A review," *Robotics and Autonomous Systems*, vol. 75, pp. 203–220, 2015.
- [35] K.-h. Chay, J.-v. Lee, Y.-d. Chuah, and Y.-z. Chong, "Upper Extremity Robotics Exoskeleton: Application , Structure and Actuation," *International journal of Biomedical Engineering and Science (IJBES)*, vol. 1, no. 1, pp. 35–45, 2014.

- [36] A. J. Veale and S. Q. Xie, "Towards compliant and wearable robotic orthoses: A review of current and emerging actuator technologies," *Medical Engineering & Physics*, vol. 38, no. 4, pp. 317–325, 2016.
- [37] A. H. Stienen, E. E. Hekman, F. C. Van Der Helm, and H. Van Der Kooij, "Self-aligning exoskeleton axes through decoupling of joint rotations and translations," *IEEE Transactions on Robotics*, vol. 25, no. 3, pp. 628–633, 2009.
- [38] M. Cempini, S. M. M. De Rossi, T. Lenzi, N. Vitiello, and M. C. Carrozza, "Self-alignment mechanisms for assistive wearable robots: A kinetostatic compatibility method," *IEEE Trans. Robot.*, vol. 29, no. 1, pp. 236–250, 2013.
- [39] T. Rahman, S. Stroud, R. Ramanathan, M. Alexander, R. Seliktar, and W. Harwin, "Task priorities and design for an arm orthosis," *Technol. Disabil.*, vol. 5, pp. 197–203, 1996.
- [40] G. Walsh, D. Streit, and B. Gilmore, "Spatial spring equilibrators theory," *Mech. Mach. Theory*, vol. 26, pp. 155–170, jan 1991.
- [41] Crimson Dynamics Technology, "CDYS Exoskeleton."
<https://www.c-dyn.com/product>.
Accessed: 2022-08-19.
- [42] Robo-Mate Project, "Robo-mate exoskeleton."
<https://www.robo-mate.eu/>.
Accessed: 2022-08-19.
- [43] EKSO Bionics, "EKSO EVO Exoskeleton."
<https://eksobionics.com/ekso-evo/>.
Accessed: 2022-08-19.
- [44] ottobock, "Paexo shoulder exoskeleton."
<https://paexo.com/paexo-shoulder/?lang=en>.
Accessed: 2022-08-19.
- [45] P. Maurice, J. Camernik, D. Gorjan, B. Schirrmeister, J. Bornmann, L. Tagliapietra, C. Latella, D. Pucci, L. Fritzsche, S. Ivaldi, and J. Babič, "Objective and Subjective Effects of a Passive Exoskeleton on Overhead Work," *IEEE Transactions on Neural Systems and Rehabilitation Engineering*, vol. 28, no. 1, pp. 152–164, 2020.
- [46] SuitX, "Shoulderx exoskeleton."
<https://www.suitx.com/shoulderx>.
Accessed: 2022-08-19.

- [47] S. Alabdulkarim, S. Kim, and M. A. Nussbaum, "Effects of exoskeleton design and precision requirements on physical demands and quality in a simulated overhead drilling task," *Applied ergonomics*, vol. 80, pp. 136–145, 2019.
- [48] skelex, "Skelet360-xfr shoulder exoskeleton."
<https://www.skelex.com/skelex-360-xfr/>.
Accessed: 2022-08-19.
- [49] A. de Vries, M. Murphy, R. Könemann, I. Kingma, and M. de Looze, "The amount of support provided by a passive arm support exoskeleton in a range of elevated arm postures," *IIEE transactions on occupational ergonomics and human factors*, vol. 7, no. 3-4, pp. 311–321, 2019.
- [50] K. S. Stadler, R. Altenburger, E. Schmidhauser, D. Scherly, J. Ortiz, S. Toxiri, L. Mateos, and J. Masood, "Robo-mate an exoskeleton for industrial use : concept and mechanical design," in *Advances in Cooperative Robotics : Proceedings of the 19th International Conference on CLAWAR 2016* (M. O. Tokhi and G. S. Virk, eds.), (London), pp. 806–813, World Scientific, 2016. 19th International Conference on CLAWAR, London, 12-14 September 2016.
- [51] J. van der Vorm, R. Nugent, and L. O'Sullivan, "Safety and risk management in designing for the lifecycle of an exoskeleton: A novel process developed in the robo-mate project," *Procedia Manufacturing*, vol. 3, pp. 1410–1417, 2015. 6th International Conference on Applied Human Factors and Ergonomics (AHFE 2015) and the Affiliated Conferences, AHFE 2015.
- [52] Ergo Santé Technologie, "Shivaexo exoskeleton."
<https://www.shivaexo.fr/en/>.
Accessed: 2022-08-19.
- [53] TILTA, "ARMOR MAN Exoskeleton."
<https://tilta.com/shop/armor-man-3-0-gimbal-support-system/>.
Accessed: 2022-08-19.
- [54] D. Anton and D. L. Weeks, "Prevalence of work-related musculoskeletal symptoms among grocery workers," *International Journal of Industrial Ergonomics*, vol. 54, pp. 139–145, 2016.
- [55] K. Abbruzzese, D. Lee, A. Swedberg, H. Talasan, and M. Paliwal, "An innovative design for an assistive arm orthosis for stroke and muscle dystrophy," in *2011 IEEE 37th Annual Northeast Bioengineering Conference, NEBEC 2011*, no. C, 2011.

- [56] L. Zhou, S. Bai, M. S. Andersen, and J. Rasmussen, "Design and Optimization of a Spring-loaded Cable-driven Robotic Exoskeleton," *25th Nord. Semin. Comput. Mech.*, pp. 205–208, 2012.
- [57] L. Zhou, S. Bai, M. Andersen, and J. Rasmussen, "Modeling and design of a spring-loaded, cable-driven, wearable exoskeleton for the upper extremity," *Modeling, Identification and Control (Online)*, vol. 36, no. 3, pp. 167–177, 2015.
- [58] L. Zhou and Y. Li, "Design optimization on passive exoskeletons through musculoskeletal model simulation," *2016 IEEE International Conference on Robotics and Biomimetics, ROBIO 2016*, pp. 1159–1164, 2017.
- [59] L. Zhou, S. Bai, and Y. Li, "Energy Optimal Trajectories in Human Arm Motion Aiming for Assistive Robots," *Modeling, Identification and Control: A Norwegian Research Bulletin*, vol. 38, no. 1, pp. 11–19, 2017.
- [60] S. Kim, M. A. Nussbaum, M. I. Mokhlespour Esfahani, M. M. Alemi, B. Jia, and E. Rashedi, "Assessing the influence of a passive, upper extremity exoskeletal vest for tasks requiring arm elevation: Part ii – "unexpected" effects on shoulder motion, balance, and spine loading," *Applied Ergonomics*, vol. 70, pp. 323–330, 2018.
- [61] K. Huysamen, T. Bosch, M. de Looze, K. S. Stadler, E. Graf, and L. W. O'Sullivan, "Evaluation of a passive exoskeleton for static upper limb activities," *Applied ergonomics*, vol. 70, pp. 148–155, 2018.
- [62] Levitate Technologies Inc, "Airframe exoskeleton."
<https://www.levitatetech.com/>
Accessed: 2022-08-19.
- [63] M. Marino, "Impacts of using passive back assist and shoulder assist exoskeletons in a wholesale and retail trade sector environment," *IISE Transactions on Occupational Ergonomics and Human Factors*, vol. 7, no. 3-4, pp. 281–290, 2019.
- [64] Cyber Human Systems, "BESK Exoskeleton."
<https://en.cyberhs.eu/besk>.
Accessed: 2022-08-19.
- [65] Exy ONE, "Exy ONE Exoskeleton webpage."
<https://exygroup.com/en/#exyone-shoulder>.
Accessed: 2022-08-19.
- [66] Human Mechanical Technologies (HMT), "LIGHT Exoskeleton."
<https://www.hmt-france.com/en/ourExoskeletons/light>.
Accessed: 2022-08-19.

- [67] Comau, "MATE-XT Exoskeleton."
<https://mate.comau.com/>.
Accessed: 2022-08-19.
- [68] Human Mechanical Technologies (HMT), "PLUM' Exoskeleton web-page."
<https://www.hmt-france.com/en/ourExoskeletons/plum>.
Accessed: 2022-08-19.
- [69] T. Rahman, W. Sample, S. Jayakumar, M. M. King, J. Y. Wee, R. Seliktar, M. Alexander, M. Scavina, and A. Clark, "Passive exoskeletons for assisting limb movement," *J. Rehabil. Res. Dev.*, vol. 43, no. 5, p. 583, 2006.
- [70] D. Ragonesi, S. K. Agrawal, W. Sample, and T. Rahman, "Quantifying anti-gravity torques for the design of a powered exoskeleton.," *IEEE transactions on neural systems and rehabilitation engineering : a publication of the IEEE Engineering in Medicine and Biology Society*, vol. 21, pp. 283–8, mar 2013.
- [71] T. Rahman, W. Sample, R. Seliktar, M. Alexander, and M. Scavina, "A body-powered functional upper limb orthosis," *Journal of rehabilitation research and development*, vol. 37, no. 6, pp. 675–680, 2000.
- [72] EKSO Bionics, "EKSO UE Exoskeleton."
<https://eksobionics.com/ekshealth/>.
Accessed: 2022-08-19.
- [73] AGADE srl website, "AGADEXO Exoskeleton."
<https://agade-exoskeletons.com/en/agade-eng/>.
Accessed: 2022-08-19.
- [74] A. Ebrahimi, "Stuttgart exo-jacket: An exoskeleton for industrial upper body applications," in *2017 10th International Conference on Human System Interactions (HSI)*, pp. 258–263, IEEE, 2017.
- [75] S. Lessard, P. Pansodtee, A. Robbins, J. M. Trombadore, S. Kurniawan, and M. Teodorescu, "A soft exosuit for flexible upper-extremity rehabilitation," *IEEE Transactions on Neural Systems and Rehabilitation Engineering*, vol. 26, no. 8, pp. 1604–1617, 2018.
- [76] R. Singer, C. Maufroy, and U. Schneider, "Automatic support control of an upper body exoskeleton—method and validation using the stuttgart exo-jacket," *Wearable Technologies*, vol. 1, 2020.
- [77] AUXIVO, "Eduexo-pro exoskeleton."
<https://www.auxivo.com/eduexo-pro>.
Accessed: 2022-08-19.

- [78] V. Bartenbach and C. Shirota, "Design and impact of a commercial educational robotic exoskeleton," in *Inclusive Robotics for a Better Society* (J. L. Pons, ed.), vol. 25, (Cham), pp. 136 – 140, Springer, 2020. 1st International Conference on Inclusive Robotics for a better Society (INBOTS 2018); Conference Location: Pisa, Italy; Conference Date: October 16-20, 2018.
- [79] D. Sui, J. Fan, H. Jin, X. Cai, J. Zhao, and Y. Zhu, "Design of a wearable upper-limb exoskeleton for activities assistance of daily living," in *2017 IEEE International Conference on Advanced Intelligent Mechatronics (AIM)*, pp. 845–850, IEEE, 2017.
- [80] C. Liu, H. Liang, N. Ueda, P. Li, Y. Fujimoto, and C. Zhu, "Functional evaluation of a force sensor-controlled upper-limb power-assisted exoskeleton with high backdrivability," *Sensors*, vol. 20, no. 21, 2020.
- [81] Innophys CO, LTD, "Muscle Suit webpage."
<https://innophys.jp/en/>.
Accessed: 2022-08-19.
- [82] H. Kobayashi and K. Hiramatsu, "Development of muscle suit for upper limb," in *IEEE International Conference on Robotics and Automation, 2004. Proceedings. ICRA'04. 2004*, vol. 3, pp. 2480–2485, IEEE, 2004.
- [83] H. Kobayashi, T. Aida, and T. Hashimoto, "Muscle suit development and factory application," *International journal of automation technology*, vol. 3, no. 6, pp. 709–715, 2009.
- [84] H.-C. Hsieh, D.-F. Chen, L. Chien, and C.-C. Lan, "Design of a parallel actuated exoskeleton for adaptive and safe robotic shoulder rehabilitation," *IEEE/ASME Transactions on Mechatronics*, vol. 22, no. 5, pp. 2034–2045, 2017.
- [85] S. Lessard, P. Pansodtee, A. Robbins, L. B. Baltaxe-Admony, J. M. Trombadore, M. Teodorescu, A. Agogino, and S. Kurniawan, "Crux: A compliant robotic upper-extremity exosuit for lightweight, portable, multi-joint muscular augmentation," in *2017 International Conference on Rehabilitation Robotics (ICORR)*, pp. 1633–1638, IEEE, 2017.
- [86] S. R. Lessard, *The Design, Construction, and Evaluation of Crux: A Tensegrity-Inspired Compliant Robotic Upper-Extremity Exosuit*. PhD thesis, University of California, Santa Cruz, 2018.
- [87] M. Xiloyannis, D. Chiaradia, A. Frisoli, and L. Masia, "Physiological and kinematic effects of a soft exosuit on arm movements," *Journal of neuroengineering and rehabilitation*, vol. 16, no. 1, pp. 1–15, 2019.

- [88] D. Chiaradia, M. Xiloyannis, C. W. Antuvan, A. Frisoli, and L. Masia, "Design and embedded control of a soft elbow exosuit," in *2018 IEEE International Conference on Soft Robotics (RoboSoft)*, pp. 565–571, 2018.
- [89] Y. G. Kim, M. Xiloyannis, D. Accoto, and L. Masia, "Development of a soft exosuit for industrial applications," in *2018 7th IEEE International Conference on Biomedical Robotics and Biomechatronics (Biorob)*, pp. 324–329, 2018.
- [90] V. R. Ham, T. G. Sugar, B. Vanderborght, K. W. Hollander, and D. Lefeber, "Compliant actuator designs: Review of actuators with passive adjustable compliance/controllable stiffness for robotic applications," *IEEE Robot. Autom. Mag.*, vol. 16, no. September, pp. 81–94, 2009.
- [91] H. Lee, B. Lee, W. Kim, M. Gil, J. Han, and C. Han, "Human-robot cooperative control based on pHRI (Physical human-robot interaction) of exoskeleton robot for a human upper extremity," *Int. J. Precis. Eng. Manuf.*, vol. 13, no. 6, pp. 985–992, 2012.
- [92] L. Aquilante, M. Tabaglio, D. Ramirez, F. Braghin, A. L. G. Pedrocchi, M. Gandolla, and S. Dalla Gasperina, "Load compensation device, in particular of gravitational loads, applicable to exoskeletons," July 14 2022. US Patent App. 17/615,306.
- [93] Z. Li and S. Bai, "A novel revolute joint of variable stiffness with reconfigurability," *Mechanism and Machine Theory*, vol. 133, pp. 720–736, 2019.
- [94] Z. Li, S. Bai, O. Madsen, W. Chen, and J. Zhang, "Design, modeling and testing of a compact variable stiffness mechanism for exoskeletons," *Mechanism and Machine Theory*, vol. 151, p. 103905, 2020.
- [95] Harmonic Drive, "Harmonic Drive Gears." <https://harmonicdrive.de/en/products>. Accessed: 2022-08-19.
- [96] K. Anam and A. A. Al-Jumaily, "Active Exoskeleton Control Systems: State of the Art," *Procedia Eng.*, vol. 41, no. Iris, pp. 988–994, 2012.
- [97] D. Bandara, J. Arata, and K. Kiguchi, "Task based motion intention prediction with eeg signals," in *2016 IEEE International Symposium on Robotics and Intelligent Sensors (IRIS)*, pp. 57–60, IEEE, 2016.
- [98] Y. Hayashi and K. Kiguchi, "Estimation of upper-limb motion in sagittal plane based on eeg signals," in *2014 Joint 7th International Conference on Soft Computing and Intelligent Systems (SCIS) and 15th International*

- Symposium on Advanced Intelligent Systems (ISIS)*, pp. 1229–1232, IEEE, 2014.
- [99] B. Beigzadeh, M. Ilami, and S. Najafian, “Design and development of one degree of freedom upper limb exoskeleton,” in *2015 3rd RSI international conference on robotics and mechatronics (ICROM)*, pp. 223–228, IEEE, 2015.
- [100] M. D. Serruya, A. Napoli, N. Satterthwaite, J. Kardine, J. McCoy, N. Grampurohit, K. Talekar, D. Middleton, F. Mohamed, M. Kogan, *et al.*, “Neuromotor prosthetic to treat stroke-related paresis,” *Medrxiv*, 2021.
- [101] M. R. U. Islam, K. Xu, and S. Bai, “Position sensing and control with fmg sensors for exoskeleton physical assistance,” in *Wearable Robotics: Challenges and Trends*, Biosystems & Biorobotics, pp. 3–7, Cham: Springer International Publishing, 2018.
- [102] A. M. Khan, D.-w. Yun, M. A. Ali, K. M. Zuhaib, C. Yuan, J. Iqbal, J. Han, K. Shin, and C. Han, “Passivity based adaptive control for upper extremity assist exoskeleton,” *International journal of control, automation, and systems*, vol. 14, no. 1, pp. 291–300, 2016.
- [103] A. M. Khan, F. Khan, and C. Han, “Estimation of desired motion intention using extreme learning machine for upper limb assist exoskeleton,” *IEEE/ASME International Conference on Advanced Intelligent Mechatronics, AIM*, vol. 2016-Septe, pp. 919–923, 2016.
- [104] T. Hayashi, H. Kawamoto, and Y. Sankai, “Control method of robot suit HAL working as operator’s muscle using biological and dynamical information,” *2005 IEEE/RSJ International Conference on Intelligent Robots and Systems, IROS*, vol. 2, no. 1, pp. 3455–3460, 2005.
- [105] J. M. P. Gunasekara, R. a. R. C. Gopura, T. S. S. Jayawardane, and S. W. H. M. T. D. Lalitharathne, “Control methodologies for upper limb exoskeleton robots,” *2012 IEEE/SICE Int. Symp. Syst. Integr. SII 2012*, pp. 19–24, 2012.
- [106] T. Ripel, J. Krejsa, J. Hrbacek, and I. Cizmar, “Active elbow orthosis,” *International Journal of Advanced Robotic Systems*, vol. 11, no. 9, p. 143, 2014.
- [107] D. Copaci, A. Flores, F. Rueda, I. Alguacil, D. Blanco, and L. Moreno, “Wearable elbow exoskeleton actuated with shape memory alloy,” in *Converging Clinical and Engineering Research on Neurorehabilitation II*, pp. 477–481, Springer, 2017.

- [108] Y. Rosales Luengas, R. López-Gutiérrez, S. Salazar, and R. Lozano, "Robust controls for upper limb exoskeleton, real-time results," *Proceedings of the Institution of Mechanical Engineers, Part I: Journal of Systems and Control Engineering*, vol. 232, no. 7, pp. 797–806, 2018.
- [109] S. Balasubramanian and J. He, "Adaptive control of a wearable exoskeleton for upper-extremity neurorehabilitation," *Appl. Bionics Biomech.*, vol. 9, pp. 99–115, 2012.
- [110] A. AIA, C. H, L. X, O. M, and A. JM, "Survey of On-line Control Strategies of Human-Powered Augmentation Exoskeleton Systems," *Advances in Robotics & Automation*, vol. 05, no. 03, 2016.
- [111] N. Hogan, "Impedance control: An approach to manipulation," in *1984 American control conference*, pp. 304–313, IEEE, 1984.
- [112] N. Hogan, "Impedance control - An approach to manipulation. I-Theory. II-Implementation. III-Applications," *ASME Journal of Dynamic Systems and Measurement Control B*, vol. 107, pp. 1–24, 1985.
- [113] N. Hogan, "On the stability of manipulators performing contact tasks," *IEEE journal of robotics and automation*, vol. 4, no. 6, pp. 677–686, 1988.
- [114] T. Kurfess, *Robotics and Automation Handbook*. Taylor & Francis, 2005.
- [115] Cyberdyne, "HAL Single Joint webpage."
<https://www.cyberdyne.jp/english/products/SingleJoint.html>.
Accessed: 2022-08-19.
- [116] C. Carignan, J. Tang, and S. Roderick, "Development of an exoskeleton haptic interface for virtual task training," *2009 IEEE/RSJ International Conference on Intelligent Robots and Systems, IROS 2009*, pp. 3697–3702, 2009.
- [117] D. Naidu, R. Stopforth, G. Bright, and S. Davrajh, "A 7 DOF exoskeleton arm: Shoulder, elbow, wrist and hand mechanism for assistance to upper limb disabled individuals," in *IEEE AFRICON Conference*, pp. 13–15, 2011.
- [118] H. S. Lo and S. S. Q. Xie, "An Upper Limb Exoskeleton with an Optimized 4R Spherical Wrist Mechanism for the Shoulder Joint," in *IEEE/ASME International Conference on Advanced Intelligent Mechatronics (AIM)*, (Besançon, France), pp. 269–274, 2014.
- [119] M. N. Castro, J. Rasmussen, M. S. Andersen, and S. Bai, "A compact 3-dof shoulder mechanism constructed with scissors linkages for exoskeleton applications," *Mechanism and Machine Theory*, vol. 132, pp. 264–278, 2019.

- [120] A. Ebrahimi, D. Gröninger, R. Singer, and U. Schneider, "Control parameter optimization of the actively powered upper body exoskeleton using subjective feedbacks," in *2017 3rd International Conference on Control, Automation and Robotics (ICCAR)*, pp. 432–437, IEEE, 2017.
- [121] D. Copaci, D. Blanco, and L. Moreno, "Wearable elbow exoskeleton actuated with shape memory alloy in antagonist movement," in *Proceedings of the Joint Workshop on Wearable Robotics and Assistive Devices, International Conference on Intelligent Robots and Systems, Daejeon, Korea*, pp. 9–14, 2016.
- [122] Myomo Inc, "MyoPro® Exoskeleton."
<https://myomo.com/>.
Accessed: 2022-08-19.
- [123] Y. Rosales, R. Lopez, I. Rosales, S. Salazar, and R. Lozano, "Design and modeling of an upper limb exoskeleton," in *2015 19th International Conference on System Theory, Control and Computing (ICSTCC)*, pp. 266–272, IEEE, 2015.
- [124] T. G. Sugar, J. He, E. J. Koeneman, J. B. Koeneman, R. Herman, H. Huang, R. S. Schultz, D. E. Herring, J. Wanberg, S. Balasubramanian, P. Swenson, and J. a. Ward, "Design and control of RUPERT: A device for robotic upper extremity repetitive therapy," *IEEE Trans. Neural Syst. Rehabil. Eng.*, vol. 15, no. 3, pp. 336–346, 2007.
- [125] L. O. Sullivan, V. Power, G. Virk, N. Masud, U. Haider, S. Christensen, S. Bai, L. Cuypers, and M. D. Havé, "End user needs elicitation for a full-body exoskeleton to assist the elderly," in *6th International Conference on Applied Human Factors and Ergonomics (AHFE 2015) and the Affiliated Conferences, AHFE 2015 End*, vol. 00, Elsevier, 2015.
- [126] S. Bai, M. Islam, V. Power, and L. O'Sullivan, "User-centered development and performance assessment of a modular full-body exoskeleton (axo-suit)," *Biomimetic Intelligence and Robotics*, vol. 2, no. 2, p. 100032, 2022.
- [127] S. Bai, S. Christensen, M. Islam, S. Rafique, N. Masud, P. Mattsson, L. O'Sullivan, and V. Power, "Development and testing of full-body exoskeleton axo-suit for physical assistance of the elderly," in *Wearable Robotics: Challenges and Trends* (M. C. Carrozza, S. Micera, and J. L. Pons, eds.), (Cham), pp. 180–184, Springer International Publishing, 2019.
- [128] AnyBody Technology, "AnyBody Modeling System."
<https://www.anybodytech.com/>.
Accessed: 2022-08-19.

- [129] M. Nilsson, J. Ingvast, J. Wikander, and H. Von Holst, "The Soft Extra Muscle system for improving the grasping capability in neurological rehabilitation," *2012 IEEE-EMBS Conf. Biomed. Eng. Sci. IECBES 2012*, no. December, pp. 412–417, 2012.
- [130] S. Bai and J. Rasmussen, "Modelling of Physical Human-Robot Interaction for Exoskeleton Designs," *Multibody Dynamics 2011, ECCOMAS Thematic Conference*, no. July, pp. 1–7, 2011.
- [131] P. Agarwal, M. S. Narayanan, L.-f. Lee, F. Mendel, and V. N. Krovi, "Simulation-Based Design of Exoskeletons Using Musculoskeletal Analysis," in *ASME 2010 International Design Engineering Technical Conferences & Computers and Information in Engineering Conference*, pp. 1357–1364, 2010.
- [132] S. Hernandez, M. Raison, L. Baron, and S. Achiche, "Refinement of exoskeleton design using multibody modeling: an overview," in *CCToMM Mechanisms, Machines, and Mechatronics Symposium*, p. 110, 2015.
- [133] M. Damsgaard, J. Rasmussen, S. T. Christensen, E. Surma, and M. de Zee, "Analysis of musculoskeletal systems in the AnyBody Modeling System," *Simulation Modelling Practice and Theory*, vol. 14, no. 8, pp. 1100–1111, 2006.
- [134] S. L. Delp, F. C. Anderson, A. S. Arnold, P. Loan, A. Habib, C. T. John, E. Guendelman, and D. G. Thelen, "Opensim: Open-source software to create and analyze dynamic simulations of movement," *IEEE Transactions on Biomedical Engineering*, vol. 54, no. 11, pp. 1940–1950, 2007.
- [135] P. Agarwal, R. R. Neptune, and A. D. Deshpande, "A simulation framework for virtual prototyping of robotic exoskeletons," *Journal of biomechanical engineering*, vol. 138, no. 6, 2016.
- [136] D. A. Winter, *Biomechanics and Motor Control of Human Movement*. Wiley, 2009.
- [137] M. R. Islam and S. Bai, "Payload estimation using forcemyography sensors for control of upper-body exoskeleton in load carrying assistance," *Modeling, Identification and Control*, vol. 40, no. 4, p. 189, 2019.
- [138] M. N. Castro, J. Rasmussen, S. Bai, and M. S. Andersen, "Validation of subject-specific musculoskeletal models using the anatomical reachable 3-d workspace," *Journal of Biomechanics*, vol. 90, pp. 92–102, 2019.

ISSN (online): 2446-1636
ISBN (online): 978-87-7573-764-2

AALBORG UNIVERSITY PRESS